Dissertation zur Erlangung des Doktorgrades
der Fakultät für Chemie und Pharmazie
der Ludwig-Maximilians-Universität München

Structural Interplay of Key Factors in the Human MicroRNA Pathway

Janina Michelle Pfaff
aus
Mannheim, Deutschland

2013

Erklärung

Diese Dissertation wurde im Sinne von §7 der Promotionsordnung vom 28. November 2011 von Herrn Prof. Dr. Klaus Förstemann betreut.

Eidesstattliche Versicherung

Diese Dissertation wurde eigenständig und ohne unerlaubte Hilfe erarbeitet.

München, den 22.04.2013

.....

Janina Pfaff

Dissertation eingereicht am	07.03.2013
1. Gutachter	Prof. Dr. Klaus Förstemann
2. Gutachter	Prof. Dr. Gunter Meister
Mündliche Prüfung am	18.04.2013

Summary

Argonaute (Ago) proteins are viewed as key players in small RNA-guided gene silencing pathways in almost all eukaryotes. Small RNAs such as short interfering RNAs or microRNAs guide Ago proteins to specific target RNAs resulting in mRNA decay or translational silencing.

In miRNA-mediated silencing, Ago proteins associate with a member of the GW182 protein family in order to achieve efficient repression. GW182 proteins comprise a N-terminal Ago-binding domain that is characterized by multiple GW-repeats and a C-terminal silencing domain with several globular domains. GW182 hooks via its GW-repeats into the PIWI domain of the Ago protein providing a binding platform for downstream silencing events. Although the general principles underlying Ago-GW interactions are well established, a detailed characterization of the GW-Ago association has not been performed.

To elucidate the molecular basis for the interaction, we established a purification protocol to obtained the desired recombinant proteins and used NMR spectroscopy, biochemical and biophysical approaches as well as crosslinking to analyze affinities and binding properties of human Ago proteins to GW182 proteins.

Hence, we found exciting new aspects: First, the tryptophan flanking glycines are not required and several other neighbors are accepted. Second, for efficient association only several specific Trps engage in binding, which reside in fully unstructured protein environments. Finally, we mapped the GW182 binding site on Ago and propose a model of the Ago-GW182 interaction.

Thus, our results will contribute to the understanding of the mechanism of miRNA-mediated gene silencing.

Publications and Presentations

Parts of this thesis are submitted for publication:

J. Pfaff, J. Hennig, F. Herzog, R. Aebersold, M. Sattler, D. Niessing and G. Meister. (2013). Structural insights into GW - Argonaute protein interactions, submitted.

J. Pfaff and G. Meister. (2013) Argonaute and GW182 proteins: an effective alliance in gene silencing. Review. Biochem Soc Trans.

J. Hauptmann, A. Dueck, S. Harlander, **J. Pfaff**, R. Merkl and G. Meister. Turning catalytically inactive human Argonaute proteins into active slicer enzymes. (2013). Nat Struct Mol Biol, accepted.

Parts of this thesis have been presented at international conferences:

J. Pfaff, S. Ruedel, J. Hennig, M. Sattler, D. Niessing and G. Meister. Biochemical dissection of human Argonaute - GW interactions. Poster. 16th annual meeting of the RNA Society 2011, Kyoto, Japan.

Contents

Summary v

Publications and Presentations vii

Contents ix

1 Introduction 1

1.1 Classes of Small RNAs . . . 1

1.1.1 MicroRNAs . . . 2

1.2 Argonaute Proteins - the Central Components of MicroRISCs . . . 5

1.2.1 Argonaute Functional Domains . . . 5

1.3 The GW182 Protein Family - Argonaute Interaction Partners . . . 8

1.3.1 GW182 Domain Organization . . . 8

1.4 Argonaute - GW-protein Interaction . . . 10

1.4.1 Mapping of Ago and GW182 Binding Sites . . . 10

1.4.2 GW-repeats as Conserved Argonaute Binding Hooks . . . 10

1.4.3 GW-repeat Binding Mode . . . 11

1.5 Subcellular Localization . . . 12

1.6 Post Translational Modifications . . . 13

1.7 Mechanisms of Small RNA Functions . . . 14

1.7.1 Posttranscriptional Silencing by SiRNA-mediated mRNA Cleavage 14

1.7.2 MicroRNA-mediated Gene Regulation . . . 14

1.8 Aim of the Thesis . . . 17

2 Results 19

2.1 Definition of Working Constructs . . . 19

2.1.1 TNRC6 Family Proteins . . . 19

2.1.2 Argonaute Family Proteins . . . 20

2.2 Identification of Argonaute 2 Interaction Motifs on TNRC6B . . . 23

2.3 Analysis of Tryptophan Flanking Amino Acids . . . 26

2.4 Tryptophan - Argonaute 2 Contacts on an Atomic Level 29
2.5 A Tryptophan-containing TNRC6B Fragment that Binds Argonaute 2 is Unstructured in Solution 34
2.6 TNRC6B Fragment Binds to Argonaute 2 with a low Micromolar Affinity 37
2.7 Tryptophan Flanking Amino Acids Contribute to Binding 40
2.8 Two Proximal Tryptophans are Necessary for Effective Binding 42
2.9 Mapping TNRC6B Contacts on the Surface of Argonaute 2 43
2.10 Model of TNRC6B - Argonaute 2 Interaction 46

3 Discussion **49**
3.1 Protein Properties 49
3.2 Argonaute 2 Binds to Distinct Tryptophan - containing Motifs on TNRC6B with Different Affinities 50
3.2.1 Definition of the Argonaute 2 Binding Site on TNRC6B 50
3.2.2 Role of Tryptophan Residues in the Argonaute - TNRC6B Interaction 51
3.3 The Argonaute 2 Surface Reveals Potential Binding Interfaces 52
3.3.1 Implications of Species Specific Surface Characteristic on GW182 Binding 54
3.4 TNRC6B Binds to the Argonaute 2 PIWI Domain Through a Combinatorial Tryptophan - Motif 56
3.4.1 Tryptophan Position 56
3.4.2 Trp Spacer Length 57
3.4.3 Relation to Known Protein Sequence Motifs 59
3.5 Functional Implications 60

4 Material and Methods **63**
4.1 Material 63
4.1.1 Consumables and Chemicals 63
4.1.2 Oligonucleotides 64
4.1.3 Plasmids 65
4.1.4 Antibodies 66
4.1.5 Bacterial Strains and Cell Lines 66
4.1.6 Media and Buffers 66
4.2 Methods 67
4.2.1 Molecular Biology Methods 67
4.2.2 Protein Expression 69

4.2.3 Protein Purification 70
4.2.4 Protein Biochemistry 71
4.2.5 Nuclear Magnetic Resonance 74

5 Appendix **77**

Abbreviations **85**

Acknowledgements **109**

Curriculum Vitae **111**

1 Introduction

After the discovery of RNA interference (RNAi) in 1998 [62], fundamental insights into the regulation of various cellular processes by small, non-coding RNAs (sRNAs) and the underlying mechanism have been gained. The phenomenon of RNA-induced gene silencing of complementary RNAs was first described in plants more than 20 years ago [153][211]. Initially, gene silencing was supposed to be an adaptive defense in plants against viruses and transposable elements [217] but soon, studies in *Caenorhabditis elegans* (*C. elegans*) revealed that there are also endogenous causes responsible for post transcriptional regulation that are well conserved throughout plants and animals [219][118][5]. To date, RNAi is a powerful tool to repress specific genes [209]. It is applied in many fields, ranging from basic research to medical therapy [197][202][69].

1.1 Classes of Small RNAs

During the last years, different species of sRNAs were identified that can be grouped into three main classes based on their structure, biogenesis or mechanism. Common to all classes is that, once processed, the sRNA is associated with a protein of the Argonaute (Ago) protein family to exert its activity.
One class, short interfering RNAs (siRNAs), are excised by the ribonuclease (RNase) III enzyme Dicer from long , double-stranded (ds) RNAs to ~21 nucleotide (nt) long RNA duplexes. These precursor RNAs are either derived from exogenous sources like viruses (exo-siRNAs) or endogenous sources (endo-siRNAs) e.g. transposable elements, natural antisense transcripts or hairpin RNAs [38][70][106][161]. Dicer processing products are characterized by 2 nt overhangs on both 3' ends and phosphate groups on the 5' ends [62][81][46]. SiRNAs are typically composed of a guide strand, which is characterized by perfect complementary to the target RNA and therefore also termed antisene strand and a passenger (sense) strand [174]. According to the asymmetry rule, the strand with the thermodynamically less stable 5' end is selected for incorporation into Ago to form the the RNA-induced silencing complex (RISC). The guide strand positions Ago on the target RNA by complementary base pairing. This leads to gene silencing through cleavage of the bound mRNA provided that the Ago protein possesses endonucleolytic activity

[190][109][176]. SiRNA biogenesis and function has been reviewed in detail [112][71][25]. Another class comprises P-element-induced wimpy testis (PIWI)-interacting RNAs (piRNAs). PiRNAs are processed in a Dicer-independent pathway to 24-31 nt long, single stranded (ss) RNAs. They are typically associated with a member of the PIWI clade of Ago proteins and have only been identified in animal germ cells [1][71][112]. Structurally, this sRNA class is characterized by a 2'-O-methylation at their 3' end [113][185]. However, the exact function of this modification is unclear. The biological significance of piRNA relies mainly in the inactivation of mobile genetic elements [23].
The last class of sRNAs, microRNAs (miRNAs), will be discussed in detail in the following section.

1.1.1 MicroRNAs

MiRNAs are endogenous, ss sRNAs that regulate gene expression. They are ~21 nt in length and expressed ubiquitously. After their discovery in *C. elegans* only two decades ago in the labs of Ruvkun [219] and Ambros [118], miRNAs have now been shown to play fundamental roles in many biological processes such as development, differentiation, apoptosis and proliferation. They are highly conserved in many different species ranging from plants, algae and viruses to mammals [78]. To date, more than 1000 miRNAs are annotated in humans and it is suggested that up to 60% of eukaryotic genes underly miRNA-mediated regulation [66][114]. Based on that, miRNAs are viewed as key-regulators of gene expression that are implicated in numerous diseases, offering great potential for therapeutic trials.

MicroRNA Biogenesis

Most commonly, miRNAs are located as clusters and transcribed from a polycistronic transcription unit in introns of protein-coding genes or untranslated regions (UTRs) [121][25]. Transcription of miRNA genes is carried out by RNA-polymerase II, and for some cases by RNA-polymerase III, resulting in hairpin-shaped primary miRNA-transcripts (pri-miRNA)(Figure 1.1.1). Pri-miRNAs are typically several kilo bases long with an imperfectly paired stem of ~33 bp and ss flanking ends. Like mRNAs, they are polyadenylated at their 3' ends and capped at their 5' ends [112][15][122]. In the canonical biogenesis pathway (Figure 1.1.1 A, B), pri-miRNas are cleaved in a first step by the microprocessor complex, containing the RNase III-enzyme Drosha and its cofactor DGCR8 in humans (Pasha in *Drosophila melanogaster* (*D. melanogaster*) and *C. elegans*) [40][77][83]. DGCR8 recognizes the ss ends and assists Drosha in excising the stem loop to create the precursor-miRNAs (pre-miRNAs) with characteristic 2 nt

overhangs at the 3' end and a phosphate group at the 5' end typical for RNase III processing [119]. The pre-miRNA is subsequently exported to the cytoplasm by Exportin 5 [12][136][226].

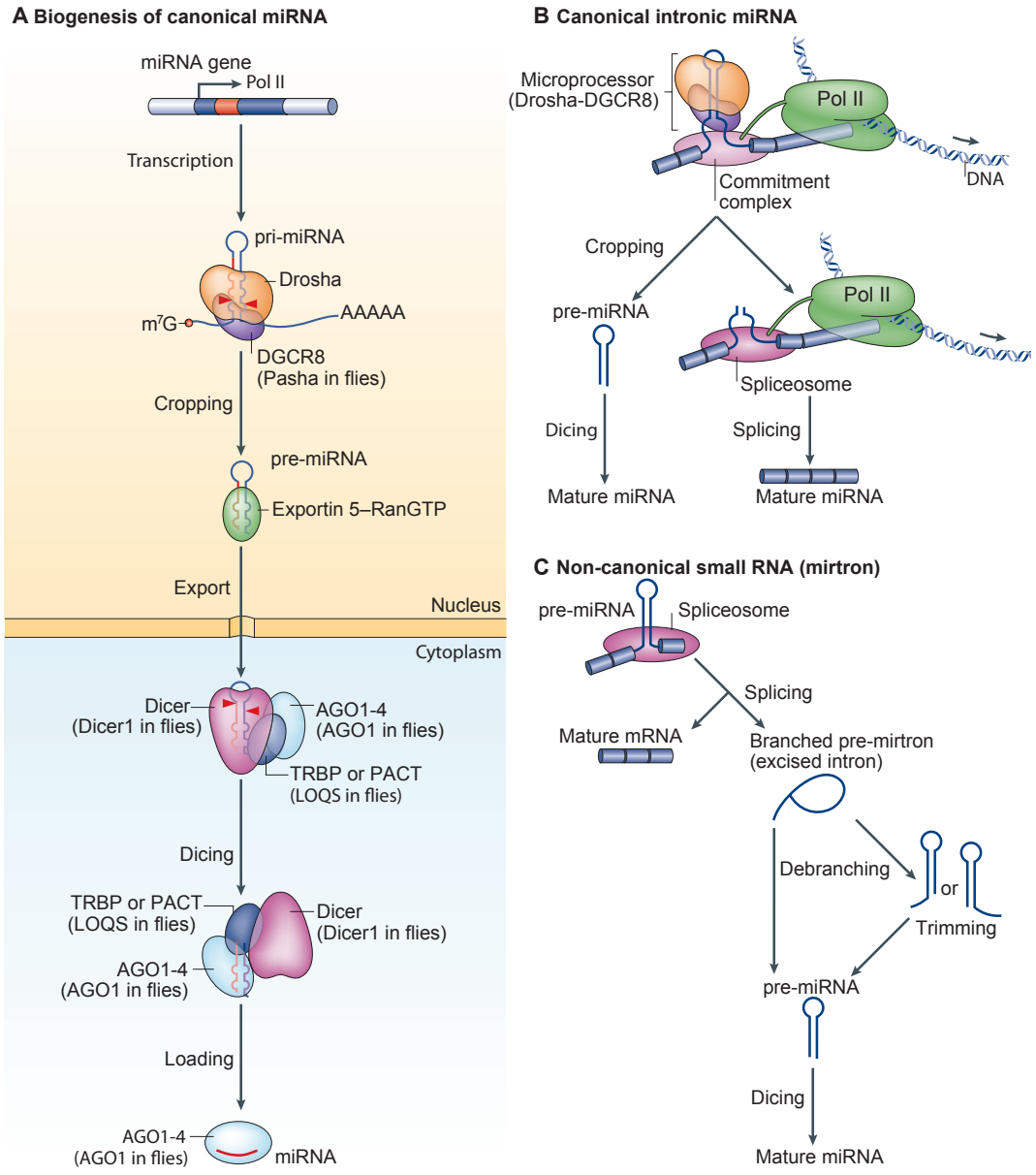

Figure 1.1.1: MiRNA biogenesis pathway. A) Canonical miRNA biogenesis pathway from non-coding RNA transcripts. B) Canonical pathway of intronic miRNAs. C) Drosha-independent non-canonical pathway for biogenesis of mirtrons from introns (adopted from[112]).

However, alternative pathways were found in vertebrates and invertebrates, which produce miRNA precursors resembling pre-miRNAs independent of the microprocessor complex. These precursors termed mirtrons are excised by the splicing machinery (Figure 1.1.1 C) and then enter the canonical miRNA processing pathway [162][180]. Recently, other non canonical pathways have been described with sRNAs derived from tRNAs [3] or small nucleolar RNAs (snoRNAs) [49].
A second processing step is carried out in the cytoplasm that involves Dicer and its cofactors TRBP an/or PACT (Loquacious (LOQS) in *D. melanogaster*) [32][63][120][184]. Dicer liberates a ~21 nt long ds miRNA with 2 nt overhangs at their 3' ends and a phosphate group at the 5' end from the stem loop [95][46]. However, recent observations also suggest a Dicer-independent maturation step of miRNA that required catalysis by Ago2 [30][34].
Usually, the miRNA passenger strand (miRNA*) is degraded, whereas the mature miRNA is incorporated into an Ago protein to form the micro-ribonucleoprotein particle (miRNP) or miRNA-induced-silencing complex (miRISC) and directs effector proteins to the RNA target.
Given the strong and general impact of miRNA-mediated gene regulation, the levels of miRNAs is crucial for the cell and have to be controlled tightly. MiRNA metabolism is regulated by multiple proteins at various levels e.g. on the level of transcription or posttranscriptionally by influencing processing steps, nuclear export or miRISC stability [207][115][220].

MicroRISC Assembly

MiRISCs are the effector complexes mediating mRNA repression. The core proteins comprising the miRISC are a miRNA bound Ago protein and a protein of the GW182 family [59].
In humans, active RISC formation is assisted by Ago, Dicer, TRBP and/or PACT (in flies Dicer1, LOQS and Ago1), together forming the RISC loading complex (RLC) [32][80][120][140][139][76]. For RISC assembly, RNA duplexes generated by Dicer processing are separated and one strand is selected for Ago loading according to the asymmetry rule [190][109][176]. This selection is sensed by Dicer or by one of its cofactors [132][133][156]. It is assumed that, after processing by Dicer, TRBP associates with the more stable duplex end, while the other end interacts with Ago [204][132].
MiRNP assembly is facilitated by the endonucleolytic (slicer) activity of Ago2 [41] which requires perfect complementary of the RNA duplex. This is the case for siRNAs, however, most miRNAs contain mismatches that prevent cleavage. Similarly, Ago1, 3 and 4

lack slicer activity and are nevertheless loaded with ssRNAs [146]. Thus, further mechanisms must exist that support RISC loading.
The endoribonuclease C3PO was shown to facilitate siRNA-initiated RISC activation in mammals and *D. melanogaster* [134][225]. A slicer independent mechanism involving RNA helicases was suggested to play a role in RISC assembly [178] in an ATP-dependent manner [159][228] by unwinding the duplex. More recently, the Hsc70/Hsp90 chaperone machinery was proposed to function in RISC assembly by inducing conformational changes in the Ago structure in an ATP-dependent way, thereby facilitating Ago loading [97] [102][149]. However, the detailed molecular mechanism of RISC loading is elusive.

1.2 Argonaute Proteins - the Central Components of MicroRISCs

Ago proteins are indispensable for miRNA/siRNA-mediated gene silencing [199]. They directly bind miRNAs, thereby recruiting effector complexes to the target mRNA which mediate regulation of gene expression. Thus, Ago proteins constitute the central components of miRISCs.
The protein family was first described in *Arabidopsis thaliana* [150] and is named after an *Arabidopsis thaliana* mutant, which phenotypically resembled a small squid termed argonaut [11]. Ago proteins are highly conserved in almost all kingdoms of life ranging from archaea and bacteria to plants and higher eukaryotes [24][89]. Organisms comprise multiple copies of Ago genes, e.g. eight in humans, five in *D. melanogaster* and 27 in *C. elegans* with different expression profiles and substrate specificities [96].
The Ago protein family is divided into three clades: germline specific PIWI proteins that bind piRNAs, ubiquitously expressed Ago proteins interacting with siRNAs and miRNAs and the worm-specific WAGO subfamily [127][24][227][60].
Humans have eight Ago proteins. Four of them belong to the PIWI subfamily, named HIWI1, HIWI2, HIWI3 and HILI, whereas the other four belong to the Ago class named Ago1, Ago2, Ago3 and Ago4. The functional difference between the four Ago proteins is unclear, however, Ago2 is the only protein possessing cleavage activity.

1.2.1 Argonaute Functional Domains

Ago functions as effector protein in miRNA/siRNA-mediated gene silencing, thus, it must bind the miRNA/siRNA in a way suitable for RNA target recognition. Initial studies on prokaryotic Ago proteins revealed a bilobal architecture comprising four globular domains: N, PIWI/Argonaute/Zwille (PAZ), middle (MID) and PIWI [196] (Fig-

ure 1.2.1). The guide DNA spans between both lobes with its 3' end anchored in the PAZ and the 5' end anchored to the MID domain [138][230][215]. Investigation of isolated domains from eukaryotic species allowed to determine nucleotide binding specificity and eukaryote-specific insertions [129][64][14][13].
Recently, two groups succeeded to crystallize full length human Ago2 providing structural insights into the mechanism of eukaryotic miRNA function [188][47]. The overall architecture resembles prokaryotic structures with a bilobal shape and a central cleft for miRNA/siRNA binding. The individual domains align well with the available structures, however, the relative position of the lobes differ from their prokaryotic counterparts. The authors also observe additional secondary structures and extended loops, which are proposed to function in RNA binding, target RNA recognition or interaction with other proteins.

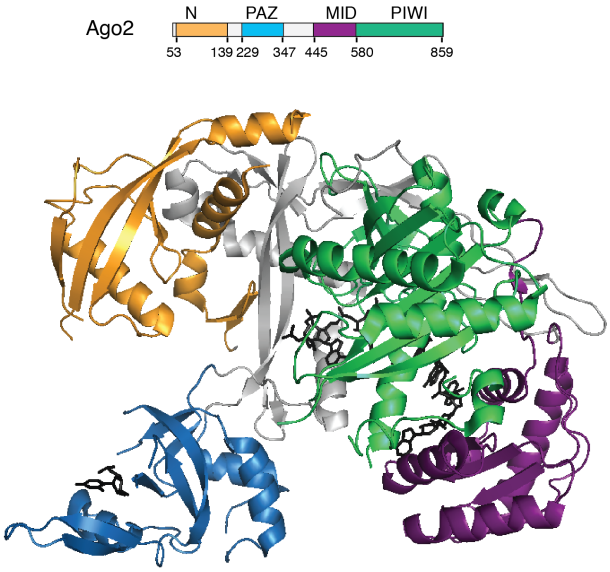

Figure 1.2.1: Crystal structure of Ago2. Ago2 crystal structure (PDB: 4EI3) [188] with its functional domains N (yellow), PAZ (blue), MID (purple) and PIWI (green) indicated. Bound miRNA is colored in black.

The N-terminal domain comprises the highest sequential variety in comparison to homologues (for alignment see appendix).
The PAZ domain resembles an oligosaccharide/oligonucleotide-binding domain or Sm-fold domain. As shown before [137][129], conserved residues of a hydrophobic pocket specifically recognize the 3' dinucleotide of the miRNA/siRNA, which result from Dicer cleavage. The last base stacks against F294 and remaining interactions are mainly mediated by the phosphate backbone and are thus sequence independent [47].

The MID domain reveals a fold similar to sugar-binding domain of the lac-repressor. As reported previously [14][64], the MID domain of human full length Ago2 forms a pocket for tethering the 5' phosphate of the miRNA/siRNA. Several residues (Y529, K533, Q545, C546 K566, K570, R812, A859) were identified that are essential for binding. In contrast to prokaryotic structures, the authors did not find a magnesium ion coordinated in the pocket [188][47]. Sequencing studies showed that human miRNA more frequently exhibit an uracil or adenine at their 5' end [90]. This was confirmed by Frank et al. who demonstrated that adenine and uracil nucleotides are indeed kinetically preferred using nuclear magnetic resonance (NMR) titration experiments with the recombinant human Ago2 MID domain [64]. However, MID domains of other species show different nucleotide preferences [70][106][147][179]. Thus, the specificity for the 5' nucleotide is provided by the MID domain.
Besides recognition of the miRNA ends, Ago2 offers extensive interactions with the phosphate backbone, thereby positioning the seed region (nt 2-8) of the miRNA suitable for target binding [188][47].
The PIWI domain comprises a RNase H fold [196]. RNase H usually catalyses hydrolysis of RNA in RNA-DNA duplices. Accordingly, prokaryotic Ago proteins were found to be DNA-guided RNase [138][230]. In contrast, Ago proteins of higher species possess cleavage activity towards RNA-RNA duplexes. The catalytic center of RNase H contains an aspartate (Asp)-Asp-glutamate (Glu)/Asp triad with two coordinated divalent metal ions required for cleavage activity [158]. Similarly, RISC-mediated cleavage is dependent on the presence of divalent metal ions, however, the active site differs. Initially the active site was assumed to comprises a catalytic Asp-Asp-histidine (His) triad [130][191], which was shown to be required but not sufficient for cleavage activity [130][145]. In humans, Ago2 and Ago3 offer the Asp-Asp-His motif but only Ago has cleavage activity towards fully complementary targets and is therefore referred to as 'slicer' [128]. Recently, a crystal structure of the ternary *Kluyveromyces polysporus* Ago complex revealed a fourth residue that pluggs into the catalytic triad thereby completing the active center of Ago to a catalytic DEDX tetrad [152]. The PIWI domain has been implicated in binding GW182, supported by the Ago2 crystal structure with two tryptophans (Trps) bound to the PIWI domain [203][126][188]. GW182 proteins were demonstrated to act as key players in miRNA-mediated gene silencing using Ago as a platform to trigger miRNA function [28][57][17]. The interaction of GW182 proteins with Ago and the functional implications will be discussed in the next section in detail.

1.3 The GW182 Protein Family - Argonaute Interaction Partners

In animals, Ago proteins bind miRNAs to mediate gene silencing [59]. Most miRNAs are not fully complementary to their target RNAs, thus, cleavage by Ago2 cannot be exerted [6]. A post transcriptional silencing mechanism involving the GW182 protein family was intensively studied during the past years and it emerged that GW182 proteins directly interact with Ago proteins thereby recruiting downstream factors leading to translational repression and mRNA degradation [235][231][224][201][175][126][92][57][51][43][31][28][17]. GW182 proteins were first described by Eystathioy et al. one decade ago. The researchers observed a 182 kDa protein containing multiple glycine (Gly)-Trp-repeats (GW-repeats) in a patients autoimmune serum suffering from motor and sensory neuropathy. The protein was shown to accumulate in discrete cytoplasmic speckles termed GW-bodies associated with mRNA and a role in posttranscriptional regulation of gene expression was suggested [55]. A subsequent report gave evidence that GW-bodies coincide with cytoplasmic structures containing markers of the mRNA degradation pathway [56]. The link to miRNA-mediated gene silencing was later established when the GW182 homologue AIN-1 was shown to interact with the miRISC in processing bodies [44]. A short time later, GW182 was demonstrated to be essential for miRNA-mediated gene-silencing [175] and a physical interaction between Ago and GW182 was proven [131][146].

1.3.1 GW182 Domain Organization

Three GW182 paralog were identified in vertebrates termed trinucleotide repeat containing protein 6 (TNRC6) A (corresponding to GW182), B and C. Insects comprise a single ortholog (GW182 or Gawky) [8]. Vertebrates and insect proteins share a similar domain organization. All proteins feature a N-terminal Ago-binding region, an ubiquitin associated (UBA)-like domain, a glutamine (Q)-rich region, a PABP-interacting motif 2 (PAM2) motif and a C-terminal RNA recognition motif (Figure 1.7.1). Multiple sequence alignment shows a high sequence variety with highly conserved stretches in the Ago-binding region, UBA domain, PAM2 motif and RRM (see appendix) [43][54]. The proteins have a molecular weight of about 180 kDa and are mainly disordered except for two globular domains: the UBA-like domain and a RRM.
UBA domains are common sequence motifs of about 45 amino acids (aa) usually occuring in proteins involved in the ubiquitin/proteasom pathway, DNA repair or cell growth. They fold into a three helix bundle with large hydrophobic patches which form the interface for binding mono- or polyubiquinated substrates [200][21]. The NMR solu-

tion structure of the TNRC6C UBA-like domain corresponds to the canonical UBA fold (PDB: 2DKL; Zhao et al. 2006, data not published). GW182 was proposed to mediate the interaction to the E3 ubiquitin ligase identified by differential display (EDD) via UBA domain dimerization and PAM2 binding [198].

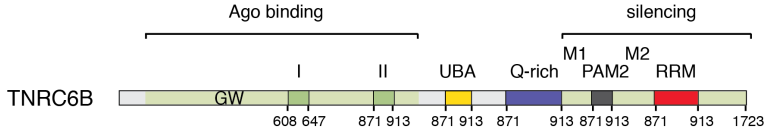

Figure 1.3.1: Schematic of TNRC6B domain organization. Schematic representation of the TNRC6B domain composition and boundaries. The basic organization is shared for vertebrate and insect proteins. Domains are color coded as follows: green: GW-rich region, dark green: GW-rich conserved motif I and II, yellow: UBA domain, purple: Q-rich-region, dark gray: PAM2 motif, red: RRM domain, linker region: gray.

RRMs usually bind single stranded RNA and adopt a fold containing four anti-parallel beta strands and two alpha helices [35]. The structure of the *D. melanogaster* GW182 RRM revealed a canonical fold with an additional C-terminal helix. The lack of RNA binding features suggests that the RRM is rather involved in protein-protein interactions [53]. The exact function of the RRM domain has not been characterized.
The PAM2 motif is responsible for association with the polyadenylate binding protein 1 (PABPC1) and is embedded in a disordered part of the proteins C-terminus between the UBA-like domain and the RRM domain. The crystal structure of PAM2 bound to the C-terminal domain of PABPC1 gave first structural insights into GW182 function [101][58][231]. As mentioned above, the PAM2 domain is also responsible for EDD binding via its PABC domain.
N-terminally to the PAM2 motif, GW182 proteins possess a Q-rich region, which is necessary for P-body localization but dispensable for the silencing activity [8][117].
Trp-motifs in the C-terminal, middle and N-terminal region of GW182 have been implicated in recruiting effector proteins as the CCR4-Not complex responsible for mRNA repression [29][57][27][28]. One report identified two CCR4-Not interaction motifs (CIM1 and CIM2) in the M1 and C-terminal region that are conserved in mammals [57]. In parallel it was published that CCR4-Not binds to several Trp-repeats in the M2 and C-terminal region [28]. The authors suggested that the Trp-motifs form a bipartite domain with autonomous silencing activity [57][51][235]. In contrast to the C-terminal Trp-motifs, several studies demonstrated that GW-repeats in the N-terminus of GW182 are important for the interaction with Ago [8][203].

1.4 Argonaute - GW-protein Interaction

1.4.1 Mapping of Ago and GW182 Binding Sites

The N-terminal GW-repeat containing region of GW182 proteins was demonstrated to be neccessary and sufficient for the interaction with the PIWI domain of Ago [45][8][126][203]. Residues important for binding GW182 in Ago were identified by mutational studies in human Ago2 and *D. melanogaster* Ago1 by different groups [51][203][52][13]. Two hotspots were identified that both abrogated GW182 binding upon mutation. One resides in the MID domain compassing the 5' binding pocket, the second one clusters around the two Trp binding sites identified by Schirle et al. [188].
MiRNA binding was only affected by mutation of residues in the 5' binding pocket. This suggests that GW182 binding either depends on miRNA binding or mutations in the MID domain induce changes that prevent binding. This results give evidence that GW182 interacts with spots approximately in the MID/PIWI domain of the Ago protein. Interestingly, not all Ago proteins are capable of GW182 binding, as shown for *D. melanogaster* Ago2 or PIWI-like proteins [8][148]. Therfore, GW182 binding capacity might be limited to Ago proteins functioning in the miRNA pathway.
Defining the binding site of Ago on GW182 proteins emerged to be more challenging. Species and method-specific difference in binding sites and affinities did not allow to draw a clear picture. Consistently, all reports showed that the N-terminal GW182 region is necessary and sufficient for Ago binding [8][203][45][117][126][201][4][235], although Lian et al. observed additional Ago affinity for GW-repeats in the C-terminus [126]. Shortly after locating the binding region, GW-repeats emerged as the key determinants for efficient binding and a high affinity region termed Ago-hook was mapped, which is however not conserved in all GW182 homologs [203]. Further studies reported that conserved motif I, II or the Ago hook provide major binding sites depending on the species and paralog, with additional repeats strengthening the interaction [8][51][117][4].

1.4.2 GW-repeats as Conserved Argonaute Binding Hooks

The importance of GW-repeats in miRNA-mediated gene silencing was recognized after the discovery of GW182 [55]. This protein quickly evolved to a key component in the miRNA pathway recruiting effector proteins to the mRNA by binding Ago through GW repeats [45][8][126][203][203]. However, GW182 is not the only protein using GW-repeats to associate with Ago proteins.
In parallel to the investigation of GW182-Ago binding, proteins involved in transcriptional gene silencing (TGS) by the RNA-induced transcriptional silencing (RITS) com-

plex in fission yeast were shown to interact with Ago in a similar way. The RITS constitutes an Ago protein, the chromodomain protein Chp1 and Tas3, which mediates transcriptional silencing [213][22]. The authors revealed an interaction module within Tas3 with high sequence conservation to the GW-repeat containing Ago-hook of GW182. This motif was essential for TGS and mutation of a single G or W residue abolished binding [167][203].
In plants, a RNAi-related mechanism known as RNA-directed DNA methylation (RdDM) silences target DNAs by methylation involving nuclear RNA polymerases that synthesize or bind scaffold RNAs [20][233]. Pol V largest subunit NRPE1 comprises a specific GW-repeat containing C-terminus that interacts with Ago4 and is required for Pol V function [45][172][125]. In the same pathway, an SPT5 homolog (KTF1) was shown to link PolV transcription with Ago4 mediated via GW-repeat interaction [86]. Further, the tetrahymenia Ago protein was shown to interact with two GW-repeat proteins termed Wag1p and CnjBp, thereby promoting genome rearrangement [7]. Recently, the interaction between the GW-repeat containing prion protein PrP (C) and human Ago2 was established. It was proposed that the prion protein facilitates formation or stability of miRISC effector complexes on multivesicular bodies (MVBs) and that the prion protein is required for efficient repression [72].
GW-proteins were also implicated in pathogen defense against the host RNAi machinery in plants. Two independent studies provide evidence that viruses use own proteins containing Ago-hooks to hijack the host Ago silencing system and are essential for viral suppressor of RNA silencing (VSR) function [2][74].
Overall, those reports indicate that GW repeats function in numerous proteins of divergent species as evolutionary conserved Ago binding platforms.

1.4.3 GW-repeat Binding Mode

GW-proteins are known to serve as universal Ago binding platforms. In posttranscriptional mRNA regulation, short linear interaction motifs (SLiMs), like the GW-repeats, are common sequence features in a variety of pathways [42][18][208][67]. SLiMs have a length of about 6-11 aa and are typically found in disordered protein regions. To characterize the binding mode of GW182 GW-repeats it might help to examine the results obtained for related SLiMs besides investigation of GW182-Ago interaction data.
Several studies gave evidence that Trp and its neighbor Gly are crucial for efficient interaction of GW-repeats and Ago [203][45][4][201]. Moreover, investigation of NRPE1 and TNRC6A GW-repeats showed little sequence conservation except for the GW-repeats, however, the aa composition was biased with a high content of Gly, serine (Ser), Trp

medium content of Glu, Asp, asparagine (Asn) and to a little extent cystein (Cys), phenylalanine (Phe), His, methionine (Met) and tyrosine (Tyr) [45]. Due to the low conservation score and variability of GW-repeats in number and length, it is very difficult to predict GW-repeat containing proteins. Using an bioinformatical approach, Karlowski et al. developed a tool to detect GW-motifs in proteins [234]. They find that the aa embedding the Trp are mainly of small, hydrophilic and charged nature and suggest that this might facilitate surface accessibility of the Trp [103].
The Ago2 crystal structure by Schirle et al. provided hints on the binding mode of GW182 to Ago. The authors found two adjacent Trp binding pockets on the surface of the PIWI domain and concluded that GW182 bind to those sites by a tandem Trp motif [188].
However, the binding mode of GW-repeats remains unclear and might also be distinct for different proteins. Thus, it is difficult to exactly predict whether and how strong a protein interacts with Ago.
There are not only GW-motifs but also well known Trp motifs comprising other neighbors than Gly, thereby exerting a completely distinct function. Thus, it is important to discriminate between GW-motifs and related Trp motifs [195][28][57]. On the other hand, there are motifs comprising other aromatic residues instead of Trp, which are also embedded in low complexity regions [65][104].
Together, SLiMs and in particular Trp-containing motifs were shown to interact with an increasing number of proteins involved in multiple processes. Defining the context of the Trp required for efficient binding will help to shed light on this complex protein network.

1.5 Subcellular Localization

Ago proteins are specifically distributed in the cell [128][145][182]. 15-20% of the Ago protein was observed to localize to the nucleus whereas the remainder resides in the cytoplasm [160]. From the cytoplasmic pool, a minor part accumulates in processing bodies (P-bodies) [124].
P-bodies are dynamic cytoplasmic mRNP aggregates that harbor translationally inactive mRNAs [9]. They assemble around components that function in posttranscriptional decay, processing and transport of mRNA, e.g. they are enriched in GW182 which is the reason why P-bodies are also named GW-bodies. In the following, P-bodies or GW-bodies will be termed P/GW-bodies. P/GW-bodies can be detected microscopically and are clearly distinguished from other foci as stress granules by their specific protein markers [194][50][166]. P/GW-body formation requires mRNAs, however, their repres-

sion and storage is a reversible process [9]. Visible P/GW-body formation is disrupted by depletion of components of the mRNA pathway, as Drosha, Dicer, Ago or GW182 [223][131][50]. This suggest a close connection between P/GW-bodies and the miRNA pathway. However, only 1.3% of the cytoplasmic Ago pool resides in P/GW bodies [124] and mRNA repression also occurs in absence of P/GW-bodies. This leads to the conclusion that P/GW bodies are rather a consequence than a cause of sRNA-mediated gene silencing [50].
Recent studies implicated a congregation of Ago and GW182 in endosomes and MVBs [73] thus, linking miRNA-mediated gene silencing to endosomal trafficking [123]. Supporting this, miRNAs have been found in exosomes [210]. However, the relation between P/GW-bodies and MVB are not clear yet and further research is required to examine the exact roles of distinct foci in the cell.
Supporting the nuclear function of Ago proteins, Ago-dependent RNAi effects were observed in the nucleus in mammalian cells during the last years [177][99][100][9][110][100]. Moreover, Importin 8 was suggested as transport factor, targeting Ago proteins to the nucleus [218].
Ago is not the only miRISC component that plays a role in the nucleus besides its cytoplasmic function. Till et al. found that human TNRC6B actively shuttles to the nucleus [203]. By immunohistochemical analysis, TNRC6A was also observed in the nucleus [229] and recently, it was even revealed that TNRC6A acts as a navigator for nuclear import of Ago [155].

1.6 Post Translational Modifications

Besides the nature of the sRNA, the cellular localization and the miRNP composition, post translational modifications (PTMs) are a factor further regulating the miRNP activity. GW182 was shown to be phosphorylated *in vivo* [55], however, further research is needed to elucidate the functional implications of GW182 PTMs.
Ago proteins comprise hydroxylation at proline P700, which is thought to support Ago stability [173]. Ubiquitination plays a role to mark Ago for proteasomal degradation [183]. Phosphorylation was first described by Zeng et al. who showed that phosphorylation of Ser S387 facilitates Ago2 localization to P-bodies [232]. Previously, it was reported that phospohorylation of Ago2 Tyr Y529, which lies in the center of the MID domain, affects sRNA binding [182].

1.7 Mechanisms of Small RNA Functions

Based on their mode of action, subcellular localization and the nature of the sRNA molecule, silencing pathways induced by sRNAs can be classified into different groups. The major pathways are discussed in the following sections.

1.7.1 Posttranscriptional Silencing by SiRNA-mediated mRNA Cleavage

In RISC-mediated cleavage, a guide siRNA recruits Ago to a perfectly complementary mRNA which is then cleaved. In humans, only Ago2 exerts slicing activity [130][145]. The minimal human RISC contains Ago2 bound to a ss siRNA [176]. Ago2 catalyses hydrolysis of the phosphate backbone between the corresponding nucleotides 11 and 12 of the guide strand [46] and release of a 5' phosphate and a 3' hydroxy terminus [191][142]. The cleaved target dissociates and is further degraded by the cellular decay machinery [164][193].

1.7.2 MicroRNA-mediated Gene Regulation

MicroRNA-mediated Translational Repression and Decay

Recruiting the miRISC to specific mRNAs, miRNAs exert their function either on the level of translational repression or mRNA destabilization.
Previous reports discussed several steps at which translation can be inhibited, which is either initiation, elongation or termination [25]. Evidence that repression of translation is exerted at the initiation step came from studies showing that miRNA-repressed target mRNAs shift to lighter fractions in polysome gradients [9][171] and it was suggested that miRNA pathway components prevent the eIF4E interaction to the 5' cap [91]. Indications that repression occurs at the elongation step were provided by studies that detected miRNA-repressed mRNAs in actively transcribing polysome fractions [141][163]. Finally, some reports proposed that translation is inhibited by premature termination [169].
In the last years, it emerged that GW182 plays a key role in miRNA-mediated silencing. GW182 was initially suggested to inhibit translational initiation by binding to PABP and thus preventing PABP-eIF4G interaction and mRNA circularization [231][58]. It was further indicated that the GW182-PABC interaction enhances deadenylation by placing the poly(A) tail in close proximity to deadenylase complexes [58]. However, the exact relevance of the GW182-PABP interaction is controversial and it is indicated that PABP might additionally play a role independent of GW182 suggesting a more active role for PABP in gene silencing [68][94].

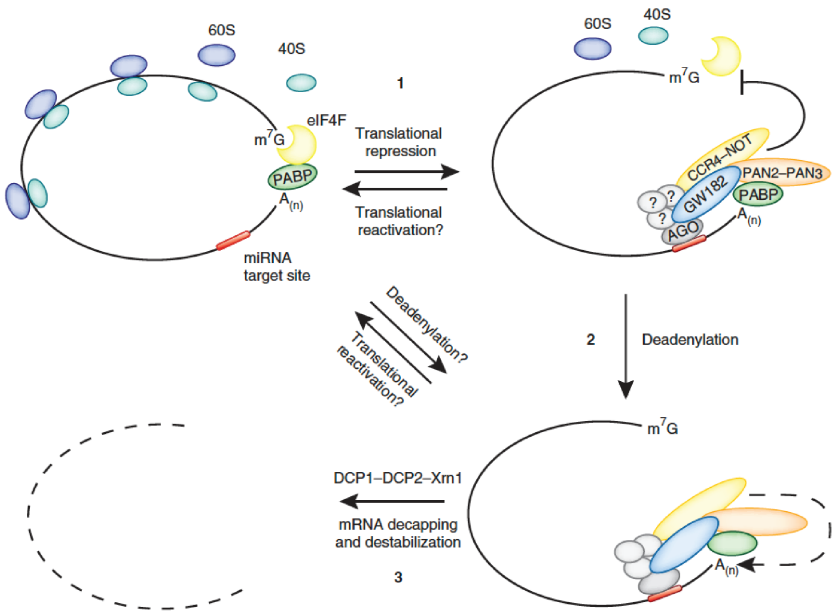

Figure 1.7.1: MiRNA-mediated translational repression and decay. One model proposes that translational initiation is inhibited by interference of the miRISC with the eIF4F-cap interaction. Association of GW182 with PABP might prevent mRNA circularization leading to repression of translational initiation. CCR4Not and PAN2/Pan3 mediate mRNA deadenylation, followed my cap removal through the DCP1/DCP2 complex and final decay by XRN1 (adopted from [59]).

Recent studies revealed that mRNA degradation is a widespread effect of miRNA-mediated repression [93]. MiRNA-mediated mRNA destabilization by decay mechanisms involve the CCR4-Not and PAN2/PAN3 deadenylase complexes [28][57][17][37][17][57]. GW182 is not only a platform for deadenylases to gain access to the poly(A) tail but also triggers DCP1/DCP2 mediated decapping and final mRNA decay by XRN1 [8].
Besides involvement of PABP and deadenylase complexes, EDD was implicated to be essential for efficient miRNA-mediated repression in mouse embryonic stem cells through direct interaction with GW182 [198]. Since EDD directly interacts with the decapping activator RCK/p54 it was suggested to assist GW182 as additional module to recruit miRNA effector proteins for translational repression [198][36][33].
As described above, miRNAs have a major impact on mRNA destabilization. However, the relative contributions and exact sequential arrangements of the different effects have not been elucidated [79]. Several studies revealed that miRNAs can repress their targets in a two step mode. First, mRNA translation is inhibited followed by subsequent deadenylation, decapping and decay [59].
Posttranscriptional gene regulation is guided by miRNAs or RNA-binding proteins (RBPs) through association with target sites in the 3' UTR. TRIM-NHL proteins have been iden-

tified as modulators of miRNA-mediated repression in mammals, flies and worms. The interaction with Ago or other miRNA components can either result in enhanced or alleviated repression [82][189] [183][154][135]. The dead end homolog 1 protein (DND1) prevents miRNA binding by association with the miRNA target site [107]. Similarly, the Hu-antigen R protein (HuR) or the pumillo homology domain family member (PUF) proteins target mRNAs to exert their regulatory functions [26][111][9]o[108][157].
Together, these studies show that a thorough knowledge of the interplay between the miRNA machinery and RBPs is necessary to understand the mechanisms of miRNA-mediated gene silencing.

MicroRNA-mediated Translational Activation

MiRNAs have been found to generally mediate posttranscriptional down regulation of gene expression. However, more and more studies reveal that miRNAs can function as translational activators depending on the RNA sequence, associated RNP factors or cellular conditions [98]. In human cells, miRNAs were observed to oscillate between repression and activation dependent on the stage of the cell cycle. Here, miR-369-3 directs the association of Ago2 and FXR1, an RNA binding protein linked to the fragile X syndrome, with the AU-rich element in the 3' UTR of TNFα to stimulate translation. Furthermore, they report that let-7 enhances translation during cell cycle arrest and represses translation in proliferating cells [212]. Another study observed that miRNA-10a interacts with the 5' UTR of mRNAs encoding ribosomal proteins to stimulate their translation during aa starvation [165]. Furthermore it was reported that the liver-specific miRNA-122 enhances Hepatitis C virus (HCV) translation by targeting sites in the 5' UTR of the HCV genome [87]. These finding highlight the complexity of miRNA-mediated gene regulation, in which the relevance of translational activation has to be clarified.

1.8 Aim of the Thesis

Ago proteins are embedded into miRNPs and constitute the central components of miRNA-mediated gene silencing. They associate with GW182 proteins which have been found to serve as a platform to recruit effector proteins triggering translational silencing or mRNA decay.

To date, much progress has been made to reveal the functional relevance of the Ago-GW182 interaction. However, there are many open questions especially about the underlying binding mechanisms of both proteins:

Why does the GW182 sequence comprise numerous GW repeats? Do all GW-repeats engage in Ago interaction? Is only one Ago protein involved or do several molecules associate with GW182 in parallel? Is there a defined sequence motif with which GW182 binds to Ago? Why do some GW-repeats interact with Ago with high affinity whereas others do not? Ago and Not1 both bind GW-repeats, are these repeats distinct motifs and how is the specificity mediated? Where and how does GW182 bind Ago and does GW182 associate with all four Ago proteins equally?

The aim of this thesis was to elucidate the molecular basis of Ago-GW182 interaction addressing the above mentioned questions.

For this purpose, recombinant proteins first needed to be obtained to perform *in vitro* studies. Therefore, a suitable expression and purification protocol had to be established. Second, the recombinant proteins should be used in biochemical and biophysical approaches to map the binding sites and clarify the binding properties of Ago and GW182. Finally, the data should be used to create a structural model displaying the Ago-GW182 interaction.

2 Results

2.1 Definition of Working Constructs

In miRNA-mediated silencing, Ago proteins associate with a member of the GW182 protein family (in human TNRC6A, B, and C) in order to achieve efficient repression. To extend our knowledge on the function of both proteins we aimed to better understand the mechanism beyond their interaction. To perform *in vitro* studies, we established a purification strategy to obtain members of both protein families in high purity.

2.1.1 TNRC6 Family Proteins

To get an overview of structural elements in TNRC6 proteins, a secondary structure prediction using Quick2D [10] was performed for TNRC6B (see appendix). Except for known domains (UBA 997-1055, Q-rich 1036-1218 and RRM 1535-1619) the protein is predicted to offer very little structural content.
In a first attempt, full length proteins of TNRC6A, B and C were purified from insect cells. All proteins were well expressed, soluble and could be enriched using a Nickel-affinity column via their 6x His-tag (Figure 2.1.1). Nevertheless, the protein was not stable upon further purification e.g. by ion exchange or size exclusion chromatography (SEC). Similarly, shorter TNRC6B constructs covering the N-terminus (aa 1-1007) expressed in *Escherchia coli* (*E. coli*) or the carboxy C -terminus (917-1723) expressed in insect cells did not yield stable protein (Figure 2.1.1). Alignment of TNRC6 family proteins using MAFFT [105] (see appendix) identified two conserved regions (aa 599-683 and aa 861-911) in the N-terminal part of TNRC6B covering sites that were reported to bind Ago in literature [54]. Both fragments were expressed in *E. coli* with an N-terminal His-GST-tag and were purified to high homogeneity using affinity chromatography. For some experiments, the His-GST-TNRC6B 599-683 preparation was further purified by tag cleavage and SEC.
GST-tagged RRM domains of TNRC6A, B and C (Figure 2.1.1) as well as TNRC6A, B, C full length, TNRC6B 599-683 and TNRC6B 861-911 were used to generate antibodies against TNRC6A, B and C respectively, in collaboration with Dr. Elisabeth Kremmer.

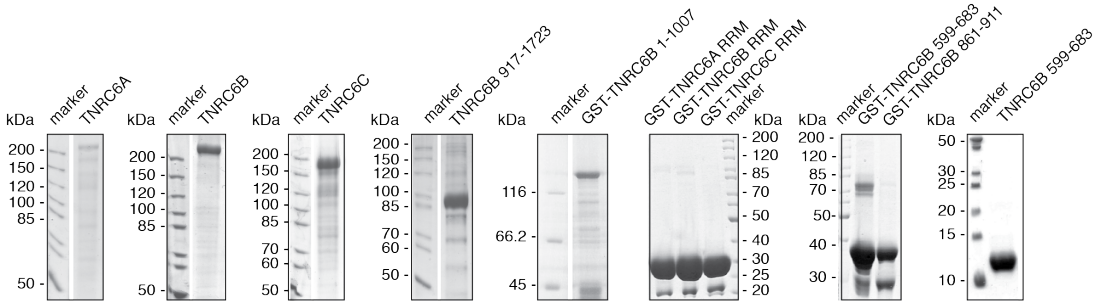

Figure 2.1.1: Purification of TNRC6 constructs. Proteins were purified as visualized by coomassie stainingg after sodium dodecyl sulfate polyacrylamid gel electrophoresis (SDS-PAGE). TNRC6A, B, C as well as TNRC6B constructs 1-999 and 917-1723 were prone to degradation, whereas the RRM domains of TNRC6A, B, C and TNRC6B constructs 599-683 and 861-911 were stable.

Figure 2.1.2 gives an overview of constructs used and the success of expression, solubility and purification.

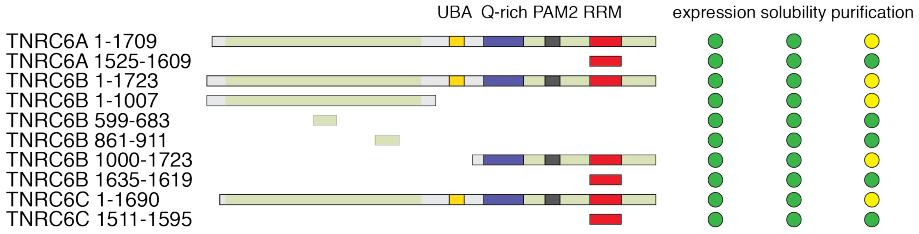

Figure 2.1.2: Schematic of TNRC6 constructs. Schematic representation of the TNRC6 domain organization and constructs used for purification attempts. Domains are color coded as follows: green: GW-rich region, yellow: UBA domain, purple: Q-rich-region, dark gray: PAM2 motif, red: RRM domain, linker region: gray. The success of expression, solubility and purification is indicated on the right in green (good), yellow (medium) and red (failed) dots.

2.1.2 Argonaute Family Proteins

On the basis of secondary structure prediction carried out using Quick2D (see appendix), several Ago2 constructs for expression in *E. coli* were designed.
All Ago2 fragments are listed in Figure 2.1.3. Expression was tested in several *E. coli* strains using different solubility tags (His, His-GST, His-Sumo, His-Trx), lysis conditions as well as co-expressing the interaction partner TNRC6B 599-681. Except for the full length protein, all protein fragments were highly expressed. However, besides Ago2 449-575 none of them yielded soluble protein.

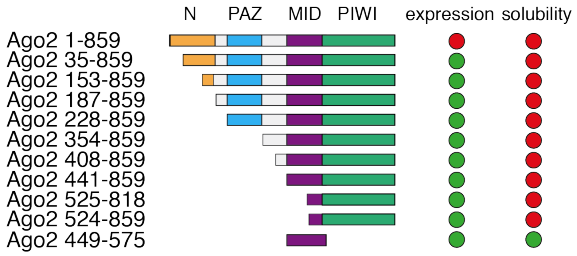

Figure 2.1.3: Schematic of Ago2 constructs. Schematic representation of the Ago2 domain organization and constructs used for purification attempts. Domains are color coded as follows: N-terminal domain: orange, PAZ: blue, MID: purple, PIWI: green, linker region: gray. The success of expression and solubility is indicated on the right in green (good), yellow (medium) and red (failed) dots.

Therefore, Ago2 449-575, expressing the Ago2 MID domain, was tested for TNRC6B 599-681 interaction in a pulldown assay (Figure 2.1.4). Recombinant Ago2 449-575 was mixed with GST-tagged TNRC6B 599-683 (lanes 2 and 3) and precipitated by glutathione (GSH) beads. After washing, bound protein was eluted with GSH (lanes 5 and 6) and visualized by SDS-PAGE followed by coomassie staining. However, the Ago2 fragment was not sufficient to mediate the interaction.
In another attempt, the Ago protein from the archaeal species *pyrococcus furiosus* (*pf*) was purified recombinantly and tested for interaction (Figure 2.1.3) as described for the MID domain fragment. Here, even the pfAgo full length protein was not able to pull down TNRC6B 599-683 (lanes 4 and 5).

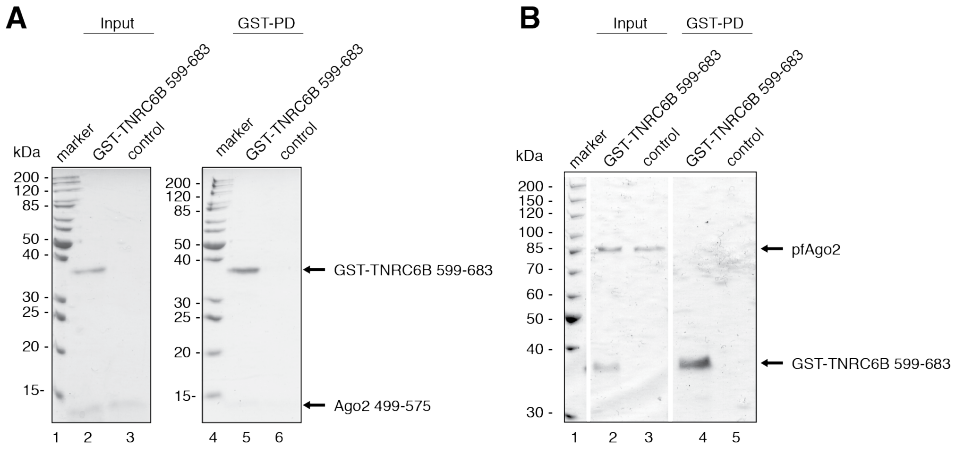

Figure 2.1.4: The Ago2 MID domain and pfAgo full length protein are not sufficient to bind TNRC6B 599-683. A) Ago2 499-575 and B) pfAgo can not be precipitated by TNRC6B 599-683 in a pull-down experiment (lanes 5, 6 and 4, 5 respectively).

Since *E. coli* expression did not reveal an Ago construct that exhibited expression/ solubility and TNRC6B binding capacity, we changed the expression system and established the purification of human Ago full length proteins from insect cells according to the Bac-to-Bac manual (Invitrogen). Ago1-4 were expressed and isolated by a three-step purification, including Nickel-affinity chromatography, tag cleavage followed by a second Nickel-affinity step and finally SEC. Due to a very low expression yield, only about 0.3 mg of pure protein were obtained from 1l culture of High Five insect cells (Figure 2.1.5 A).

We used recombinant full length Ago2 protein for analytical limited proteolysis (Figure 2.1.5 B) to find smaller interaction domains, that, after identification of their boundaries, could then be used for expression in *E. coli*. Samples were subjected to proteases of different concentrations, incubated and separated by SDS-PAGE followed by coomassie staining.

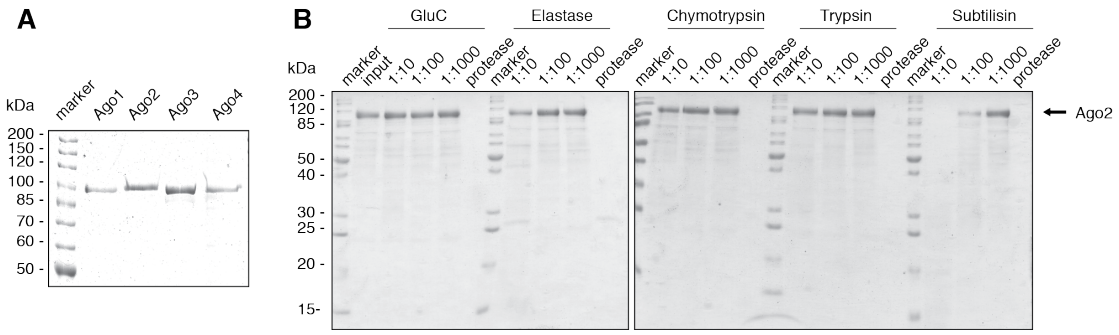

Figure 2.1.5: Purification and limited proteolysis of Ago. A) SDS-PAGE showing that Ago1-4 was purified to homogeneity. B) Ago2 was incubated with different concentration of several proteases and the digestion products were resolved by SDS-PAGE.

However, Ago2 was highly stable in presence several proteases. Only after addition of the protease subtilisin it was susceptible to degradation, even though no stable subfragments could be observed.

Taken together, we find that handling of TNRC6 full length protein or longer constructs beyond purification by affinity chromatography is impractical, whereas domains (RRM) or smaller constructs are highly stable. Strikingly, all four human Ago proteins are available in high purity. For the following experiments, we chose the full length protein of Ago2 to study the interaction with TNRC6B.

2.2 Identification of Argonaute 2 Interaction Motifs on TNRC6B

It emerged from the literature that different GW-containing regions of TNRC6B are capable of Ago binding. However, a clear picture about the number of binding sites in the TNRC6B sequence and their affinities to Ago2 did not arise. Here, we comprehensively investigated the Ago2 TNRC6B interaction sites using a peptide array. The selected N-terminal half of TNRC6B containing the GW-motifs required for Ago binding is (except for the RRM) predicted to be unstructured. This is a good prerequisite for a successful *in vitro* peptide scanning experiment in which short unstructured peptides are used. Recombinant human Ago2 was isolated from insect cells and purified to high homogeneity as described above (Figure 2.2.1 A). Figure 2.2.1 B schematically illustrates the setup of the peptide array. 20-meric peptides overlapping in 15 aa and covering almost the complete TNRC6B sequence were synthesized and spotted onto a nitrocellulose membrane (Figure 2.2.1 C). The membrane was incubated with recombinant Ago2 and binding was indirectly revealed by western blotting using a specific primary (anti-Ago2 11A9) [181] and secondary (HRP- conjugated anti-rat IgG) antibody.

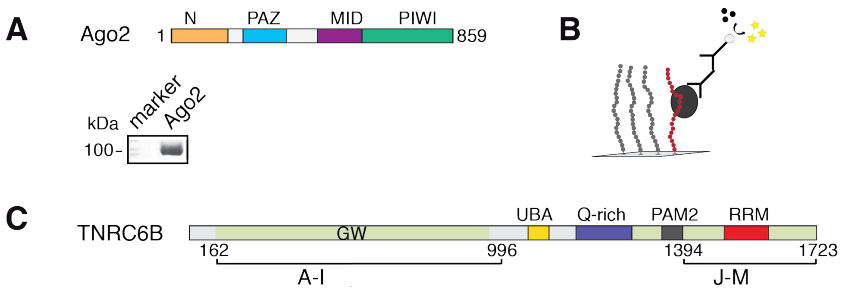

Figure 2.2.1: Experimental setup of peptide array. A) Domain organization of Ago2 and preparation of recombinant Ago2 used in the experiment. Domains are color coded as follows: N-terminal domain: orange, PAZ: blue, MID: purple, PIWI: green, linker region: gray. B) Schematic illustration of the peptide array setup used to identify Ago2 interaction sites on TNRC6B. C) Domain organization of TNRC6B. Domains are color coded as follows: green: GW-rich region, yellow: UBA domain, purple: Q-rich-region, dark gray: PAM2 motif, red: RRM domain, linker region: gray. The regions that were covered by peptides are indicated as A-I and J-M.

The membrane incubated with Ago2 shows distinct regions within the TNRC6B N-terminal as well as the C-terminal fragment that are capable of Ago2 binding (Figure 2.2.2 A and B). Intensities of peptides A-I that offered binding were quantified using the software ImageJ and normalized to peptide E11, that was binding the strongest (Figure 2.2.2 C).

We find three hotspots that strongly interact with Ago2 (Figure 2.2.3 black circles), as well as several sites with medium (grey circles), weaker (light grey circles) and faint (white circles, not included in quantification) binding. Of note, all peptides that bind Ago2 share the presence of at least one Trp in the sequence. Surprisingly, not all peptides that bind with high affinity to Ago2 require a Gly flanking the Trp, as seen for peptide D3 containing an SWD and SWN motif.
In the control experiment, in which Ago2 has been omitted from the reaction, primary and secondary antibodies used for immuno-detection of bound Ago2 showed almost no unspecific binding besides the spots L9-12 and M3 (Figure 2.2.2 B).

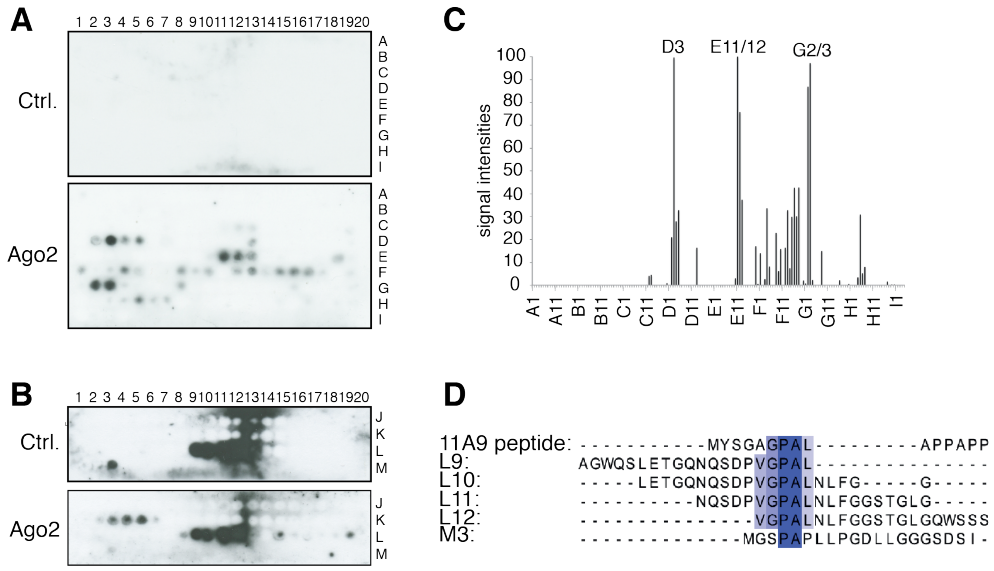

Figure 2.2.2: Peptide array identifies distinct Ago2 binding sites on TNRC6B. Several TNRC6B peptides allow Ago2 binding. 20-meric TNRC6B peptides of A) regions A-I and B) regions J-M with an offset of 5 aa were covalently coupled to a nitrocellulose membrane, incubated with recombinant Ago2 followed by specific Ago2 detection with the 11A9 antibody [181]. Upper panel: Control experiment carried out lacking Ago2 incubation step. Lower panel: Incubation with Ago2 before monitoring TNRC6B binding. C) Signals in the peptide array A) were quantified using the ImageJ software (http://rsb.info.nih.gov/ij/), showing different levels of affinity. D) Alignment of the peptide used for 11A9 antibody generation and peptides of TNRC6B sequence unspecifically binding the 11A9 antibody in the control experiment displays a consensus sequence highlighted in blue.

Interestingly, alignment of those peptides with the peptide used for generation of the anti-Ago2 antibody 11A9 [181] reveals a conserved sequence motif consisting of the aa sequence (A/V)GPAL within peptides 11A9 and L9-12 (Figure 2.2.2 D). M3 only partially covers the complete sequence explaining the weaker binding. From the 15-meric peptide this short 5 aa stretch is most likely the epitope necessary and sufficient to be recognized by the 11A9 antibody.

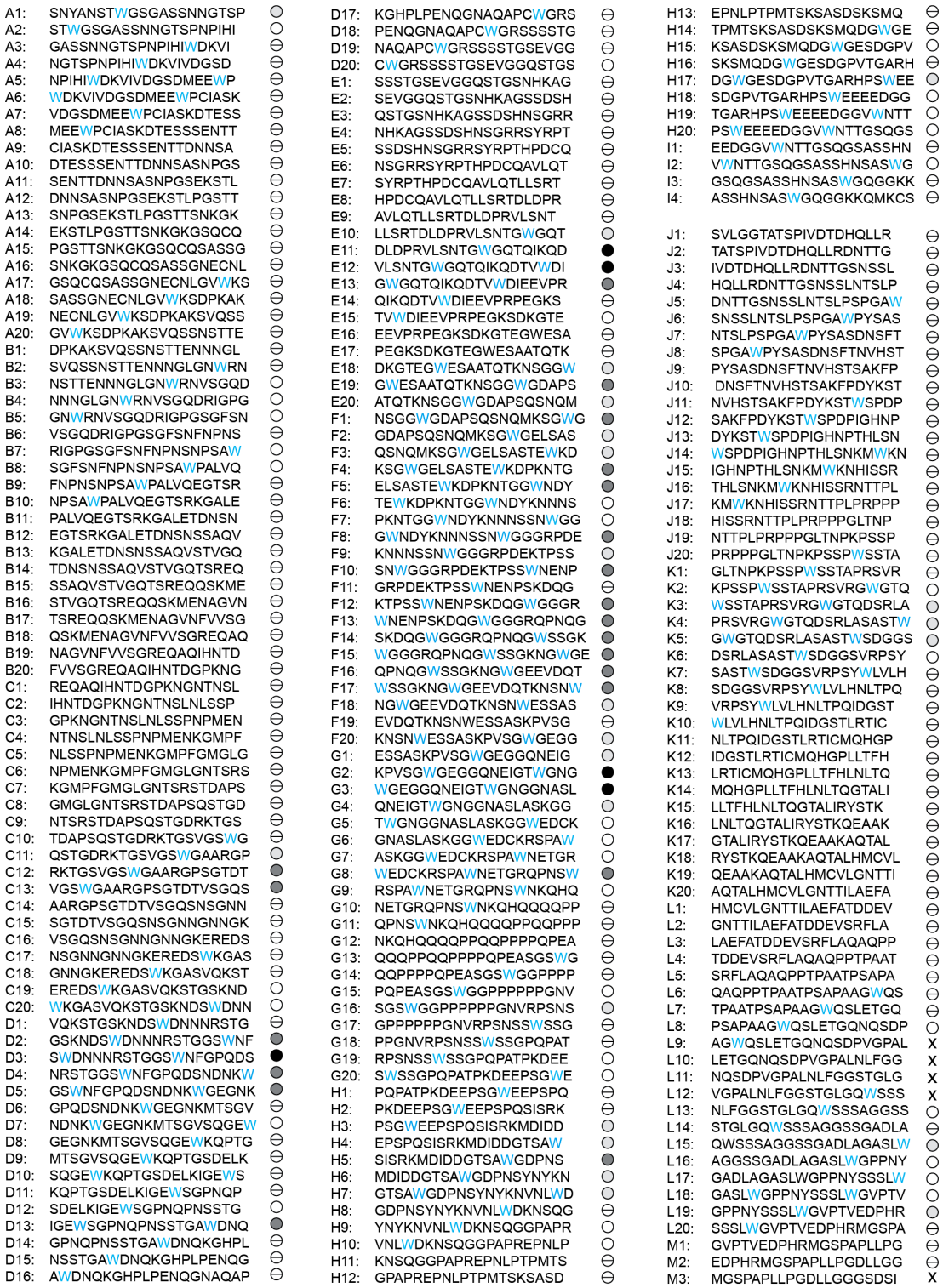

Figure 2.2.3: List of TNRC6B peptides spotted on the membrane with their Ago2 affinity indicated. Set of TNRC6B peptides used in the peptide array. The Ago2 binding strength is illustrated by black (strong binding), grey (medium binding), light grey (weaker binding), white (faint binding) and dashed white (no binding) dots. Trps are highlighted in blue.

In conclusion, we find sites in the N-terminal region of TNRC6B that specifically interact with Ago2. Interestingly, not all Trps engage in Ago binding and Gly flanking the Trp appear not to be a requirement for efficient binding.

2.3 Analysis of Tryptophan Flanking Amino Acids

Our peptide scan revealed that not all peptides containing Trps which might be suitable for Ago2 binding, interact with Ago2. Therefore, we performed a second peptide array to further elucidate Ago2 binding requirements (Figure 2.3.1).
For this, we set up a mutational screen based on peptide E11, that had one of the strongest interactions with Ago2. Several peptides were designed and analyzed by peptide array probing using Ago2 and immuno-detection with 11A9 antibody (Figure 2.3.1). To exclude artifacts of the signal strength e.g. by unequal washing or antibody binding, several wild type (wt) peptides were spread over the membrane to ensure comparable results (Figure 2.3.1 A: A1; D: C16, D5; E: E14; F: F5)

Alanine Scan of Peptide E11

To test the requirements for aa flanking the Trp, we first performed an alanine (Ala) scan by substituting each aa of the peptide sequence flanking the Trp to the left with Ala (Figure 2.3.1 A: A2-A12). Here, no influence on Ago2 binding was observed, whereas introducing an Ala at the position of the Trp (A13) completely abolished binding. Substitution of aa flanking the Trp to the right (A14-B1) did not have a significant impact on Ago2 binding in comparison to wt (C16). This suggests, that a single aa does not have an impact on Ago2 binding, however, the presence of a Trp is strictly required.

Multiple Alanine Substitutions in Peptide E11

The Ala scan showed that substitution of a single aa does not influence binding to Ago2. Next, we aimed to find out if substitution of multiple aa shows an effect. Thus, we systematically replaced all aa N-terminal to the Trp by Ala (Figure 2.3.1 B: B2-B11). This did not lower binding, whereas substitution of C-terminal aa decreased the affinity (B12-B17).
Replacing the entire peptide except for the central Trp or Gly/Trp/Gly by Ala (B18-C1) had an even stronger effect. Here, binding was reduced indicating that the composition of the Trp flanking aa is indeed important for efficient binding. Similar to A13, insertion of Ala at the positions of the central Gly/Trp/Gly tripeptid completely abolished binding,

whereas substitution of only the Trp flanking Glys by Ala did not affect binding (C2, C3). This confirms the key role of the Trp.

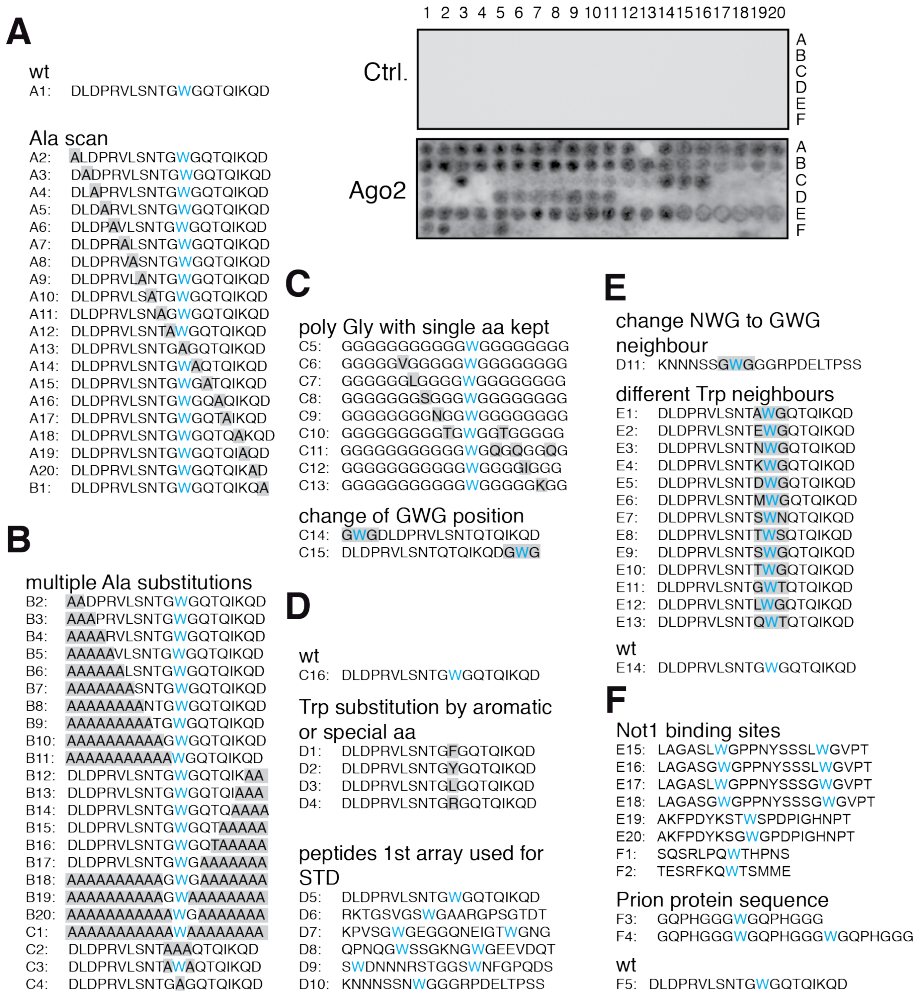

Figure 2.3.1: Peptide array for mutational analysis of peptide E11. Peptide array showing different effects of aa substitutions in peptide E11 (Figure 2.2.3). Upper panel: Control experiment carried out lacking Ago2 incubation step. Lower panel: Incubation with Ago2 before monitoring TNRC6B binding. List of designed peptides with the type of mutation indicated above and highlighted in gray. Trps are highlighted in blue. A) Ala scan of peptide E11. B) Multiple Ala substitutions in peptide E11. C) Role of single aa and Trp position. D) Role of single aa and Trp position. E) Impact of aa neighboring the Trp. F) Ago2 binding efficiency of Not1 binding sites and the prion protein.

Role of Single Amino Acids and the Tryptophan Position

Substitution of multiple aa indicated that the overall aa composition indeed plays a role in Ago2 binding. We thus chose a polyGly peptide and tested whether the insertion

of single aa occurring at its position in peptide E11 might contribute to binding and enhances the affinity to Ago2 (Figure 2.3.1 C: C5-13).
Similar to the polyAla peptide (C1), a polyGly peptide containing one Trp showed reduced affinity (C5). Based on that, we inserted valine (Val) (C6), leucine (Leu) (C7), Ser (C8), Asn (C9), threonine (Thr) (C10), glutamine (Gln) (C11), isoleucine (Ile) (C12) and lysine (Lys) (C13), however, none of them increased the affinity, suggesting that single aa do not determine the binding properties.
Unexpectedly, changing the position of the GWG tripeptide to the very N- and C-term (Figure 2.3.1 C: C14-15), respectively, did not lower the affinity compared to the wt (C16), leading to the conclusion that also the position of the key Trps within the peptide is not a crucial factor.

Tryptophan Requirements

Having proven that the Trp is a key requirement for efficient binding in the peptide sequence, we next characterized its role by replacing it with aa featuring related characteristics of Trp (Figure 2.3.1 D: D1-D4).
To test whether the aromatic ring is necessary for binding, we replaced the Trp by the aromatic residues Phe and Tyr, respectively (D1-2). Faint binding was found for the the Phe peptide, whereas the Tyr peptide completely lost its affinity. This is consistent with a previous report [188] where the authors found phenol from the crystallization condition bound to the protein.
Peptide D3 and D4 were used to check whether the hydrophobic (Leu) or bulky (arginine (Arg)) property of the Trp are sufficient to facilitate binding. This is not the case, since the interaction was completely lost.
In Figure 2.3.1 D: D5-D10, peptides from the first peptide array (Figure 2.2.2), that were later used for further experiments, were again spotted.

Impact of Amino Acids Neighboring the Tryptophan

Finally, we screened for possible neighboring aa of the Trp. Changing a Asn/Trp/Gly tripeptide (D10) to a Gly/Trp/Gly tripeptide (D11) does not have an effect. Next, we replaced the directly flanking aa by a set of aa that is also abundant in the TNRC6B sequence (Figure 2.3.1 E: D11-E13). Here, for all variations the interaction remained at wt level, suggesting that a Gly/Trp Trp/Gly dipeptid is preferred but not an absolute requirement for efficient binding.

Argonaute 2 Binding Efficiency of Not1 Binding Sites and the Prion Protein

Recent publications revealed binding sites for Not1 on GW182 [57][28]. The corresponding TNRC6B peptides (Figure 2.3.1 F: E15, E19, F1, F2) and mutations (E16, E17, E18, E20) were tested in a peptide array for Ago2 binding in comparison to peptide E11 (F5). For peptides E15-E20 the so-called "ring spot effect" was noticed, caused by too tight peptide density. Consequently, the binding can only be assessed qualitatively. In comparison to peptide E11 (F5), peptide F1 shows diminished binding, whereas binding of peptide F2 to Ago2 seems to be equivalent to E11.
Recently, it was published that the Gly/Trp/Gly containing prion protein is able to bind Ago, thereby promoting accumulation of miRNA effector complexes [72]. Thus, a peptide stretch derived from the prion protein sequence containing one or two Gly/Trp/Gly, respectively, was compared with peptide E11 (Figure 2.3.1 F: F3, F4), which had the strongest affinity in the first peptide array. Notably, only very faint binding was observed. The additional Gly/Trp/Gly (F4) enhanced the affinity to Ago2. Thus, Not1 and the prion protein can bind Ago2, however, with weaker affinity than peptide E11 derived from the TNRCB sequence.

In summary, we found that a single aa within the TNRC6B peptide does not have influence on Ago2 binding. Rather the overall aa composition seems to be the determining factor with the aromatic ring of Trp mainly engaged in binding .

2.4 Tryptophan - Argonaute 2 Contacts on an Atomic Level

Based on the findings we gained from the peptide arrays, which showed that one Trp was sufficient for binding, we further investigated the binding of TNRC6B to Ago2 in molecular detail. We analyzed the interaction on an atomic scale using saturation transfer difference (STD)-NMR. STD-NMR allows to measure transient binding of small ligands to larger protein receptors and detection of the ligand parts involved in binding.
One advantage of this technique is that only small quantities of unlabeled protein are needed. This method is ideal for studying large proteins, that are difficult to express and are therefore not available in larger quantities.
The principle underlying this approach is illustrated in Figure 2.4.1 A. Protons of a large receptor protein (Ago2) are selectively saturated for a defined period of time (saturation time) by irradiation of spectral regions containing "wings" of broad resonances (in this experiment -1 ppm). Those "wings" are, due to the structured nature of proteins, specific for macromolecules and do not occur in small ligands like peptides. Rapid intramolec-

ular propagation of the saturation by spin diffusion results in transfer of saturation to the bound ligand (here the TNRC6B peptide) if protons are in close proximity (< 5 Å) to Ago2 protons.
This saturation leads to bleaching of the corresponding signals in the NMR spectrum. Finally, a comparison of a saturated and unsaturated NMR spectrum allows the identification of the binding area after assignment of protons in the peptide sequence.
Six peptides with different affinities were chosen from the peptide array for STD-NMR measurements (Figure 2.2.3 C12, D3, E11, F9, F16, G). STD-NMR spectra were recorded as exemplarily represented for peptide E11. Figure 2.4.1 B shows a section of a typical one dimensional (1D) -proton (^{1}H) -NMR spectrum. Chemical shifts of protons are plotted on the x-axis. For proteins, they are typically in the range of 0-10 ppm and rely on the molecular structure, solvent, temperature, neighboring groups and the magnetic field in which the spectrum was recorded. Using statistics (www.bmrb.wisc.edu), the chemical shift of each proton in an aa can be assigned to a certain region in the NMR spectrum. The y-axis displays the relative intensity of each signal.

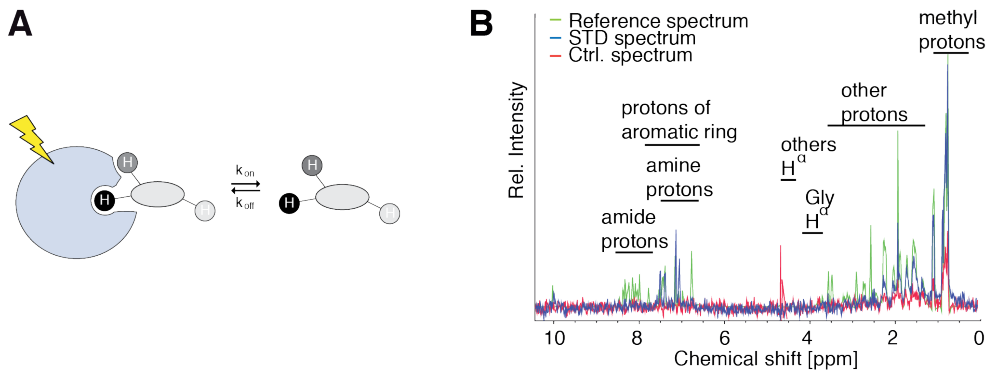

Figure 2.4.1: Schematic illustration of STD-NMR experiment applied to the protein receptor (Ago2) and ligand (peptide) complex. A) Selective saturation of receptor signals is transferred to the peptide protons by spin diffusion. The stronger the receptor ligand contact between two protons, the stronger is the STD effect. B) The set-up involves recording three 1D-^{1}H-NMR spectra. A standard 1D-^{1}H-NMR spectrum as a reference (green), a difference spectrum of the reference spectrum and a 1D-^{1}H-NMR spectrum with selective saturation of the receptor named STD-spectrum (blue) and a difference spectrum without addition of Ago2 as control (red). The difference spectrum only shows signals corresponding to bound ligand protons. Indicated are chemical shift regions corresponding to the respective protons.

First, a 1D-^{1}H-NMR reference spectrum of the TNRC6B peptide was recorded (green). As described above, each peak corresponds to a proton of an aa in the peptide. Protons of amides can be observed at around 8 ppm, protons of aromatic rings as well as amine protons at around 6.5-7.5 ppm, $H\alpha$ proton appear in a range of 3-4.5 ppm, whereas the

region between 0-1 ppm is typical for methyl protons.
In the following, the difference between the reference and the saturated spectrum will be called STD-spectrum. In this spectrum (blue), only protons of the E11 peptide bound to Ago2 are visible as clarified above. Comparison of this spectrum with the reference spectrum reveals that the STD-spectrum lacks some peaks e.g. in the areas from 8-9 ppm or 2-4 ppm. This loss of signals is due to protons that were not bleached by saturation transfer and thus, do not interact with Ago2.
The control spectrum (red) was recorded with the same conditions as the STD-spectrum without adding Ago2. Peaks appearing here, are due to unspecific irradiation of the ligand and are subtracted from the STD-spectrum (corrected STD-spectrum). Since Ago2 was specifically irradiated at -1 ppm, hydrophobic residues that contain methyl protons, which have a chemical shifts close to the irradiation frequency of about 0-1 ppm (see Figure 2.4.1 B), are most likely affected by unspecific irradiation in comparison to those of the indole ring (7-7.5 ppm).
Analysis of the spectrum shown in Figure 2.4.1 B leads to two observations: First, most likely the peaks appearing at 7-7.5 ppm are resulting from the Trp typically expected in this region. Second, there is no peak in the chemical shift range of Gly (3.8-4.2 ppm). This leads to the assumption that the Trp is strongly involved in binding whereas its directly neighboring aa Gly completely lacks binding. To better assess the absolute magnitude of the STD effect Mayer and Meyer [144] introduced the STD amplification factor described by the following equation:

$$\textit{STD amplification factor} = \frac{I_0 - I_{sat}}{I_0} * \textit{ligand excess}$$

In this equation, I_0 represents the reference spectrum and I_0-I_{sat} describes the intensity of the corrected STD spectrum, normalized with a concentration dependent factor (ligand excess) (Figure 2.4.1 B).
TNRC6B peptides that were proven to interact with Ago2 in the peptide array (Figure 2.2.2) were chosen for STD-NMR analysis. Prior to the actual STD-NMR measurements, backbone assignment of the aa in the TNRC6B peptide sequence was performed using two dimensional total correlation spectroscopy (2D-TOCSY) and natural abundance ^{13}C-heteronuclear single quantum coherence (HSQC) measurements. In 2D-NMR, two frequency axes, representing chemical shifts, are used to enhance resolution and thus, providing more information. In the TOCSY experiment, cross peaks of coupled protons are detected which give characteristic signal patterns for each aa, allowing to assign the peaks to aa in the peptide sequence. Assignment is further facilitated by

combining the information provided by 2D-TOCSY with ^{13}C-HSQC. Here, correlations between nuclei of two different types, in our case ^{1}H and the naturally abundant ^{13}C, that are separated by one bond are observed. The resulting patterns are characteristic for the proteins structural integrity as they depend on the chemical environment of each atom; therefore the HSQC spectrum can be considered as a fingerprint of the protein.
After assignment of signals to the corresponding aa, STD-NMR spectra were recorded as exemplarily described above. Integrals of the peaks with a width of 0.3 ppm were obtained and used for calculation of the STD amplification factor, as described above.
The diagrams in Figure 2.4.2 display the STD amplification factors. Plotting the STD amplification factor against the saturation time results in a curve reaching a plateau. This plateau is due to TNRC6B peptides dissociating from Ago2 and emitting their saturation before recording the NMR spectrum, if the period of saturation time is too long.
In each diagram, one aa is represented by the same color (e.g. blue for Trps). Each proton of the respective aa side chain is displayed as a symbol (e.g. triangle for a $H\zeta 2$ proton).
As expected, a plateau is reached after a certain saturation time, for most protons in the range of 4-8 s. For all tested peptides, protons of the Trp indole ring (blue) show the strongest binding.
Inspection of their STD amplification factors shows that similar intensities were obtained for peptide C12 and E11 (between 3-14) as well as for peptides F16 and G2 (between 1-8), whereas D3 reaches much higher values (up to 25) and F9 much lower values (0-1.5). The difference of binding affinity in the peptide array and the values of the STD amplification factors in comparison to the different peptides is reasonable since proximity and binding strength do not directly correlate with each other.
Peptides D3, G2 and F16 contain two Trps in the sequence that can both be designated in the spectrum. Figure 2.4.2 F shows two curves for the $H\delta 1$ as well as for the $H\eta 2$ proton originating from different Trps. Thus, both Trp bind Ago2, although from this data it cannot be clarified whether they bind at the same time or successively. Less significantly, several other aa were in close proximity to Ago2, possessing weak signals. Of note, the Trp neighboring Gly do not bind at all.
The relative STD of each proton in the Trp is illustrated on the right side of the graphs. Here, the proton with highest STD amplification factor ($H\eta 2$ highlighted in red) was set to 100%. On the basis of this, values for the other protons were calculated.
Strikingly, for most of the measured peptides, protons $H\eta 2$ and $H\zeta 2$ of the Trp offer the highest relative STD leading to the assumption that those protons must be most deeply buried into a pocket on Ago2.

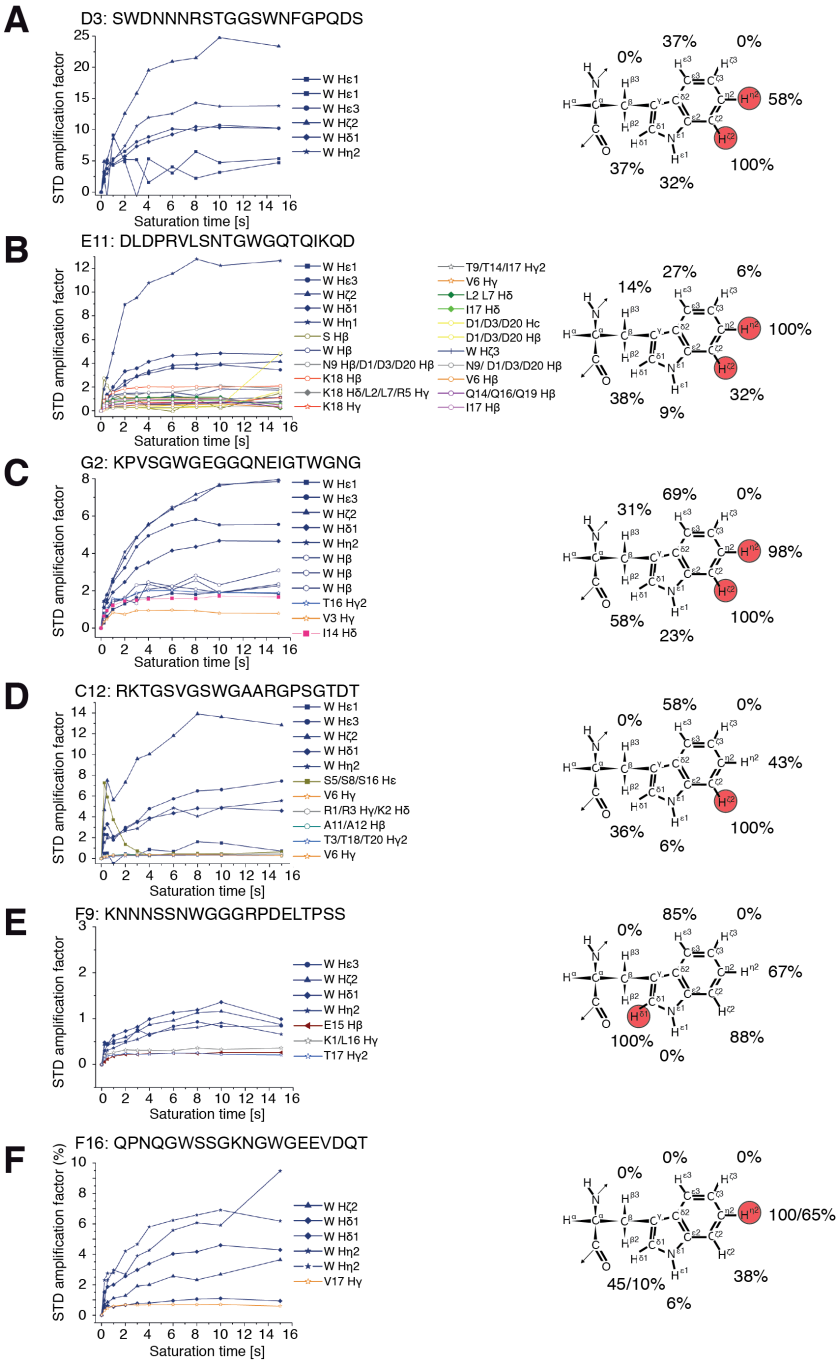

Figure 2.4.2: STD amplification factors of measured peptides Left panels: Time course of STD amplification factors plotted against the saturation transfer time calculated for several peptides from peptide array (Figure 2.2.2), A: D3, B: E11, C: G2, D: C12, E: F9, F: F16. Different amino acids are highlighted by colors, while different symbols are used for protons observed. Right panels: Structure of tryptophane with proton names annotated. The value of the proton with the highest STD amplification factor was set to 100% and is highlighted in red and relative values are then indicated for the other protons, accordingly. STD-NMR measurements were recorded by Dr. Janosch Hennig from the lab of Prof. Michael Sattler.

With this knowledge, results from the second peptide array (Figure 2.3.1) are explainable. The major interaction is mediated by the benzole part of the indole ring. The benzole ring is also available in a Phe, although its lacking the pyrrole what is most likely decreasing the affinity. In the Tyr molecule a hydroxy group is sitting at the position of the $H\eta 2$ proton, hindering the molecule to properly bind into the pocket.
Taken together, we found that mainly the Trp is binding and that this binding is mainly mediated by $H\eta 2$ and $H\zeta 2$ protons. Weak signals of the remaining aa might be due to supporting affinity, the spatial proximity to Ago2 by flanking the Trp, or unspecific irradiation.

2.5 A Tryptophan-containing TNRC6B Fragment that Binds Argonaute 2 is Unstructured in Solution

STD-NMR experiments elucidated that all TNRC6B peptides bind to Ago2 through their Trps. In case two Trps are present both are involved in binding (Figure 2.4.2 A, C, F). Thus, we were wondering how the binding is facilitated in the context of a larger fragment. To test this, we chose a 83 aa long TNRC6B construct ranging from aa 599-683. This region covers peptides E8-F2 (Figure 2.2.3) including peptide E11, which binds Ago2 efficiently in our peptide array experiments. In order to identify important residues for function and folding, we analyzed cross species conservation of this region. In contrast to most of the N-terminal GW regions, this section is conserved (see appendix) (Figure 2.5.1).

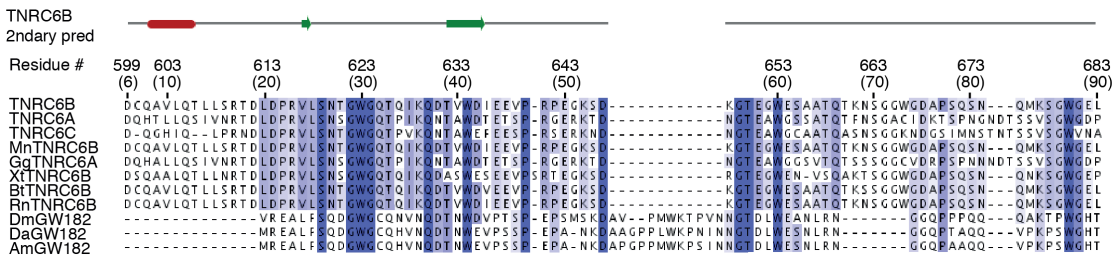

Figure 2.5.1: Multiple sequence alignment of TNRC6B 599-683 orthologs. TNRC6B orthologs from selected organisms were aligned with MAFFT [105] using the Jalview software [216]. Conserved sequence motifs are shaded in blue. Predicted secondary structure elements are displayed above the sequence.

The Gly/Trp/Gly (GWG 29-31 corresponding to TNRC6B aa 622-624) tripeptide of E11 is conserved in vertebrates and insects, as well as some flanking aa, such as S26 (S619) and Q37 (Q630). However, most of the other Trps (W41, W60, W87 corresponding to

TNRC6B W634, W653, W680) are also conserved. Secondary structure analysis only identifies local secondary structure elements whereas the overall structure is predicted to be disordered (Figure 2.5.1).

To find out whether TNRC6B 599-683 exhibits local secondary structure elements that might contribute to binding *in vitro*, the secondary structure of recombinant TNRC6B 599-683 (Figure 2.1.1) was assessed by circular dichroism (CD) spectroscopy (Figure 2.5.2 A). The experimental folding analysis reveals a random-coil-like spectrum with no significant structural content. Unlikely, but local structural elements that could be important for binding can not be fully excluded.

We then recorded relaxation experiments of the construct to investigate protein backbone dynamics (Figure 2.5.2 B). Relaxation describes the process by which spins return to their equilibrium state after excitation. The return back to equilibrium is described by two constants, T1 and T2. T1 is the longitudinal relaxation time describing the return of the magnetization in z-direction while T2 describes the vanishing of magnetization in the xy-plane. These two constants can be directly related to the protein dynamics. While slower global movements are reflected in the T1 value, fast local motions on the ns time scale are affecting the T2 relaxation.

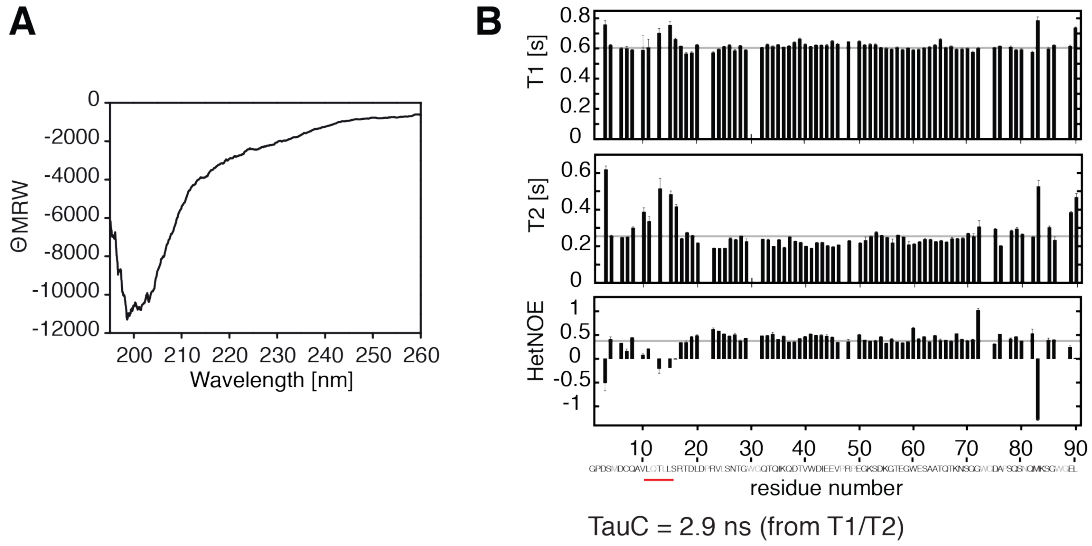

Figure 2.5.2: CD spectrum, ^{15}N NMR relaxation data and heteronuclear NOE of TNRC6B 599-683. A) CD spectrum of TNRC6B 599-683 reveals a random-coil-like structure. B) Average relaxation times are 0.6 s (T1) and 0.25 s (T2), the average value for heteronuclear NOE is about 0.4 as indicated with a gray line. A flexible stretch with enhanced T1, T2 relaxation time and reduced heteronuclear NOE is marked in red. From T1 and T2 the rotational correlation time was estimated to be t=2.9 ns. NMR measurements were performed by Dr. Janosch Hennig.

For backbone assignment of TNRC6B 599-683, the protein was $^{15}N^{13}C$-labeled during expression using M9 minimal medium. Purification was performed in three steps using GST-affinity chromatography, tag-cleavage and SEC. Backbone resonances were assigned using standard triple resonance techniques as HNCA, CBCACONH and HNCACB [187]. The correlation time describing the molecular tumbling in solution estimated from T1 and T2 is t=2.9 ns. This is lower than the correlation time expected for a globular 10 kDa protein (t=5-6 ns), due to the unfolded nature of the protein.
Data gained from this measurements are interpreted on a residue-by-residue basis. The protein shows no internal dynamics except for the termini and a stretch (LQTLLS) in the N-terminal part which showed elevated relaxation rates meaning more flexibility. Thus, this stretch might have a special role in folding or function of the protein. Together, also the NMR relaxation experiments suggest an unfolded TNRC6B fragment
To solidify our findings, backbone heteronuclear NOE rates of TNRC6B 599-683 were measured, which identify motions of N-H bonds. Decreased values occur if an individual motion is faster than the overall tumbling, whereas negative values imply the occurrence of very fast large motions, which are very frequent in unfolded proteins. For a folded protein values between 0.5 and 0.8 would be expected. Our measurements demonstrate a rather flexible unstructured protein with values of about 0.5. Consistently, the area found to have different dynamics in T1 and T2 relaxation has even greater flexibility with values below zero.

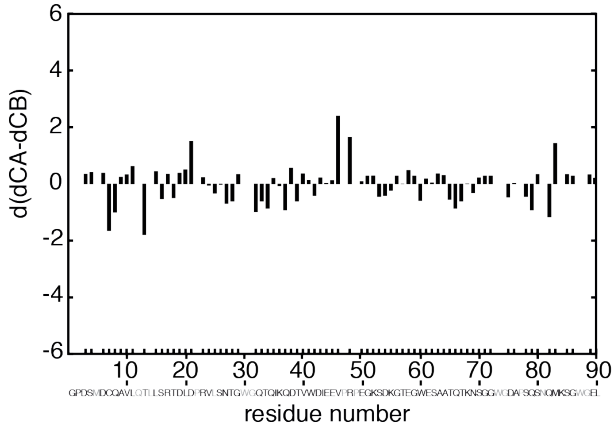

Figure 2.5.3: Secondary chemical shifts calculated for TNRC6B 599-683. Secondary structure analysis based on the ^{13}C secondary chemical shifts of the free TNRC6B 599-683 fragment indicating the absence of significant population of secondary structure. NMR measurements were performed by Dr. Janosch Hennig.

Further, secondary structure prediction based on the difference of measured C_α and C_β

chemical shifts to random coil chemical shifts of the same nuclei (Figure 2.5.3) [192][221] confirms the results found before. Values of all residues are below ±6 ppm, statistically indicating that no secondary structure is present. Taken together, all our measurements imply that TNRC6B 599-683 is a highly flexible protein with no preformed defined folds or structural elements that might contribute to the Trp recognition by Ago2.

2.6 TNRC6B Fragment Binds to Argonaute 2 with a low Micromolar Affinity

As NMR and CD analysis helped to reveal the structural properties of TNRC6B 599-683 itself, we next addressed the binding affinity of TNRC6B 599-683 to Ago2. First, we tested which proteins of HeLa lysate are able to bind to TNRC6B 599-683 in a biochemical pulldown assay (Figure 2.6.1). Therefore, GST-tagged TNRC6B 599-683 was coupled to GSH beads and incubated with HeLa whole cell lysate followed by elution with GSH. The pulldown quality was ensured by SDS-PAGE and visualized by silver staining. A gel slice containing proteins precipitated by GST-TNRC6B 599-683 was cut out as depicted in figure 2.6.1 and analyzed by mass spectrometry (MS). All four human

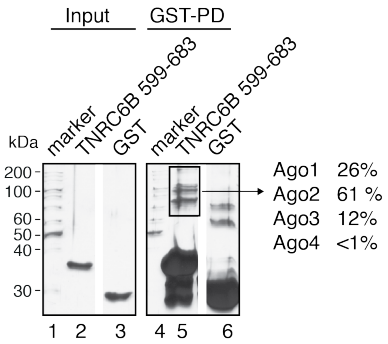

Figure 2.6.1: Pulldown of proteins from HeLa lysate by TNRC6B 599-683. Whole cell HeLa lysate was incubated with GST-tagged TNRC6B 599-683 followed by GST-pulldown. Precipitated proteins were analyzed by SDS-PAGE and visualized by silver staining. 5% input samples (lanes 2 and 3) and 30% eluates (lanes 5 and 6) were loaded. The gel was cut above the 50 kDa marker band and proteins were identified by MS. The ratio of pulled down Ago fractions are indicated on the right.

Ago proteins were identified by MS. The distribution of bound Ago1-4 was determined from the peptide intensities to 26% Ago1, 61% Ago2, 12% Ago3 and less than 1% Ago4. This is in agreement with a previous report [170], where the authors found 20-25% Ago1, 60% Ago2, 15% Ago3 and about 1% Ago4 of the total Ago protein pool in HEK 293T or HeLa S3 cells. Thus, there is no preference of TNRC6B 599-683 to one of the Ago proteins.

Table 2.6.1 lists all proteins that were pulled down from HeLa lysate with at least five identified peptides.

Protein name	Gene name	Uniprot	Peptides	Intensity
Argonaute-2	EIF2C2	Q9UKV8	167	5.3E+08
Heat shock 70 kDa protein 5	HSPA5	P11021	49	2.6E+08
Argonaute-1	EIF2C1	Q9UL18	128	2.2E+08
Trinucleotide repeat-containing gene 6B protein	TNRC6B	Q9UPQ9	43	1.7E+08
Argonaute-3	EIF2C3	Q9H9G7	105	1.1E+08
Heat shock 70 kDa protein 8	HSPA8	Q53HF2	32	2E+07
Heat shock 70 kDa protein 1	HSPA1A	Q5SP16	42	1.7E+07
MMS19 nucleotide excision repair protein homolog	MMS19	Q96T76	24	6057500
Argonaute-4	EIF2C4	Q9HCK5	48	6011494
Elongation factor 2	EEF2	P13639	20	3066700
Interferon-induced protein with tetratricopeptide repeats 5	IFIT5	Q13325	11	1769400
Protein RCC2	RCC2	Q9P258	12	1494600
Carbamoyl-phosphate synthase	CPS1	P31327	20	1479400
Pyruvate kinase isozymes M1/M2	PKM2	P14618	14	1462600
60 kDa heat shock protein	HSPD1	P10809	15	1128100
Heat shock protein HSP 90-beta	HSP90AB1	P08238	10	876770
Polyadenylate-binding protein 1	PABPC1	P11940	13	876570
Nucleolin	NCL	P19338	8	765490
DNA damage-binding protein 1	DDB1	Q16531	11	633100
Heterogeneous nuclear ribonucleoprotein U	HNRNPU	Q00839	7	628890
Heterogeneous nuclear ribonucleoprotein K	HNRNPK	P61978	10	599130
cDNA FLJ78440	GIG12	A8K494	8	398270
WD repeat-containing protein 23	WDR23	Q8TEB1	6	396060
Heterogeneous nuclear ribonucleoprotein M	HNRNPM	P52272	6	390090
ATP synthase subunit alpha	ATP5A1	P25705	7	374470
Clathrin heavy chain 1	CLTC	Q00610	12	346730
Phosphoglycerate dehydrogenase	PHGDH	O43175	7	334190
T-complex protein 1 subunit beta	CCT2	P78371	6	251270
Heat shock protein HSP 90-alpha	HSP90AA1	P07900	6	133610

Table 2.6.1: Table of proteins pulled down together with TNRC6B 599-683 from HeLa lysate Several proteins were precipitated by GST-tagged TNRC6B from HeLa lysate and identified by MS. Bound proteins are listed with their protein names, gene names, Uniprot ID, Peptide count and Intensity.

We demonstrated that a recombinant TNRC6B fragment is suitable to pull down endogenous Ago protein. Next, we tested whether the same fragment also binds recombinantly expressed Ago2 and proved the interaction by an biochemical *in vitro* pulldown assay (Figure 2.6.2 A). Recombinant proteins were mixed and then incubated with GSH beads. After elution with GSH, samples were analyzed by SDS-PAGE and visualized by coomassie staining. In comparison to the control sample (lane 6), recombinant Ago2 is clearly precipitated by TNRC6B 599-683 (lane 5).
In summary, TNRCB 599-683 not only efficiently binds endogenous Ago2 but also the recombinant protein. Based on that, we designed *in vitro* experiments using recombinant proteins to further characterize the interaction.
To assess whether the proteins oligomerize or aggregate upon binding dynamic light scattering (DLS) was conducted (Figure 2.6.2 B). Small molecules are constantly moving in solution due to their Brownian motion. Recording this diffusion by analyzing the intensity of scattered light using the autocorrelation function allows to determine the hydrodynamic radius (R_H) of proteins as a parameter of its size.
Before the measurement, recombinant proteins were filtered and centrifuged to remove aggregates. DLS shows that TNRC6B 599-683 and Ago2 measured alone are monodis-

perse and have a hydrodynamic radius of 1.34 nm and 3.05 nm, respectively. After mixing both proteins, two peaks corresponding to a R_H of 1.17 nm and 3.76 nm are apparent. No high molecular weight peaks are found. Thus, Ago2 and TNRC6B do not aggregate upon binding under our experimental conditions.

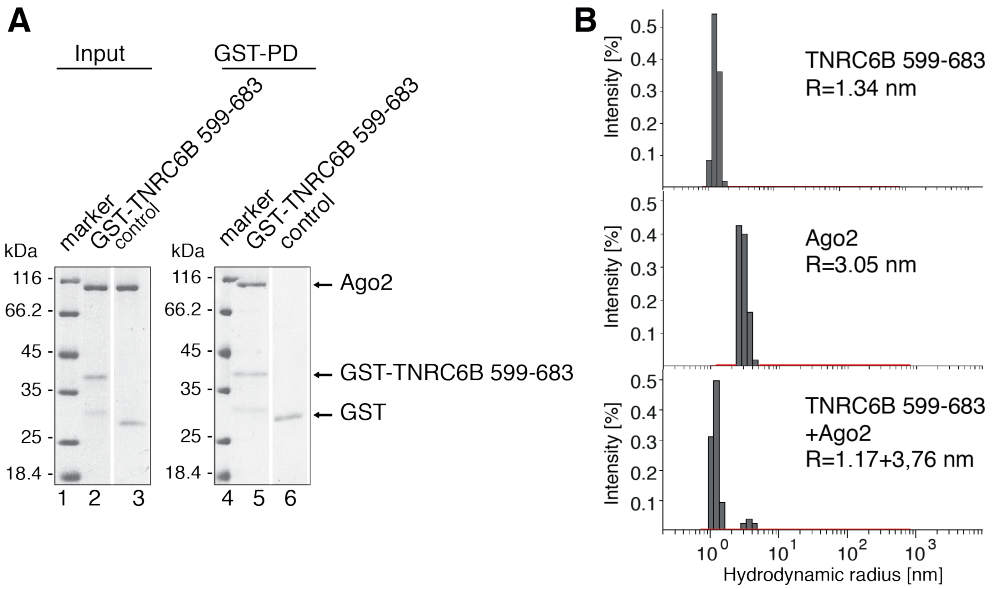

Figure 2.6.2: TNRC6B 599-683 directly interacts with Ago2 and the complex does not aggregate upon binding. A) Ago2 can be efficiently precipitated by TNRC6B 599-683 in a GST-pulldown assay. Recombinant proteins were mixed, bound protein precipitated using GSH beads and analyzed by SDS-PAGE followed by coomassie staining. 5% input samples (lanes 2 and 3) and 30% eluates (lanes 5 and 6) were loaded. B) DLS data shows small particles for TNRC6B 599-683 and Ago2 alone (R_H=1.34 nm and 3.05, respectively) as well as for the complex (R_H= 1.17 nm and 3.78 nm). Intensities were normalized for molecular weight as indicated by a red mark.

Following DLS, we established a biophysical assay based on fluorescence polarization (FP) spectroscopy to measure the affinity of the TNRC6B Ago2 interaction. Polarization of fluorescent light depends on the motion and thus, size of the analyzed molecule. TNRC6B was labeled with a fluorescence dye at a Cys in the very N-terminus of the sequence and mixed with recombinant Ago2 at increasing concentrations. Equilibrium dissociation constants (K_D) of 1.1±0.2 µM and 1.9±0.5 µM for the interaction of TNRC6B 599-683 and Ago2 were acquired in two independent measurements (Figure 2.6.3). A K_D in the low µM range is reasonable assuming an involvement of only a few aa.
Together, TNRC6B 599-683 efficiently associates with endogenous Ago1-4 and recombinant Ago2 with an affinity determined *in vitro* in the low µM range.

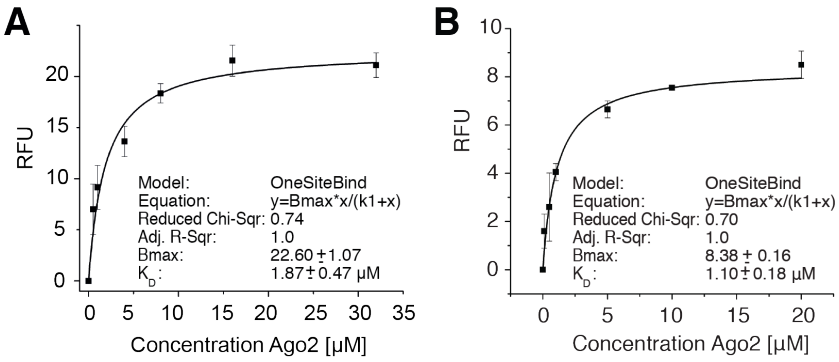

Figure 2.6.3: FP measurement of TNRC6B 599-683:Ago2 interaction. In FP measurements, the K_D of TNRC6B 599-683:Ago2 interaction was A) 1.1±0.2 µM and B) 1.9±0.5 µM, respectively (mean and deviation were calculated from a triple measurement for each sample).

2.7 Tryptophan Flanking Amino Acids Contribute to Binding

Previous experiments (Figure 2.3.1, Figure 2.4.2) indicated that aa flanking the Trp might contribute to binding. To examine this in molecular detail, we performed NMR titration experiments using ^{15}N-HSQC measurements.

Here, the correlation in the protein backbone amides between ^{15}N and ^{1}H is recorded. The resulting spectrum displays one dimension for the ^{1}H nucleus and one dimension for the ^{15}N nucleus, with one peak for each ^{1}H attached to a ^{15}N. For this, ^{15}N was incorporated into the TNRC6B 599-683 protein during expression using M9 medium. Purification was performed using a GST-affinity step, followed by tag cleavage and SEC. A series of ^{15}N-HSQC spectra was recorded at increasing Ago2:TNRC6B 599-683 ratios. Ideally, a concentration dependent movement of single aa peaks, termed chemical shift perturbation (CSP), is observed, resulting from a change of the chemical environment in case direct interaction occurs. On the other hand, the intensity of the peak can decrease upon environmental change due to line broadening. Both factors are used to map the interaction site of Ago2 on TNRC6B 599-683.

Figure 2.7.1 A shows a superposition of the ^{15}N-HSQC reference spectrum of free TNRC6B 599-683 (blue) and the bound form in the presence of Ago2 (red) in a molar ratio of 1:1. With increasing Ago2 concentrations a set of signals decreases in its intensity levels, e.g. signal corresponding to aa L15, T18 or T28. Few resonances undergo a chemical shift, like aa D21, R23 or V40. Some resonances demonstrate both signs of direct interaction.

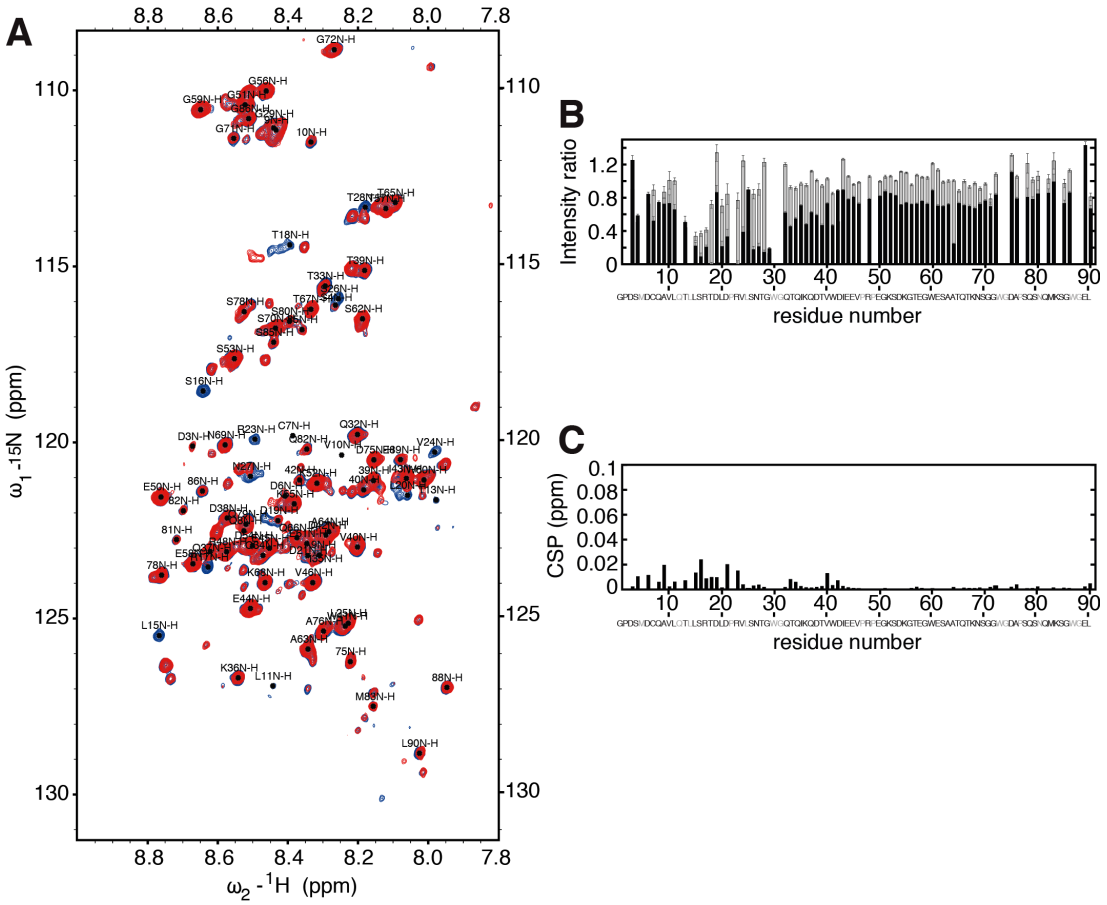

Figure 2.7.1: NMR titration experiments of TNRC6B 599-683 and Ago2. A) Overlay of $^{1}H^{15}N$-HSQC spectra of TNRC6B 599-683 alone (blue) and after addition of 1:1 ration of Ago2 (red). aa corresponding to the peaks are indicated. B) NMR titration experiments were used to calculate the peak intensity ratios of a 0.1:1 (gray) and 1:1 (black) TNRC6B 599-683:Ago2 compared to the free TNRC6B 599-683 reference spectrum. Reduced intensity is observed for T13-W41 (TNRC6B 606-634). C) CSP correspond to the region with reduced affinity. aa colored in gray could not be assigned. NMR titration experiments were performed by Dr. Janosch Hennig.

For analysis, peak intensities of free TNRC6B 599-683 (blue spectrum) and after addition of Ago2 (red spectrum) were calculated and set in relation to display the differences. Ratios of peak intensities were plotted for each residue after addition of molar ratios of 1:0.1 TNRC6B 599-683:Ago2 (gray) and 1:1 TNRC6B 599-683:Ago2 (black) (Figure 2.7.1 B). If no interaction occurs, peak intensity ratios of free TNRC6B 599-683 and the sample containing Ago2 are supposed to be 1 (Figure 2.7.1 B gray bars), since environmental conditions should theoretically be constant. However, higher protein concentrations in the sample also influence the ligand even without binding. In our experiment, the baseline shows a general decrease in intensity upon addition of higher protein concentrations

(1:1 TNRC6B 599-683:Ago2) down to 0.8 (Figure 2.7.1 B black bars). For CSP analysis, distances of the same peaks in the blue and red spectrum were calculated (Figure 2.7.1 B).
Residues highlighted in gray in the sequence below the plots could not be assigned, thus no conclusion about the binding can be drawn from that. A reason for this might be that it is not possible to distinguish between resonances exactly lying on top of each other. Here, this is the case for three out of five Trps and their C-terminally flanking Gly. Since all Trp are part of a GWG tripeptide the very similar environment, in contrast to the Trp lying within a TWD or GWE, leads to the same chemical shift. A possible reduction in intensity and thus interaction to Ago2 can only be assessed from neighboring residues. Intensities of residues T13-T28 (TNRC6B 606-621) are strongly reduced, also the region from Q32-W41 (TNRC6B 625-634) is diminished, covering the Trps W30 (TNRC6B W623) and W41 (TNRC6B W634). Chemical shift perturbations are rather weak but cover the same region as we see for the intensity decrease. This is in accordance with the data we have obtained in the peptide array.
In summary, we observed that the N-terminal region comprising residues T606- W634 ofTNRC6B 599-683 clearly interacts with Ago2.

2.8 Two Proximal Tryptophans are Necessary for Effective Binding

In NMR titration experiments we identified a region covering only two out of five possible Trps that contribute to Ago2 binding. We used GST-pulldown assays to further define the role of all Trps. Mutations were introduced into TNRC6B 599-689, substituting five Trps in the TNRC6B fragment with Ala in different combinations in order to investigate their role in complex formation. Mutants were expressed and purified as described for the wt protein (Figure 2.1.1). GST-tagged TNRC6B 599-683 and the mutants were incubated with recombinant Ago2 and immobilized on GSH beads. After washing, bound protein was analyzed by SDS-PAGE followed by coomassie staining (Figure 2.8.1).
Individual mutation of W623 or W634 completely abolished Ago2 binding (lower panel: lanes 3 and 4), whereas the mutation of W653, W666 or W680 did not affect binding at all (lower panel: lanes 5, 6 and 7). This is consistent with the NMR data suggesting impact on exactly those residues upon titration of Ago2. Intriguingly, the presence of only one Trp, with all other Trps substituted by Ala, is not sufficient for binding (lower panel: lanes 3 and 4). Having observed this, we designed constructs offering both W623 and W634 (lower panel: lane 17) as well as W653, W666 and W680 (lower panel: lane

18) together, with the remaining Trps mutated to Ala. Here, the W653/666/680A construct showed binding comparable to wt (lower panel: lane 16), whereas the W623/634A construct completely lost its affinity for Ago2.
This results leads to the conclusion that W623 and W634 are necessary and sufficient for binding.

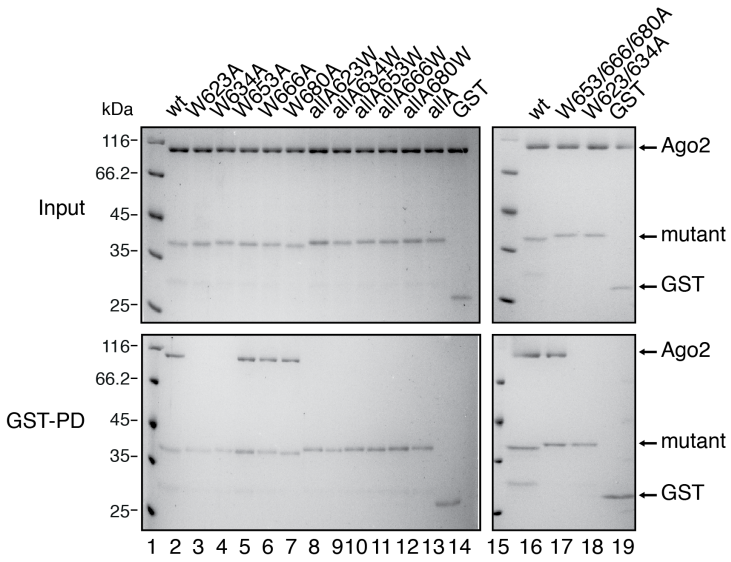

Figure 2.8.1: The TNRC6B 599-683 :Ago2 interaction is mediated by Trps. Upper panel: Input for pull-down assay with respective mutants indicated above. Lower panel: Ago2 precipitation by GST-pull-downs with TNRC6B 599-683 mutants. Mutations W623A and W634A impaired binding, whereas W653A, W666A and W680A had no effect. The combination of W623 and W634 are sufficient to restore binding to wt level.

Comparing those results with the peptide array, we noticed that peptide E11 containing only one Trp (W623) was actually able to bind Ago2 alone, whereas peptide E14 containing only W634 was not. The reason for this might be that the pull down assay was not appropriate to detect this transient interaction. Nevertheless, the results from the peptide array are consistent with the NMR titration results, were the region surrounding W623 was stronger affected than the region flanking W634. This suggest that W623 binds with a higher affinity, whereas W634 assists binding. However, binding in the context of a larger fragment might be different.

2.9 Mapping TNRC6B Contacts on the Surface of Argonaute 2

Having characterized the binding of Ago2 to TNRC6B, we next located the interaction site of TNRC6B on the Ago2 surface. Thus, we subjected the TNRC6B 599-683:Ago2 complex to chemical crosslinking followed by mass spectromic analysis [88]. Therefore, both proteins were purified to high homogeneity (Figure 2.1.5 A and Figure 2.1.1) and crosslinked by incubation with isotope-labeled disuccinimidyl suberate (DSS). DSS is an

11 Å crosslinker that contains an amine-reactive N-hydroxysuccinimide (NHS) ester at each end, reacting with primary amines e.g. in Lys side chains. Crosslinking efficiency was monitored by SDS-PAGE (Figure 2.9.1 A). The sample was loaded on a gelfiltration column and a defined complex was slightly shifted towards higher molecular weight in comparison to Ago2 alone, whereas free TNRC6B 599-683 and impurities were separated (Figure 2.9.1 B). The pure complex was again visualized by coomassie staining after SDS-PAGE (Figure 2.9.1) suggesting that the chemical crosslink was efficient and that crosslinked proteins can be used for further analysis.

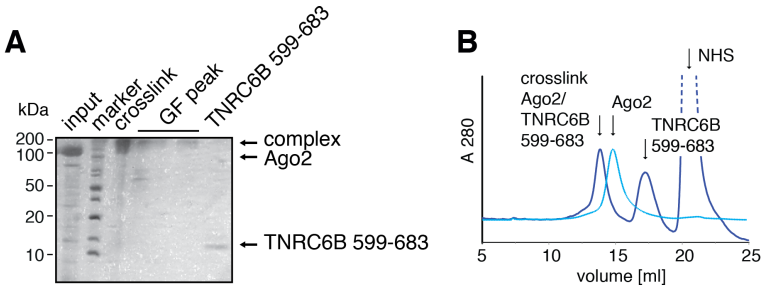

Figure 2.9.1: Crosslinking of TNRC6B 599-683:Ago2. A) SDS-PAGE of crosslinked TNRC6B 599-683:Ago2 complex with defined DSS concentration before (crosslink) and after (GF peak) separation by SEC. The purified sample was subjected to MS analysis. B) After crosslinking of TNRC6B 599-681 and Ago2 the complex was separated from free TNRC6B 599-683 (blue line) and is slightly shifted towards lower elution volume in comparison to free Ago2 (light blue line).

The crosslinked complex was digested with Lys-C and trypsin and finally analyzed my MS as described in [88][214]. The analysis revealed 35 intra- and 5 intermolecular crosslinks that are summarized in Table 2.9.1.
The intermolecular crosslinks connecting TNRC6B and Ago2 are illustrated in Figure 2.9.2 A. Four Lys of Ago2 crosslinked with three Lys of TNRC6B 599-683 in different combinations. However, K648 on TNRC6B 599-683 seems to be preferred. All Lys on TNRC6B are positioned C-terminally of the interacting region we identified before.
For Ago2, intermolecular crosslinks were mainly observed in the PIWI domain, which corresponds to literature. Lys K655, K693 and K844 are exposed on the surface of the PIWI domain whereas K425 is a part of a linker between N-terminal and MID domain, although it is close to the PIWI domain. Recently a crystal structure of Ago2 was published [188]. The authors succeeded to co-crystallize Ago2 with two Trp molecules bound to the surface of the PIWI domain. This is in good agreement with the data we have obtained in the pulldown experiment. Here, we reported that two Trps next to each other within a sequence are necessary and sufficient for binding.

ID	Protein 1	Protein 2	Abs Pos1	Abs Pos2	Mz	z	Error_rel [ppm]	nseen	TIC	ID-Score	MS2
GTEGWESAATQTKNSGGWGDAPSQSNQMK-NKAIATPVQGVWDMR-a13-b2	TNRC6B 599-683	Ago2	661	425	1209.08	4	6.9	1	0.46	32.52	7
SDKGTEGWESAATQTK-EACIKLEK-a3-b5	TNRC6B 599-683	Ago2	648	693	941.8	3	4.4	4	0.39	31.74	3
SDKGTEGWESAATQTK-NKAIATPVQGVWDMR-a3-b2	TNRC6B 599-683	Ago2	648	425	880.44	4	3.5	3	0.41	31.15	1
SDKGTEGWESAATQTK-ELLIQFYKSTR-a3-b8	TNRC6B 599-683	Ago2	648	655	808.415	4	4.7	2	0.38	30.41	6
QDTVWDIEEVPRPEGKSDK-DHQALAKAVQVHQDTLR-a16-b7	TNRC6B 599-683	Ago2	645	844	859.846	5	6.6	1	0.46	24.06	2
SAPDRQEEISKLMR-LFCTDKNER-a11-b6	Ago2	Ago2	381	720	745.626	4	4.4	5	0.71	38.83	7
VEITHCGQMKR-DRHKLVLR-a10-b4	Ago2	Ago2	276	317	422.902	6	2.3	4	0.71	37.68	4
VGKSGNIPAGTTVDTK-LFCTDKNER-a3-b6	Ago2	Ago2	726	720	955.488	3	0.9	20	0.54	36.41	6
EIVEHMVQHFKTQIFGDR-KPVFDGRK-a11-b1	Ago2	Ago2	83	91	660.354	5	5.1	8	0.42	36.25	4
IDIYHYELDIKPEKCPR-GLKVEITHCGQMK-a14-b3	Ago2	Ago2	65	266	638.665	6	4.4	5	0.4	35.72	4
IDIYHYELDIKPEKCPR-VEITHCGQMKR-a11-b10	Ago2	Ago2	62	276	614.979	6	0.8	1	0.66	35.66	5
KPSIAAVVGSMDAHPNR-FTKEIK-a1-b3	Ago2	Ago2	608	260	531.29	5	0.3	6	0.61	35	2
TIKLQANFFEMDIPK-LFCTDKNER-a3-b6	Ago2	Ago2	39	720	779.401	4	5.7	5	0.48	34.8	4
KPSIAAVVGSMDAHPNR-KLTDNQTSTMIR-a1-b1	Ago2	Ago2	608	355	824.432	4	2.8	7	0.48	34.76	5
IDIYHYELDIKPEKCPR-IFKVSIK-a11-b3	Ago2	Ago2	62	129	632.951	5	4.2	2	0.55	34.31	5
KLTDNQTSTMIR-EIKGLK-a1-b3	Ago2	Ago2	355	263	744.75	3	2.5	4	0.36	32.14	2
SIEEQQKPLTDSQR-VKFTK-a7-b2	Ago2	Ago2	248	257	806.77	3	2.4	4	0.32	31.79	2
IDIYHYELDIKPEK-KNLYTAMPLPIGR-a11-b1	Ago2	Ago2	62	98	678.172	5	6.2	3	0.72	30.31	1
IDIYHYELDIKPEKCPR-VEITHCGQMKR-a14-b10	Ago2	Ago2	65	276	737.775	5	2.6	2	0.59	30.06	7
KLTDNQTSTMIR-FTKEIK-a1-b3	Ago2	Ago2	355	260	770.752	3	1.5	4	0.38	30.02	3
RPASHQTFPLQQESGQTVECTVAQYFKDR-HKLVLR-a27-b2	Ago2	Ago2	313	317	1078.556	4	-2.1	20	0.47	29.64	3
NKAIATPVQGVWDMR-NKQFHTGIEIK-a2-b2	Ago2	Ago2	425	440	785.174	4	5	8	0.45	29.29	1
YHLVDKEHDSAEGSHTSGQSNGR-DHQALAKAVQVHQDTLR-a6-b7	Ago2	Ago2	820	844	654.897	7	5.3	14	0.32	29.09	4
SAPDRQEEISKLMR-EACIKLEK-a11-b5	Ago2	Ago2	381	694	697.616	4	0.7	2	0.51	28.71	3
SAPDRQEEISKLMR-KLTDNQTSTMIR-a11-b1	Ago2	Ago2	381	355	801.917	4	3.2	1	0.36	28.61	3
GLKVEITHCGQMK-KLTDNQTSTMIR-a3-b1	Ago2	Ago2	266	355	762.144	4	-0.5	2	0.38	28.48	1
GLKVEITHCGQMK-VKFTK-a3-b2	Ago2	Ago2	266	257	452.849	5	-3.5	7	0.4	28.07	3
IDIYHYELDIKPEKCPR-KNLYTAMPLPIGR-a14-b1	Ago2	Ago2	65	98	950.758	4	3.9	2	0.59	27.88	4
YHLVDKEHDSAEGSHTSGQSNGR-KLTDNQTSTMIR-a6-b1	Ago2	Ago2	820	355	811.99	5	2.3	3	0.31	27.15	2
SIEEQQKPLTDSQR-FTKEIK-a7-b3	Ago2	Ago2	248	260	513.076	5	1.3	4	0.23	26.15	3
VEITHCGQMKR-EIKGLK-a10-b3	Ago2	Ago2	276	263	728.396	3	2.5	5	0.25	26.05	3
DKVELEVTLPGEGKDR-VEITHCGQMKR-a14-b10	Ago2	Ago2	124	276	820.926	4	4.7	1	0.33	25.8	5
YHLVDKEHDSAEGSHTSGQSNGR-FTKEIK-a6-b3	Ago2	Ago2	820	260	569.779	6	-0.7	3	0.27	23.32	4
DHQALAKAVQVHQDTLR-EACIKLEK-a7-b5	Ago2	Ago2	844	693	612.333	5	5.3	1	0.19	20.49	0
YHLVDKEHDSAEGSHTSGQSNGR-EIKGLK-a6-b3	Ago2	Ago2	820	264	556.779	6	2.6	8	0.11	20.33	2

Table 2.9.1: Table of crosslink pairs identified by MS. Listed are 5 intermolecular (highlighted in violet) and 35 intramolecular crosslinks detected the TNRC6B 599-683:Ago2 complex by MS. Analysis of the crosslinks was performed by Dr. Franz Herzog.

Strikingly, all Lys identified by crosslinking are in close proximity to those Trps (Figure 2.9.2 B, crosslinked Lys in violet).

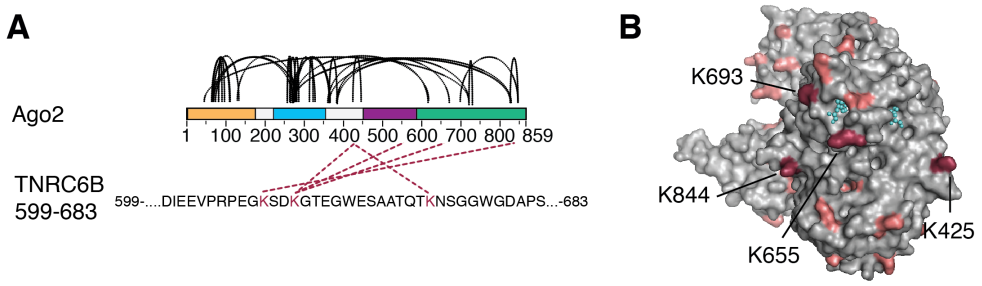

Figure 2.9.2: Crosslink map of TNRC6B 599-683:Ago2 analysis. A) The crosslink map illustrates the crosslinks found between Ago2 and TNRC6B 599-683 (violet) and the Ago2 intramolecular crosslinks (black dashed lines). Upper panel: Domain organization of Ago2: N-terminal domain (orange), PAZ domain (blue), MID domain (purple) and PIWI domain (green). Lower panel: Lys crosslinked in TNRC6B 599-683 are highlighted in violet. B) Surface presentation of Ago2 crystal structure (PDB: 4EI1) aligned with Trp (cyan) co-crystallized (PDB: 4EI3). Lys on Ago2 that crosslinked with TNRC6B Lys are highlighted in violet. All other Lys present in the Ago2 sequence are highlighted in salmon to show possible crosslinking sites.

To illustrated the availability of Lys that could possibly react with the crosslinker, all surface exposed Lys on Ago2 are highlighted in pink. We assume the distance between C_α atoms of crosslinked Lys to be not more than 30 Å [88], calculated from the length of the DSS spacer (11 Å), the length of each Lys side chain (two times 6.5 Å) and an error due to the Lys side chain flexibility that was estimated to 3 Å. Since there are Lys available for crosslink above the Trp binding site that did not react, TNRC6B 599-683 most likely binds below the Trp binding site.
Together, we revealed by crosslinks followed by mass spectromic analysis that TNRC6B 599-683 specifically binds a patch on the surface of the Ago2 PIWI domain and thus, provide the first structural insights into the interaction of a longer TNRC6B fragment with Ago2.

2.10 Model of TNRC6B - Argonaute 2 Interaction

Combination of all data obtained by the peptide arrays, biophysical and NMR experiments as well as the crosslinks allows us to postulate a model of the binding mechanism of TNRC6B and Ago2 (Figure 2.10.1).

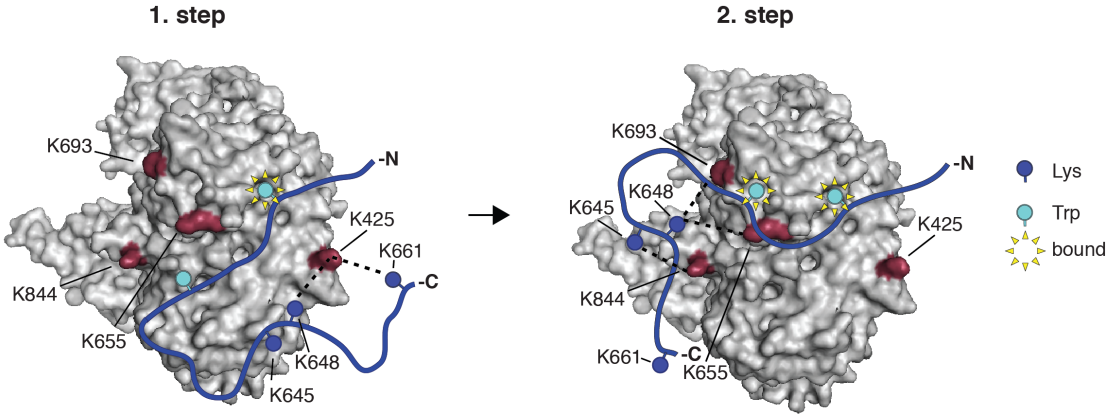

Figure 2.10.1: Schematic model of Ago2:TNRC6B 599-683 binding mode. In a first step, TNRC6B 599-683 binds with its first Trp (W623) to one Ago2 Trp binding pocket. All Lys in the TNRC6B 599-683 sequence are flexible and can reach Ago2 Lys for crosslinking. In a second step binding of the second Trp (W634) to the other pocket completes the affinity.

The TNRC6B 599-683 peptide probably binds with its first Trp (here W623 corresponding to PDB: 4EI3 W901) to one Trp binding pocket on Ago in an initial step. W623 has been shown to offer a stronger interaction with Ago2 both in the peptide array and in the NMR titration experiments. At this stage, the second Trp (here W634 corresonding to PDB: 4EI3 W902) would still be flexible and thus, all Lys come in appropriate distance

for crosslinking their identified partner Lys. In a last step the second Trp binds to the other pocket, fixing the peptide in its orientation resulting in full affinity.
To illustrate how the TNRC6B 599-683 fragment would bind Ago2, we loaded the Ago2 structure bound to two Trps (PDB: 4EI3) in the program coot [48]. On the basis of the Trp positions we completed the remaining polypeptide chain of TNRC6B 599-689, corrected it for bond angles, plane errors and rotamer positions (Figure 2.10.2). The shortest way for the 10 aa polypeptide linker from one to the other Trp was assessed to be spanning below the Arg nose sticking out of the Ago2 surface.

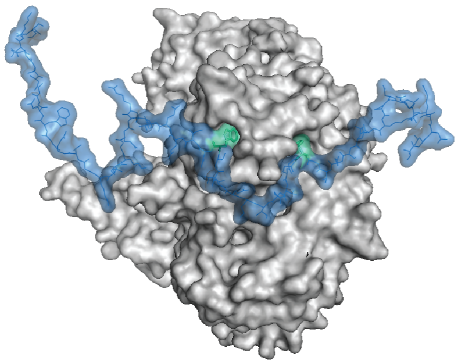

Figure 2.10.2: Model of Ago2:TNRC6B 599-683 interaction. TNRC6B 599-683 wraps along the surface of Ago2 bound through two Trp in hydrophobic pockets.

If we now take a closer look at the TNRC6B polypeptide, some requirements for efficient binding become obvious. First, the inner neighbors of the Trps do not necessarily have to be Gly but rather small aa, otherwise proper binding to the Ago2 pocket is not ensured. Second, the linker polypeptide sequence between both Trps must have a certain length, to span from one site to the other, favoring the unstructured nature and flexibility of the protein.
In conclusion, this model illustrates that the TNRC6B 599-683 is bound transiently to the PIWI domain of Ago2 through two Trps, with the spacing polypeptides between the two Trps spanning below the nose.

3 Discussion

Ago proteins are viewed as key players in small RNA-guided gene-silencing pathways in almost all eukaryotes. The association of GW182 proteins with Ago proteins is essential for efficient repression [52][43][146][175]. Thereby, GW182 binds via evolutionary and functionally conserved GW-repeat motifs to the PIWI domain of Ago proteins [203][52][4][126][29][45], providing a binding platform for downstream silencing events [235][231][224][201][175][126][92][57][51][43][31][28][17]. The functional relevance of this interaction has been well established, whereas the mechanism beyond the interaction itself remained elusive.
In this study, we dissected the role and nature of TNRC6B GW-motifs in Ago2 binding and mapped the binding sites using biophysical and biochemical approaches. Finally, we defined a model on the binding mode of both proteins.

3.1 Protein Properties

Prior to *in vitro* studies, recombinant TNRC6 as well as Ago protein needed to be acquired. TNRC6 purification was challenging since full length proteins or longer constructs seemed to be unstable upon purification, even with high concentration of protease inhibitors. This is pertinent to the recognition that intrinsically disordered proteins (IDPs) are extremely susceptible to proteolytic degradation *in vitro* [205]. It has been shown that the half-life of a protein rather negatively correlates with the length of the polypeptide chain and with various measures of structural disorder than with the presence of degradation signals [206]. Consistent with this, purification of globular domains (RRM) and smaller conserved sequence sections of TNRC6 proteins was successful.
The sequence of GW182 proteins responsible for Ago binding shows strong similarity to FG-nucleoporines except for exhibiting WG instead of FG repeats. Over the last decade, FG-nucleoporines were intensively studied. Those proteins are intrinsically disordered and crucial for building a permeability barrier in the nuclear pore complex [65]. In a recent study, RNA-binding-proteins (RBPs) offering low complexity regions that contain several YG-repeats were investigated [104]. Both studies showed that at high

concentrations the protein sequences containing F/YG-repeats were able to form so-called hydrogels *in vitro*.
Notably, in this work at very high concentration of TNRC6B 599-683 to about 10 mM, reversible formation of a hydrogel was observed (data not shown). However, those results were not reproducible. Thus, besides degradation, the full length protein being even more prone to hydrogel formation, could be stuck during the purification procedure, e.g. in the concentrator.
Ago proteins were obtained in low yield, however, in high purity. Attempts to reduce Ago2 to the minimal TNRC6B binding domain were not successful since expression of all constructs tested yielded insoluble protein. The results of analytical limited proteolysis implies that the protein is highly resistant towards proteolytic digestion. This is in accordance with a recent publication [47]. The authors separated Ago2 complexed with small RNAs from its unloaded species and showed that, after digestion, only unloaded protein was proteolysed, whereas the complex was stable.

3.2 Argonaute 2 Binds to Distinct Tryptophan - containing Motifs on TNRC6B with Different Affinities

Several studies contributed on the definition of the Ago binding site on GW182 proteins. It is known that the N-terminal GW-rich region [8][203][201][45][4][52][203], together with the Ago PIWI domain [8][148] are crucial for the interaction [126].

3.2.1 Definition of the Argonaute 2 Binding Site on TNRC6B

We used a peptide array to obtain comprehensive information about the number and affinities of Ago2 binding sites on TNRC6B. We found multiple distinct regions within the TNRC6B sequence that allow Ago2 binding. All peptides possessed at least one Trp whereas the remainder sequence composition seemed to be random. Within those peptides, we identified three sites having a strong affinity as well as several sites with medium, weaker and no affinity. Most of the binding sites were located in the N-terminal part of TNRC6B, although a Trp-containing aa stretch in the C-terminal part comprises weak Ago2 affinity, too. The three hotspots cover the aa TNRC6B 467-501, TNRC6B 612-641 and TNRC6B 767-791.
TNRC6B 612-641 corresponds to a WG/GW-rich region of GW182 that was before described as evolutionary conserved platform for Ago recruitment. Baillat et. al [4] reported that this region (termed domain I) is necessary and sufficient for the association of TNRC6B with Ago2 and that deletion of this region abrogated binding. These results

are partially in contrast to our findings, since the authors observed that one specific domain is responsible for the interaction, whereas we find multiple distinct binding sites. Supporting our results, other investigators found that in context of the full length protein, this region (termed motif I) of *D. melanogaster* (Dm) GW182 seems to be the major binding site for Ago1 [51]. Deletion of a single GWG-repeat strongly impaired binding. However, the authors conclude that additional GW-repeats strengthen the interaction by providing low affinity binding sites.
A report in context of full-length TNRC6A, B and C [117] showed that two conserved motifs (termed motif I and II) provide major binding sites in TNRC6C with additional repeats providing low affinity binding sites. In contrast, the impact on Ago interaction upon deletion of motif I and II in TNRC6A and TNRC6B isoform 1 was marginal. This is in accordance with our data showing that multiple GW-repeats contribute to the interaction.
Similarly, it was demonstrated that three fragments within TNRC6A that correspond to motif I, motif II and the Ago-hook were sufficient for Ago binding. Although, in our study, peptides of motif II offered only medium binding affinity.
In agreement with the results of Lian et al. [126], we did not only observe binding of the N-terminal repeats in the peptide array, but also for a stretch lying in the C-terminal sequence. Due to the small number of GW repeats and thus lower affinity, this interaction could most probably only be detected in a more sensitive peptide array and not in pull-down assays.

3.2.2 Role of Tryptophan Residues in the Argonaute - TNRC6B Interaction

In previous studies Trps were shown to play an important role in Ago:GW182 binding [45][203][201]. We now strengthened those results and identified Trps as key residues mediating the interaction. Substitution of Trp to Ala, Tyr, Leu and Arg completely abolished binding. Interestingly, substitution of Trp to Phe, did not prevent the peptide from interacting with Ago2, even though the affinity was alleviated. This suggests that the benzole ring, abundant in both Trp and Phe, mediates the major interaction possibly by sticking into a binding pocket on Ago. This would be prevented by the additional hydroxy group present in Tyr. In contrast, replacement of Trp by Phe was shown before to abrogate binding [45][203] what is, however, not in accordance with a recent report where Ago was cocrystallized with phenol [188].
We further found that the context of the Trp also contributes to the interaction. In the first peptide array it appears that several aa before and after the Trp is needed for

optimal binding. Substitution of the complete sequence or only parts (except for the Trp) by Gly or Ala lead to very low affinity, however, binding was still detectable. Here, the polyGly or polyAla peptide probably adopted secondary structure. Thus, its rather the structural property of the entire peptide than the absence of specific residues that determines the binding capacity. This is supported by the fact, that the binding affinity was not affected upon substitution of single Trp flanking aa. This is in contrast to an experiment, were it was shown that Gly are indeed necessary as well as substitution of specific residues affected binding [203].
With this information we tried to identify a general Trp-motif comprising efficient Ago binding. Alignment of the peptides did not reveal a conserved motif except for the presence of at least one Trp. It appeared that the presence of two Trps increased the affinity. However, we were not able to identify a binding motif surrounding Trps that engage in Ago binding.
Taken together, our results confirm and extend the knowledge about the binding site of Ago2 on TNRC6B and the role of Trps. The focus on investigation of GW/WG-repeats has to be corrected towards Trp-repeats, since we have found that a flanking Gly is preferred but not absolutely necessary for binding. Instead, it appears that Trp neighbors have to be rather small, hydrophilic residues. Furthermore the aa composition plays a role in terms of structural integrity. Generally, comparison of reports on GW182:Ago interaction leads to the assumption that binding sites on GW182 proteins can differ species- and homologue-wise. Moreover the method used for the experiments seems to influence the results.

3.3 The Argonaute 2 Surface Reveals Potential Binding Interfaces

In the first part of the study, we characterized the Ago2 binding site on TNRC6B. Inspection of the Ago2 surface reveals features that might be involved in TNRC6B binding. Figure 3.3.1 shows the crystal structure of Ago2 (PDB: 4EI1) with the two bound Trps (PDB: 4EI3) aligned. In Figure 3.3.1 A, hydrophobic residues are colored in orange. The two Trp binding pockets exhibit a clearly hydrophobic character, however, some other hydrophobic patches are visible that could serve as binding sites for additional hydrophobic interactions of the peptide. Surface charges (Figure 3.3.1 B) are equally distributed all over the protein. Besides the positively charged inner protein core, which is involved in miRNA binding, no defined charged patches can be observed. A small pocket below the Trp binding site is positively charged originating from Arg/Lys inside

the PIWI domain. This pocket could play a role in binding negatively charged or phosphorylated aa in the vicinity of bound Trps. Ago2 sequence conservation was plotted on the surface using the ConSurf server illustrated in Figure 3.3.1 C. In contrast to the aa forming the inner core of the protein, the aa lying on the Ago2 surface are less conserved. An exception are the aa forming the Trp binding pockets and a stretch of aa lying in a groove below the Trp binding pocket comprising the hydrophobic and positively charged pocket described before. This region might play a role in GW18 binding, although it could be an interaction site for another protein.

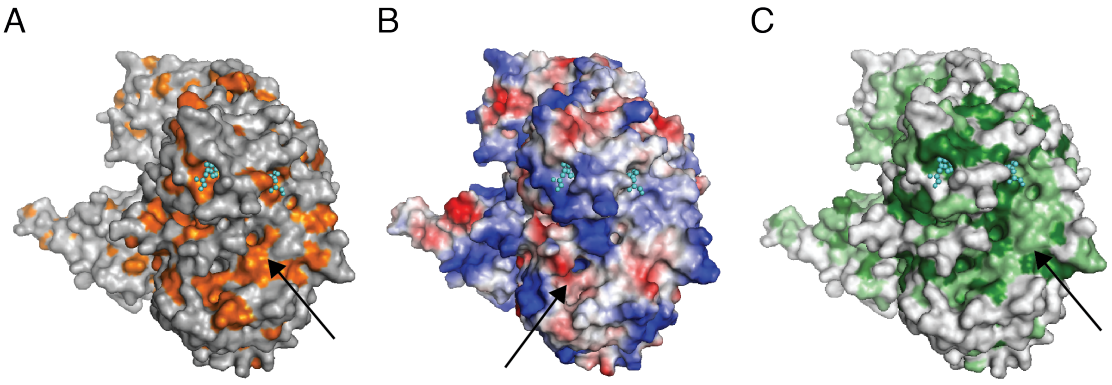

Figure 3.3.1: Surface properties of Ago2. Surface presentation of Ago2 crystal structure (PDB: 4EI1) aligned with Trp (cyan) cocrystallized (PDB: 4EI3). A) Hydrophobic residues are colored in orange. A hydrophobic patch is indicted by an arrow. B) Electrostatic potential. A positively charged pocket is indicated by an arrow. C) Conservation. Conserved aa stretch is indicated by an arrow.

Before the crystal structure of Ago2 was obtained, several groups tried to determine the GW182 binding site on Ago by mutational analysis. Till et al. [203] mutated several residues in the PIWI domain as well as in the MID domain of Ago2 to Ala, leading to strong (orange) and mild (light orange) decrease in affinity (Figure 3.3.2). Residues R583, R647 and K660 are directly involved in formation of the hydrophobic Trp binding pocket, thus, mutation of those residues completely abrogates binding. Other residues with strong and mild impact are not directly involved in the Trp interaction but might destabilize the surface conformation leading to impaired binding. Residues F470 and F505 (termed F2V2 mutant) are indicated in yellow. Here, single residue mutation did not impair the interaction [52] whereas double substitution completely abolished binding [52][148], probably due to aggregation of the MID domain. GW182 interaction to Ago has been described to be independent of miRNA binding [182]. Thus, loss of binding by mutation of residues in the MID domain is probably not a consequence of impaired miRNA binding but rather results from a conformational change of the MID domain

towards the PIWI domain or aggregation. Mutation of residues comprising the positively charged pocket described above (Figure 3.3.1 B) K533 and R812 strongly affects binding. Since these mutations are far away from the identified Trp binding pockets, those results might point towards an additional binding site, maybe in the groove described above between PIWI and MID domain Figure 3.3.1. Some of the mutations showed by Till et al. were verified in a later studies [51][52][13].

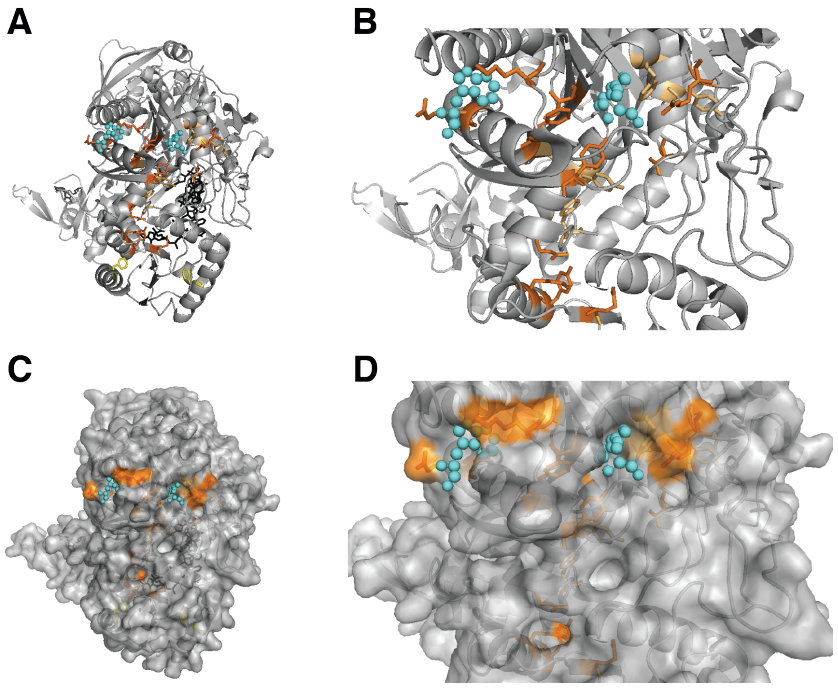

Figure 3.3.2: Ago mutations impairing GW182 binding. Ago2 crystal structure (PDB: 4EI1) aligned with Trp (cyan) cocrystallized (PDB: 4EI3). A) Mutations with strong impact on GW182 binding are colored in orange, mutations with mild impact are colored in light orange and residues of the F2V2 mutant are colored in yellow. B) close up of a). C) surface presentation of A) displaying residues important for Trp binding. D) close up of C).

3.3.1 Implications of Species Specific Surface Characteristic on GW182 Binding

We suggest that the residues between both Trp are spanning below the Arg residue (R658). Thus, we were interested whether this residue plays a role in positioning the peptide. Figure 3.3.3 A shows a sequence alignment of different species covering Ago2 R658. This residue is only conserved in higher vertebrates as human, mouse and frog. Inspection of the surface composition of available Ago structures (Figure 3.3.3 B) reveals that the hydrophobic pockets needed for anchoring the two Trps are only available in

the structures of human proteins (PDB: 4EI1 and 4F3T).

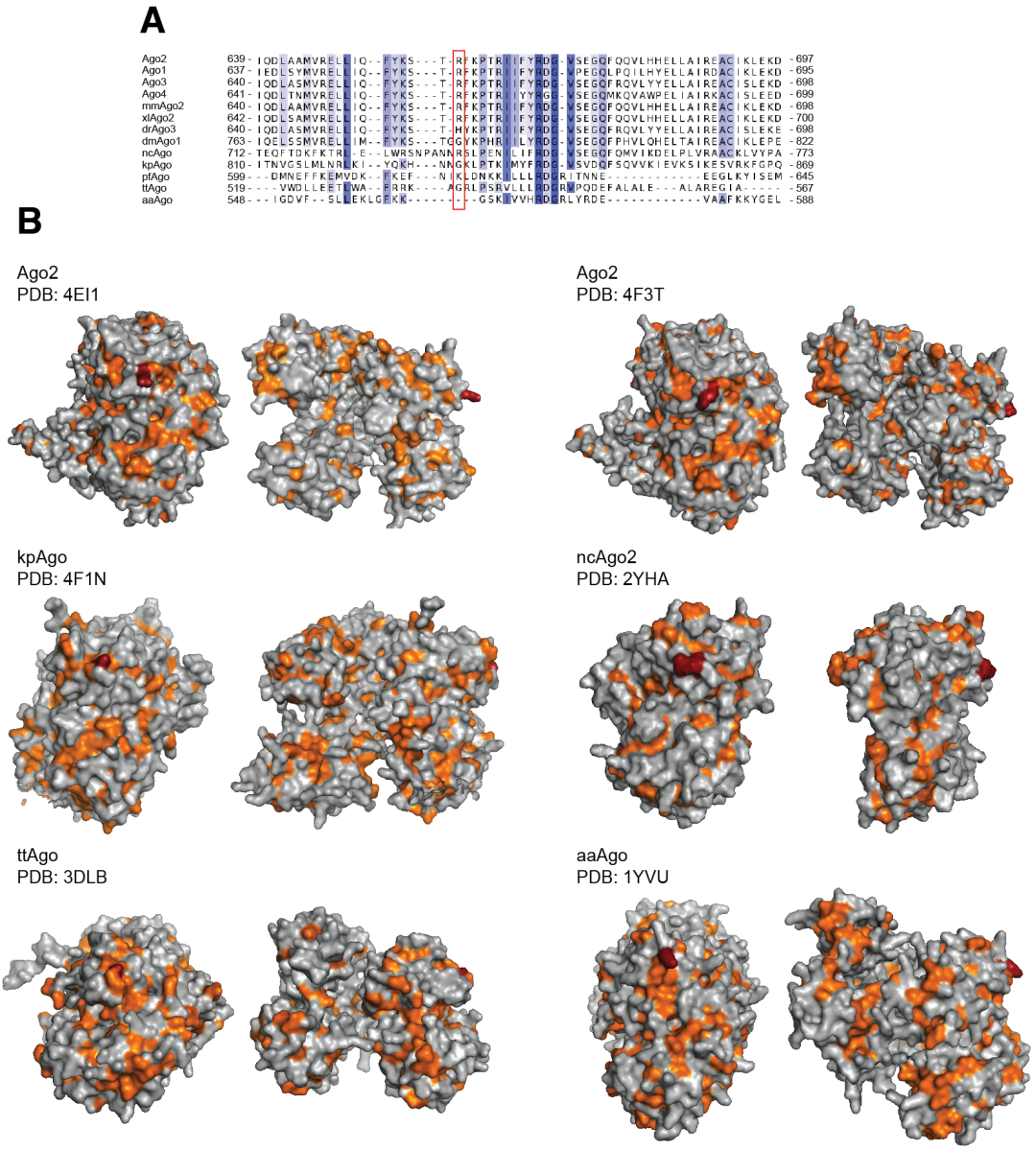

Figure 3.3.3: Surface characteristics of Ago structures from different species. A) alignment of the sequence surrounding Ago2 R658 with different species. B) Surface presentation of Ago structures from different species. Hydrophobic residues are colored in orange, Ago2 R658 and its corresponding residues are highlighted in red.

Neither structures of yeast (*Kluyveromyces polysporus*), fungi (*Neurospora crassa*), eubacteria (*Thermus thermophilus*) or bacteria (*Aquifex aeolicus*) comprise comparable GW182 interaction sites. This is in agreement with the results obtained in this study

were we showed that pfAgo cannot interact with TNRC6B.
According to that, only higher eukaryotes are able to bind GW182 and exert downstream pathways. This is reasonable since GW182 homologues are only known in miRNA-mediated gene silencing of higher eukaryotes. In contrast, Till et al. found that the archaeal *Archaeoglobus fulgidius* PIWI protein directly bound to a TNRC6B fragment [203]. However, it might be possible that the *Archaeoglobus fulgidius* PIWI protein functions in a sRNA-mediated gene silencing-like pathway interacting with other GW-proteins.

3.4 TNRC6B Binds to the Argonaute 2 PIWI Domain Through a Combinatorial Tryptophan - Motif

3.4.1 Tryptophan Position

Having observed that besides Trp no other aa directly interacts with Ago in the peptide array, we confirmed our assumption by STD-NMR measurements on an atomic level. Measurements of peptides containing two Trps show that both Trps interact with Ago2. However, we cannot tell apart which peaks originated from which Trp, and also not, whether both Trps bind at the same time or successively. In agreement with that, the Ago2 crystal structure [188] confirms that both Trps can bind at the same time.
Exact inspection of how the two Trps are bound to the pocket (Figure 3.4.1) gives evidence that W901 is stronger coordinated to surrounding Ago residues than W902. However, in context of a peptide, the exact position of the Trps might slightly differ.

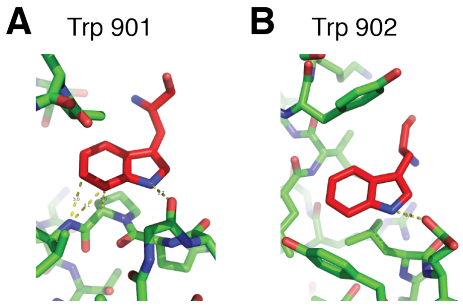

Figure 3.4.1: Trp coordination in Ago2 binding pockets. Different coordination of Trps A) W901 and A) W902 in the Ago2 binding pocket (PDB: 4EI3).

Interestingly, comparing STD-amplification factors of protons within the indole ring shows that protons $H\eta 2$ and $H\zeta 2$ possess the highest values for all peptides tested (ex-

cept for peptide F9 that had generally a very weak affinity), thus probably being closest to Ago.
If we now reconsider the published Ago2 structure and the positions of the two Trp bound, those results are reasonable. Both Trps stick with their benzole rings into Ago, thereby allowing an efficient transfer of magnetization to $H\eta 2$ and $H\zeta 2$. Here, the results from the second peptide array, were we showed that Phe but not Tyr instead of Trp allows binding, fit very well. Tyr exhibits an additional hydroxy group at the top of the benzole ring, thereby abolishing binding either sterically or due to its charge. In contrast, Phe features the same benzole ring as Trp making it possible to perform equal interactions. However, it lacks the additional affinity mediated by the pyrrol part, thus, showing reduced affinity.
To investigate, which TNRC6B 599-683 residues are affected upon Ago2 binding we performed NMR titration experiments. We found that only 2 out of 5 Trps undergo chemical shift perturbations and intensity changes. W623 is highly affected whereas the impact on W634 is milder. This leads to the conclusion that W623 binds stronger to Ago than W634, in agreement with Figure 3.4.1.
Pulldown assays confirm an important role of W623 and W634 within TNRC6B 599-681 shown by NMR titration experiments, since binding is completely abolished after substitution of Trp by Ala. According to a study by Takimoto et al. [201], mutation of residues corresponding to TNRC6B W623 and W634 in TNRC6A 431-520 completely abolished binding to Ago2 in a pulldown assay, whereas substitution of the Trp corresponding to TNRC6B W653 had no influence. Similarly, in further pulldown assays using TNRC6A 431-520 and TNRC6B 584-673, the interaction of the W623A mutant was completely abolished, although W634A only scarcely interacted with Ago2. Differences for W634A binding within the study and also to our results might have methodical reasons. However, this data match to the titration experiments, were we observed a stronger binding for W623. In contrast to the study by Takimoto et al. we did not only show that substitution of a single Trp to Ala abrogates binding but also, that this two Trps act synergistically and are sufficient for wt binding.

3.4.2 Trp Spacer Length

Investigation of the three binding hotspots identified by the peptide array reveals that the spacer between the two Trp for all hotspots is exactely 10 aa in length. This prompted us to systematically compare spacer lengths within TNRC6B (Figure 3.4.2). Indeed, most of the other spacing regions are either longer or shorter. In total, we find seven regions with a Trp distance of 10 aa, three of them are our high affinity binding sites. Inspection

of the other spacers shows that they either contain hydrophobic, aromatic residues (Tyr) which might lead to a hydrophobic collapse of the peptide or a Pro residue, which limits the flexibility of the peptide spacer, thereby hindering the Trp to properly access the binding pocket. This suggests that a certain spacing of Trp side chains may suffice to provide significant affinity to Ago2.

Figure 3.4.2: Spacing between TNRC6B Trps. Sequence of TNRC6B with all Trps colored in blue. The aa distance between each Trp is indicated by a black line, with the sequence upstream of W623 pointed out with a bold line. The binding hotspots are highlighted in gray.

In summary, combination of our data from the peptide arrays, NMR measurements, pulldown assays and crosslinking allows to define some requirement for binding Ago: First, the Trp neighbor must be a rather small, hydrophilic residue. Second, the Trp containing peptide must be flexible for proper Trp accessibility. Third, binding affinity is enhanced by simultaneous contacts of two Trp side chains separated by defined spacing.

3.4.3 Relation to Known Protein Sequence Motifs

Remarkably, in NMR titration experiments not only the region surrounding those two Trps shows signs of binding, but also some residues N-terminally of that region.
In post-transcriptional mRNA regulation, many proteins were shown to contain short linear interaction motifs (SLiM) [42] (about 6-11 aa) in disordered protein regions that mediate low μM affinity interactions to globular domains of other proteins. Many of them are unfolded in solution, however, parts of the protein that are close to the motif adopt secondary structure upon binding. This fold can then exert additional affinity and play a role as specificity factor. Similarly to GW182 proteins, those motifs occur in multiple copies to mediate high affinity interactions.
Recently, a direct interaction between the decapping factor DCP1 and the exonuclease XRN1 was identified, which couples mRNA decapping to 5' exonucleolytic degradation [18]. The authors presented a NMR structure oft the *D. melanogaster* proline-rich DCP1-binding motif (DBM) of XRN1 bound to the hydrophobic cleft of the DCP1 EVH1 domain. The XRN1 DBM peptide is unfolded in the free state but, after binding, partially folds upstream to its proline-rich sequence into a helix. This leads to additional contacts of the XRN1 DBM peptide on DCP1 EVH1 that contribute to affinity, specificity and determination of the peptide orientation. It was further discovered that the XRN1 motifs required for DCP1 binding differ in different species (*D. melanogaster* and *H. sapiens*), however, fulfilling the same function. This evolutionary plasticity might also explain contradicting results when mapping the Ago binding site on GW proteins in different species.
Several other studies report similar results, e.g. the crystal structure of the human DDX6 C-terminal RecA-like domain bound to a highly conserved FDF sequence motif in the decapping activator EDC3 [208] or the yeast EDC3 LSm domain in complex with a short helical leucine-rich motif (HLM) from DCP2 [67].
In agreement with that, TNRC6B 606-621, lying upstream to W623 and W634, is not only affected in NMR titration experiments but the very N-terminus of this part (residues VLQTLLS) also shows a greater flexibility in relaxation experiments in comparison to the other residues.
The european linear motif (ELM) data bank lists this sequence as nuclear receptor box motif (LXXLL) that confers binding to nuclear receptors. Usually, this motif is exposed and resides in natively disordered polypeptides.
As an example, Figure 3.4.3 shows the structure of the glucocorticoid receptor ligand binding domain bound to a TIF2 coactivator motif (PDB: 1M2Z).

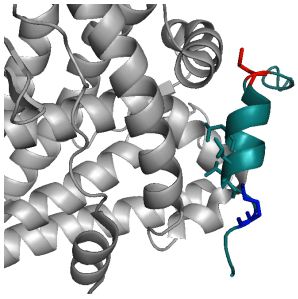

Figure 3.4.3: Exemplary crystal structure for LXXLL motif binding. Crystal structure of the glucocorticoid receptor ligand binding domain (gray) bound to a TIF2 coactivator motif (cyan) (PDB: 1M2Z). Residues comprising the charge-clamp are highlighted in red (Glu) and blue (Lys).

The LXXLL peptide forms an alpha helix that binds via its three Leu to a hydrophobic groove positioned by a so-called charge-clamp.
TNRC6B 599-681 is unfolded in free form and might also adopt secondary structure after binding. The VLQTLLS stretch could potentially form an alpha helix as shown in Figure 3.4.3, positioned by the negatively charged D599 and the positively charged R610.
Taking a closer look at the TNRC6B sequence, the distance upstream to W623 to the next Trp containing the VLQTLLS stretch is remarkably big in comparison to the spacing between the Trps in surrounding regions, allowing formation of secondary structure (Figure 3.4.2).
Corresponding to considerations about the Ago2 surface above, the groove between PIWI and MID domain below the Trp binding pockets might be a possible binding site for this additional interactions. Extra contacts might serve as specificity factor towards other GW regions in Ago binding. e.g. the Not1 binding sites on GW182 identified in two studies [28][57] contain Trps that are important for Not1 interaction, but, at the same time also have affinity towards Ago as shown in Figure 2.3.1. Here, discrimination of Trp-motifs that are either essential for Ago or Not1 interaction would help to further explain GW182 function.
However, another explanation for the results of the titration experiments is that due to the higher flexibility of this part only the dynamic property changes. This would result in lower signals, even if the part is not directly involved in binding. To get a clear picture about the role of this region in Ago binding, further experiments like pulldown assays with protein mutants or NMR titration experiments with much higher concentrations in order to get the structure of bound TNRC6B 599-681 would be required.

3.5 Functional Implications

It has been shown that one Ago protein cannot associate with multiple GW182 molecules [201]. However, we demonstrated that one GW182 protein can potentially bind multiple

Ago proteins as confirmed by other reports [4][45]. In our study, TNRC6B was able to interact with all four human Ago proteins, thus, not having a preference for a specific Ago protein [117].
We found binding of TNRC6B 599-683 and Ago2 with an equilibrium dissociation constant in a low μM range, what is consistent for an interaction of only a small number of residues. The weak affinity might suggest that GW182-Ago binding is a dynamic process with a rapid exchange. This kinetically enhances complex formation which would permit efficient recruitment of the translational repression machinery to the mRNA for several Ago proteins by a single GW182 but also allows the disassembly at a later stage.
Ago and GW182 are enriched in cytoplasmic GW/P-bodies [56][55][194]. This foci are sites of mRNA degradation and silencing [168][50]. Our observation, that TNRC6B formed a hydrogel at very high protein concentrations, could be interpreted in a way that the long unstructured protein forms soluble aggregates at certain conditions. Thereby, it interacts with other GW182 and RBPs [104], which then become visible as GW/P-bodies. Thus, all factors needed for silencing can assemble and are spatially compressed. Hydrogel formation has been shown to be phosphorylation dependent and it is speculated that the dynamics are regulated by post translational modifications [84]. Since GW182 is phosphorylated *in vivo* [55], it is tempting to speculate hydrogel formation to be a major determinant in GW182-dependent gene regulation. However, clarifying this process requires further studies.
Moreover, the TNRC6B599-683 construct, that was characterized in this work might be used as general inhibitor of Ago-GW182 (or GW protein) interaction. Upon further investigation, this fragment could be applied in basic research or medical therapy to prevent downstream processes in miRNA-mediated gene-silencing.

4 Material and Methods

4.1 Material

4.1.1 Consumables and Chemicals

All chemicals were purchased from Amersham Biosciences (Buckinghamshire, UK), Biorad (Hercules, USA), Roth (Karlsruhe, Germany), Merck (Darmstadt, Germany), Qiagen (Hilden, Germany), Roche (Basel, Switzerland), and Sigma-Aldrich (Munich, Germany), unless stated otherwise. Enzymes, nucleotides and molecular weight markers were purchased from New England Biolabs (Ipswich, USA), Invitrogen (Darmstadt, Germany), and Fermentas (Burlington, Canada). Components for bacterial growth media were ordered from Becton Dickinson (Heidelberg, Germany). Insect cell media were obtained from Invitrogen and Thermo Scientific (Waltham, USA). Equipment for liquid chromatography was purchased from GE Healthcare (Munich, Germany). DNA oligonucleotides were synthesized by Metabion (Martinsried, Germany), and Thermo Scientific. Peptides were provided by Peptide Specialty Laboratories (Heidelberg, Germany), and the peptide service of the Core Facility at the Max Planck Institute of Biochemistry (Martinsried, Germany). Peptide arrays were obtained from JPT Peptide Technologies (Berlin, Germany).

4.1.2 Oligonucleotides

Oligonucleotides for cloning:

Name	Sequence (5'—> 3')
JP_O1	GATCGGATCCTATGGATGCTGATTCTGCC
JP_O2	GATGGTCGAGTTACATGGACTCTCCACC
JP_O3	GATCGGATCCTATGAGAGAGAAGGAGCAAG
JP_O4	GATCAAGCTTTCAGATTGAATCCGACCC
JP_O5	GATCGGATCCTATGAGGAAACAATGATTCATGGATC
JP_O6	CCAGGGGCCCGACTCGATGAGAGAGAAGGAGCAA
JP_O7	CAGACCGCCACCGACTGCTTAATTCATCCATGAATCATTGT
JP_O8	GATCGTCGACTTATGGCTACAGGGAGTGA
JP_O9	GATCAAGCTTCTACAGGGACTCCCCGCT
JP_O10	GATCGGATCCATGAGAATAACAAATTGGCTTGTT
JP_O11	GATCGAATTCCTATTGTGCAAAGAAACGACTG
JP_O12	GATCGGATCCATGCGTCCTAGTTACTGGCT
JP_O13	GATCGAATTCCTATTGTGCCAGAAAGCGG
JP_O14	GATCGGATCCATGAGAACCAGCAGCTGGC
JP_O15	GATCGAATTCCTATTGGGCTAAGAAGCGATT
JP_O16	CCAGGGGCCCGACTCGATCCATTGTCAGGCTGTCTTGCAG
JP_O17	CAGACCGCCACCGACTGCTTAGAGCTCCCCCCATCCAGA
JP_O18	CCAGGGGCCCGACTCGATGGGGCCACAGCCTGCAACA
JP_O19	CAGACCGCCACCGACTGCTTAATTCTTATCCCACAGATTCACATTC
JP_O20	ATCTGGCCGGCCCATGGAAGCGGGACCCTCGGGAGCAG
JP_O21	ATCTGGCGCGCCTTATCAAGCGAAGTACATGGTGCGCAGAG
JP_O22	ATCTGGCCGGCCCATGTACTCGGGAGCCGGCCCCGCAC
JP_O23	ATCTGGCGCGCCTTATCAAGCAAAGTACATGGTGCGCAGAGTG
JP_O24	ATCTGGCCGGCCCATGGAAATCGGCTCCGCAGGACCC
JP_O25	ATCTGGCGCGCCTCATTAAGCGAAGTACATTGTGCGTAAGGTA
JP_O26	ATCTGGCCGGCCCATGGAGGCGCTGGGACCCGGACCTC
JP_O27	ATCTGGCGCGCCTTATCAGGCAAAATACATCGTGTGCTGGGTATC

Oligonucleotides for Quickchange Mutagenesis:

Name	Sequence (5'—> 3')
JP_O28	CTCTCAAACACTGGCGCCGGCCAAACTCAAATT
JP_O29	AATTTGAGTTTGGCCGGCGCCAGTGTTTGAGAG
JP_O30	AAGCAGGACACAGTGGCCGACATTGAAGAGGTG
JP_O31	CACCTCTTCAATGTCGGCCACTGTGTCCTGCTT
JP_O32	AAAGGAACTGAGGGGGCCGAGAGCGCTGCCACA
JP_O33	TGTGGCAGCGCTCTCGGCCCCCTCAGTTCCTTT
JP_O34	AAGAACTCAGGGGGCGCCGGAGATGCACCCAGC
JP_O35	GCTGGGTGCATCTCCGGCGCCCCCTGAGTTCTT
JP_O36	CAAATGAAGTCTGGAGCCGGGGAGCTCTGA
JP_O37	TCAGAGCTCCCCGGCTCCAGACTTCATTTG
JP_O38	CTCTCAAACACTGGCTGGGGCCAAACTCAAATT
JP_O39	AATTTGAGTTTGGCCCCAGCCAGTGTTTGAGAG
JP_O40	AAGCAGGACACAGTGTGGGACATTGAAGAGGTG
JP_O41	CACCTCTTCAATGTCCCACACTGTGTCCTGCTT
JP_O42	AAAGGAACTGAGGGGTGGGAGAGCGCTGCCACA
JP_O43	TGTGGCAGCGCTCTCCCACCCCTCAGTTCCTTT
JP_O44	AAGAACTCAGGGGGCTGGGGAGATGCACCCAGC
JP_O45	GCTGGGTGCATCTCCCCAGCCCCCTGAGTTCTT

4.1.3 Plasmids

All plasmids created are based on the following vectors:

Name	Application	Tag	Cleavable	Source
pEC-K-3C-GST	Bacterial expression of proteins	N-terminal 6xHis+GST	3C	Elena Conti
pGEX-6P-1	Bacterial expression of proteins	N-terminal GST	3C	GE Healthcare
pFastBacHTA	Insect cell expression of proteins	N-terminal 6xHis	TEV	Invitrogen

Cloned plasmids:

Name	Insert	Vector	Primer	Insertion sites
JP_P1	TNRC6A	pFastBacHTA	JP_O1, JP_O2	BamHI, XhoI
JP_P2	TNRC6A 1525-1609	pGEX-6P-1	JP_O10, JP_O11	BamHI, EcoRI
JP_P3	TNRC6B	pFastBacHTA	JP_O3, JP_O4	BamHI, HindIII
JP_P4	TNRC6B 1-1007	pEC-K-3C-GST	JP_O3, JP_O7	LIC 3C
JP_P5	TNRC6B 1000-1723	pFastBacHTA	JP_O5, JP_O4	BamHI, HindIII
JP_P6	TNRC6B 599-683	pEC-K-3C-GST	JP_O16, JP_O17	LIC 3C
JP_P7	TNRC6B 861-911	pEC-K-3C-GST	JP_O18, JP_O19	LIC 3C
JP_P8	TNRC6B 1635-1619	pGEX-6P-1	JP_O12, JP_O13	BamHI, EcoRI
JP_P9	TNRC6C	pFastBacHTA	JP_O8, JP_O9	BamHI, HindIII
JP_P10	TNRC6C 1511-1595	pGEX-6P-1	JP_O14, JP_O15	BamHI, EcoRI
JP_P11	Ago1	pFastBacHTA	JP_O20, JP_O21	FseI, AscI
JP_P12	Ago2	pFastBacHTA	JP_O22, JP_O23	FseI, AscI
JP_P13	Ago3	pFastBacHTA	JP_O24, JP_O25	FseI, AscI
JP_P14	Ago4	pFastBacHTA	JP_O26, JP_O27	FseI, AscI
JP_P15	TNRC6B 599-683 W623A	JP_P6	JP_O28, JP_O29	LIC 3C
JP_P16	TNRC6B 599-683 W634A	JP_P6	JP_O30, JP_O31	LIC 3C
JP_P17	TNRC6B 599-683 W653A	JP_P6	JP_O32, JP_O33	LIC 3C
JP_P18	TNRC6B 599-683 W666A	JP_P6	JP_O34, JP_O35,	LIC 3C
JP_P19	TNRC6B 599-683 W680A	JP_P6	JP_O36, JP_O37	LIC 3C
JP_P20	TNRC6B 599-683 allA	JP_P6	JP_O28, JP_O29, JP_O30, JP_O31, JP_O32, JP_O33, JP_O34, JP_O35, JP_O36, JP_O37	LIC 3C
JP_P20	TNRC6B 599-683 allA623W	JP_P20	JP_O38, JP_O39	LIC 3C
JP_P21	TNRC6B 599-683 allA634W	JP_P20	JP_O40, JP_O41,	LIC 3C
JP_P22	TNRC6B 599-683 all653A	JP_P20	JP_O42, JP_O43,	LIC 3C
JP_P23	TNRC6B 599-683 allA666A	JP_P20	JP_O44, JP_O45,	LIC 3C
JP_P24	TNRC6B 599-683 allA680W	JP_P6	JP_O28, JP_O29, JP_O30, JP_O31, JP_O32, JP_O33, JP_O34, JP_O35,	LIC 3C

4.1.4 Antibodies

Name	Origin	Source
anti-hAgo2 (11A9)	rat monoclonal hybridoma supernatant	Dr. Elisabeth Kremmer [11]
anti-rat IgG	goat, peroxidase conjugated	Jackson Lab. West Grove, USA

4.1.5 Bacterial Strains and Cell Lines

Bacterial strains:

Strain	Species	Genotype
XL1-blue	E. coli	recA1 endA1 gyrA96 thi-1 hsdR17 supE44 relA1 lac [F'proAB lacIqZΔM15 Tn10 (Tetr)]
BL21 (DE3) Star	E. coli	F-ompT hsdSB(rB-, mB-) gal dcm rne131
BL21 (DE3) Gold pRARE	E. coli	B F- dcm+ Hte ompT hsdS(rB- mB-) gal endA Hte [argU ileX leuW proL metT glyT tyrU thrU Camr]
DH10Bac	E. coli	F- mcrA Δ(mrr-hsdRMS-mcrBC) Θ80lacZΔM15 ΔlacX74 recA1 endA1 araD139 Δ(ara, leu)7697 galU galK λ- rpsL nupG /pMON14272 / pMON7124

Cell lines:

Cell line	Description
Sf21	Derived from Spodoptera frugiperda ovarian cells. Used to isolate and propagate recombinant baculovirus stocks.
High Five	Derived from the Trichopulsia in cell line. Used to express recombinant proteins upon baculovirus infection.
HeLa	Derived from cervical cancer cells from Henrietta Lacks. Used for whole cell lysate preparation.

4.1.6 Media and Buffers

Medium	Composition	Cell type
LB	1% (w/v) Bacto Trypton, 0.5% (w/v)\ NaCl, 0.5% (w/v)\ Yeast extract	E. coli
Minimal medium	10% M9 medium (10x), 1% trace elements solution, 0.4% (w/v) ^{13}C glucose, 1 mM $MgSO_4$, 0.3 mM $CaCl_2$, 1 μg/ml Biotin, 1 μg/ml Thiamine	E. coli
M9 medium (10x)	0.44 M Na_2HPO_4, 0.22 mM KH_2PO_4, 85 mM NaCl, 95 mM $^{15}NH_4Cl$	E. coli
Trace elements solution (100x)	17 mM EDTA, 3 mM $FeCl_3$, 0.6 mM $ZnCl_2$, 76 μM $CuCl_2$, 42 μM $CoCl_2$, 0.16 mM H_3BO_3, 8.2 μM $MnCl_2$	E. coli
SOC	2% (w/v) Bacto Trypton, 0.05% (w/v) NaCl, 0.5% (w/v) Yeast extract, 2.5 mM KCl, 10 mM $MgCl_2$, 20 mM glucose	E. coli
Sf-900 III SFM	Protein-free insect cell culture medium	insect cells
HyClone SFX	Protein-free insect cell culture medium	insect cells
DMEM	DMEM with high glucose (PAA, Pasching, Austria) with 10% fetal bovine serum (Biochrom, Berlin, Germany) and 10% Penicillin/Streptomycin	mammalian cells

Buffer	Composition	Application
Ni-A	20 mM HEPES/NaOH (pH 7.5), 300 mM NaCl, 10mM Imidazole, 2mM ßMe	Protein purification
Ni-A salt	20 mM HEPES/NaOH (pH 7.5), 1 M NaCl, 10mM Imidazole, 2mM ßMe	Protein purification
Ni-A ATP	20 mM HEPES/NaOH (pH 7.5), 300 mM NaCl, 150 mM KCl, 2mM ATP, 10 mM $MgSO_4$, 10mM Imidazole, 2mM ßMe	Protein purification
Ni-B	20 mM HEPES/NaOH (pH 7.5), 300 mM NaCl, 250mM Imidazole, 2mM ßMe	Protein purification
GST-A	20 mM HEPES/NaOH (pH 7.5), 300 mM NaCl, 5mM DTT	Protein purification
GST-B	20 mM HEPES/NaOH (pH 7.5), 300 mM NaCl, 25 mM glutathione, 1mM DTT	Protein purification
SEC	20 mM HEPES/NaOH (pH 7.5), 150 mM NaCl, 1mM DTT	Protein purification
NMR	20 mM NaH_2PO_4 /Na_2HPO_4 (pH 6.0), 150 mM NaCl, 1mM DTT	Protein purification
CD	10 mM NaH_2PO_4 /Na_2HPO_4 (pH 7.5)	Protein purification
PBS	3.2 mM Na_2HPO_4, 0.5 mM NaH_2PO_4 (pH 7.4), 135 mM NaCl, 1.3 mM KCl	Cell culture
Lysis buffer	20 mM HEPES/NaOH (pH 7.4), 150 mM KCl, 2 mM EDTA, 1mM NaF, 0.5% (v/v) NP-40, 5% (v/v) glycerol	Cell culture
TBE	89 mM Tris-HCl (pH 6.8), 89 mM boric acid, 2.5 mM EDTA	DNA elektrophoresis
TGS	25 mM Tris-HCl (pH 8.6), 192 mM glycine, 0.1 % SDS	Protein elektrophoresis
Silver fix	50 % (v/v)\ methanol, 12 % (v/v) acetic acid, 0.5ml/l 37% formaldehyde	Silver staining
Silver wash	30 % ethanol	Silver staining
Silver thio	0.2 g/l NaS_2O_3, 0.5 ml/l 37 % formaldehyde	Silver staining
Silver nitrate	0.2 g/l $AgNO_3$, 0.75ml/l 37 % formaldehyde	Silver staining
Silver dev	60 g/l $NaCO_3$	Silver staining
Silver stop	50 % (v/v) methanol, 12% (v/v) acetic acid	Silver staining
TBS-T	20 mM Tris-HCl (pH7.6), 137 mM NaCl, 0.1% (v/v) Tween-20	Western blotting

4.2 Methods

4.2.1 Molecular Biology Methods

Standard molecular biology methods were performed as described by Sambrook et al. [186]. Genes were amplified from template DNA using Phusion^{TM} DNA Polymerase (Finnzymes, Espoo, Finnland), analyzed by agarose gel electrophoresis in 1x TBE running buffer. After staining with GelRed (Biotium), PCR products were purified with the NucleoSpin gel and PCR clean-up kit (Macherey Nagel, Düren, Germany).
For conventional cloning, vector DNA and PCR products were digested with the respective restriction enzymes and ligated using T4 DNA Ligase (Fermentas, Burlington, Canada) according to the manufacturer's instructions.
For ligation independent cloning (LIC) (Aslanidis and deJong, 1990) the pEC series of vectors generated by Jerome Basquin and Florence Martin in the laboratory of Elena Conti was used according to the following protocol.

Processing of insert:

Component	Amount
gel purified PCR product	600 ng
T4 DNA Pol. buffer (10x)	2 μl
dATP (25 mM)	2 μl
DTT (100 mM)	1 μl
T4 DNA Pol. LIC qualified (Novagen)	0.4 μl
H_2O	add to 20 μl

Vector processing:
Before processing, 2 ug vector were linearized by digestion with 60 u of SacII (or 20 u ZraI for 3C LIC vectors) and gel purified

Component	Amount
linearized vector	450 ng
T4 DNA Pol. buffer (10x)	3 ul
dTTP (25 mM)	3 μl
DTT (100 mM)	1.5 μl
T4 DNA Pol. LIC qualified (Novagen)	0.6 μl
H_2O	add to 30 μl

After incubation for 30 min at RT, reaction mixes were inactivated at 75°C for 20 min. For annealing, 2 μl of processed insert and processed vector were incubated for 10 min at RT. 1 μl EDTA (25 mM) was added and the mix was incubated for 10 min at RT. For transformation into *E. coli* 2 μl were used.
Point mutations were introduced using the QuickChange II site directed mutagenesis kit (Agilent Technologies).
Plasmids were transformed into chemically competent *E. coli* cells prepared according to Hanahan, 1983 [85]. Isolation of plasmid DNA was carried out using the NucleoBond® XtraMini Kit (Macherey Nagel, Düren, Germany). The success of the cloning procedure was confirmed by DNA sequencing (Core Facility at the Max Planck Institute of Biochemistry or Eurofins MWG Operon).

4.2.2 Protein Expression

Protein Expression in *E. coli*

For all constructs in the present work, expression was first tested in small scale with conditions. Expression levels were assessed by small-scale pull down experiments with the appropriate affinity resin.
For large scale expression, colonies of freshly transformed BL21(DE3) Gold pRARE were used to inoculate 20 ml LB medium supplemented with the respective antibiotics over night. 3 l of LB medium were inoculated 1:1000 with preculture and then grown in baffled Erlenmeyer flasks at 37°C under constant agitation (160 rpm). At an OD_{600} of about 0.4 the culture was cooled to 18 °C. Expression was induced at an OD_{600} of 0.7 by adding 0.1 mM Isopropyl-β-D- thiogalactopyranosid (IPTG). After 10 h cells were harvested (4400 x g, 15 min, 4°C), flash frozen with liquid nitrogen, and stored at -80°C. For NMR spectroscopy experiments TNRC6B 599-683 was $^{15}N^{13}C$-labeled during protein expression in minimal medium. As preculture, freshly transformed *E. coli* BL21 (DE3) Gold pRARE cells carrying the plasmid JP_P6 were grown in 20 ml medium containing 1:1000 kanamycin (50mg/ml) and chlormaphenicol (34 mg/ml) over night at 37 °C. One liter of minimal medium supplemented 1:1000 with kanamycin (50mg/ml) and chlormaphenicol (34 mg/ml) was inoculated with 5 ml of the preculture and grown at 37°C to an OD_{600} of 0.8. After induction of expression with 0.1 mM IPTG, cells were grown for 10 h, harvested (4400 x g, 15 min, 4°C), flash frozen with liquid nitrogen, and stored at -80°C.

Protein Expression in Insect Cells

Recombinant baculovirus was prepared essentially as described in the Bac-to-Bac manual (Invitrogen). A culture of 500 ml High Five cells with a density of 1x 10^6 cells/ml was infected with 30 ml P2 viral stock and cultivated for 72 h at 27.5 °C with 85 rpm shaking. Cells were then harvested (1000 x g, 20 min), flash frozen with liquid nitrogen and stored at -80°C.

Culturing Mammalian Cells

Mammalian cells were cultured in DMEM at 37° C and 5% CO_2. In order to split cells, the medium was removed, cells were washed once with PBS and were detached by treatment with Trypsin-EDTA (PAA, Pasching, Austria). Detached cells were pelleted

by centrifugation at 200 x g for 5 min and plated on fresh plates.
For whole cell lysate preparation, cells were cultured to 80-90% density, washed three times with PBS, scraped off and pelleted at 200 x g for 10 min. Cell pellets were flash frozen in liquid nitrogen and stored at -80°C. 3 ml of cell pellet was then thawed on ice, resuspended in 15 ml lysis buffer freshly supplemented with DTT and protease inhibitor (Roche, Basel, Switzerland) by pipetting up and down and incubated on ice for 20 min. Cell debris was pelleted by centrifugation (17000 x g, 10min, 4°C) and the supernatant was transferred to a fresh reaction tube.

4.2.3 Protein Purification

Purification of proteins expressed in *E. coli*

Proteins were expressed in *E. coli* BL21 (DE3) Gold pRARE cells according to the protocol detailed above. All steps were carried out at 4 °C. Typically, 3 l of culture were resuspended in GST-A buffer supplemented with one tablet of EDTA-free protease inhibitor cocktail (Roche, Basel, Switzerland) and 0.4 mM PMSF to a total volume of 100 ml. After sonication (4 x 4 min, amplitude 30%, output: 6), the lysate was clarified by centrifugation (39000 x g, 30 min), loaded onto two 5 ml GSTrap columns (GE Healthcare) connected in series, equilibrated in buffer GST-A, and washed with 20 column volume (cv) of GST-A. His-GST tagged protein was eluted in 5 cv of buffer GST-B. For tag cleavage, a volume of 5 ml GST-A supplemented with 100 µg of 3C (PreScission) protease was applied to the column. Both ends of the column were connected and the flow rate was set to 0.3 ml/min for 10 h. Cleaved protein was eluted directly on a 5 ml HisTrap column (GE Healthcare) collecting the flow through.
Proteins were filtered with a 0.22 µM filter, and concentrated by ultrafiltration with an Amicon Ultra centrifugal filter (Milipore, Billerica, MA, USA). Finally, purification was completed by size exclusion chromatography (Superdex 75 10/300 gl) carried out in SEC buffer. Purified protein was usually concentrated to 5-10 mg/ml by ultrafiltration. Quality was ensured by SDS-gel electrophoresis and UV-spectroscopy. Aliquots were flash frozen in liquid nitrogen and stored at -80°C.

Purification of Proteins Expressed in Insect Cells

All steps were carried out at 4 °C. Insect cell pellets of 5 l culture were resuspended in Ni-A buffer supplemented with one tablet of EDTA-free protease inhibitor cocktail and 0.4 mM PMSF to a total volume of 300 ml. After sonication (4 x 1 min, amplitude 30%,

output: 6), lysate was clarified by centrifugation (39000 x g, 45 min) and applied onto a XK16/20 column (GE Healthcare) filled with 5 ml of Ni-resin (GE Healthcare), following three washing steps with buffers Ni-salt, Ni-ATP and 8% Ni-B and elution in 5 cv Ni-B. For purification of Ago proteins, the eluate was supplemented with 100 µg of TEV protease and dialyzed against 2 l buffer SEC containing 2 mM EDTA. After incubation, the sample was passed over a HisTrap column (GE Healthcare). Unbound flow through was collected, concentrated and resolved by size exclusion chromatography (Superdex 200 10/300 gl) in SEC buffer. The protein was pure as assayed by SDS gel electrophoresis and was concentrated to 1-5 mg/ml, flash frozen with liquid nitrogen and stored at 80°C.

4.2.4 Protein Biochemistry

Concentration Determination

Protein concentration was determined by measurement of the A_{280} using the NanoDrop ND-1000 UV-Vis spectrophotometer (Peqlab) or by Bradford Protein Assay (Biorad, Hercules, USA). The respective extinction coefficient was calculated with ProtParam (www.expasy.org).

Gel Electrophoresis and Protein Visualisation

Depending on size, proteins were separated on 8% -19% sodium SDS-gels as described by Laemmli, 1970 [116]. Coomassie staining of gels was performed with PageBlue protein Staining solution (Thermo Scientific).
For silver staining gels were fixed in Silver fix buffer for 1 h and washed with buffer Silver wash three times for 20 min . Silver thio buffer was applied for 1 min followed by rinsing three times with water for 20 sec. After soaking with buffer Silver nitrate for 20 min, the gel was rinsed with water two times for 20 sec. Developer (Silver dev) was applied until the desired stain intensity was reached and the reaction was stopped by discarding the developer followed by rinsing with water. The gel was then incubated in stopping solution (Silver stop) for 10 min and transferred into water.

Analytical Limited Proteolysis

For analytical limited proteolysis 10 μl protein (0.6 mg/ml) were subjected to protease of different concentrations (0.1 mg/ml, 0.01 mg/ml, 0.001 mg/ml) in SEC buffer. After

incubation on ice for 30 min, the reaction was stopped by addition of 1μl 100 mM 4-(2-Aminoethyl) benzenesulfonyl fluoride hydrochloride (AEBSF). Samples were separated by SDS-gel electrophoresis.

In Vitro Pull-down Assay

For each pulldown, the respective resin was washed two times (5000 x g, 1 min) with water and two times with SEC buffer. For pull-down from whole cell lysate, an excess of GST-tagged protein was bound to 50 μl Glutathione Sepharose 4B beads (GE Healthcare) for 1h at 4°C, washed three times with SEC buffer and added to 15 ml whole cell lysate, followed by incubation for 3 h on a rotating wheel at 4°C.
Recombinant proteins were mixed in a total volume of 100 μl and incubated for 30 min on ice. The resin was resuspended in SEC buffer, added to the protein mixture and incubated for 1 h on a rotating wheel.
After incubation, the resin was washed twice with 1 ml SEC buffer and once with 1 ml SEC buffer supplemented with additional 150 mM NaCl. The supernatant was removed and bound protein was eluted either by boiling for 10 min in 5x SDS loading dye or by addition of 50 μl SEC buffer containing 500 mM imidazole (for His-tagged proteins) or 50 mM GSH (for GST-tagged proteins). Eluted protein samples were analyzed by SDS gel electrophoresis.

Peptide Array

Custom peptide membranes were obtained from JPT Peptide Technologies GmbH (Berlin, Germany). For mapping protein interaction sites, the sequence of the desired protein was synthesized as linear 20 meric peptides that are redundantly displayed overlapping in 15 residues. Peptides were C-terminally covalently bound to a cellulose-PEG-membrane and N-terminally acetylated. Each of the spots carried approximately 5 nmol of peptide. Prior use, the membrane was rinsed with a small volume of methanol, subsequently equilibrated three times with TBS for 5 min and blocked with TBS containing 1% (w/v) milk powder at RT. Before incubation with the protein, peptides were first checked for unspecific interactions with antibodies used for detection of the bound protein. For this, the membrane was incubated in TBS 1% (w/v) milk powder supplemented with Ago2 (11A9, 1.5 mg/ml) primary antibody diluted 1:1000 for 2 h. Following three washing steps with TBS-T, the membrane was subjected to peroxidase-conjugated anti-rat antibody in TBS1% (w/v) milk powder according to the manufacturers instructions. Three washing steps with TBS-T removed unbound antibody. Visualization was achieved using the Pierce ECL substrate (Thermo Scientific). The membrane was then either exposed

to light-sensitive films (GE Healthcare) or analyzed with the LAS-3000 mini imaging system (Fujifilm, Düsseldorf, Germany).
Removal of bound antibody was achieved by incubation with buffer containing SDS and ß-Me at 50°C for four times 30 min each. The membrane was subsequently incubated in 10x PBS (3 x 20 min) followed by a washing step in TBS-T (20 min) and TBS (5 x 10 min). To analyze protein-protein contacts, prior to incubation with the primary antibody, the membrane was incubated overnight at 4°C with 30 µg/ml Ago2 protein in TBS with 1% (w/v) milk powder and washed three times in TBS-T for 5 min at RT. Detection of bound Ago2 was achieved as described above. Quantification of signals was carried out with the ImageJ software (http://rsb.info.nih.gov/ij/).

Circular Dicroism Spectroscopy

Secondary structure was analyzed by circular dicroism spectroscopy (CD)-spectroscopy. Proteins were desalted into CD buffer using SEC (Superdex 75 10/300 gl). Protein concentration was adjusted to a final concentration of 0.3 mg/ml and CD spectra were recorded in a 0.5 mm cuvette on a JASCO CD-spectrometer (260-195 nm, 0.1 nm data pitch, accumulation: 10, bandwidth 1nm, 20°C).

Dynamic Light Scattering

To determine the size distribution of particles in solution, dynamic light scattering (DLS) was performed using a PDDLS/cool Batch 90T with PD 2000 DLS Plus detector system. After centrifugation (20000 x g, 20 min), samples were mixed and measured in a micro cuvette at 20°C. Ten measurements were recorded and the distribution of the hydrodynamic radius was obtained from the autocorrelation function using the Precision Deconvolve32 Software (Precision Detectors, Bellingham, USA).

Fluorescence Polarization

For fluorescence polarization (FP) measurements, TNRC6B 599-683 was Cys labeled with Atto488 Maleimid (Atto-Tec). Measurements were performed at 20°C in 70 μl reactions on an Envision Multilabel reader (Perkinelmer). Labeled protein was dissolved to a concentration of 50 nM and incubated with increasing Ago2 concentrations in SEC buffer. The excitation and emission wavelengths were 485 nm and 535 nm, respectively. The dissociation constant was calculated by fitting the data with the one-site binding model included in the program origin (OriginLab). The experiment was performed as a duplicate.

Crosslinking and Mass Spectrometry

The Ago2:TNRC6 B599-683 complex was crosslinked using isotopically coded disuccinimidyl suberate (DSS-H12/D12, Creative Molecules Inc.). To screen for ideal crosslinking conditions, proteins were incubated in a 1:1 and 2:1 ratio with a concentration of 1 mg/ml for 30 min. 5 µg of the protein complex was mixed with with 25 mM DSS stock solution dissolved in dimethylformamide (DMF, Pierce Protein Research Products) to a final crosslinker concentration of 0 mM, 0.04 mM, 0.08 mM, 0.16 mM, 0.4 mM, 1 mM, 2 mM and 4 mM, respectively. After incubation (35 min, 30°C, 1000 rpm) the reaction was quenched with 1 μl of 100 mM NH_4HCO_4 (15 min, 30°C, 1000 rpm). The sample was mixed with 7 μl SDS loading dye and 2 μl were resolved on a SDS gel followed by visualization of the bands by silver staining. The best crosslinker concentrations (0.16 mM and 0.4 mM in the 1:1 reaction) converted most of the protein to a higher molecular weight complex but still avoiding oligomerization. For the final reaction 200 µg (1mg/ml) of a 1:1 complex of Ago2 and TNRC6B 599-683 was mixed with DSS to a concentration of 0.16 and 0.4 mM, respectively, and incubated at 1000 rpm for 35 min at 30°C. The reaction was stopped by addition of NH_4HCO_4 to a concentration of 100 mM (15 min, 30°C, 1000 rpm). The crosslinked complex was applied to size exclusion chromatography (Superdex 200 10/300 gl) in SEC buffer (with a NaCl concentration of 300 mM) and separated peaks of crosslinked protein (from 0.16 mM and 0.4 mM DSS reaction) were pooled.
After treatment with two sample volumes of 8 M urea, proteins were reduced and alkylated using 5 mM Tris(2-carboxyethyl)phosphine (TCEP) and 10 mM iodoacetamide, respectively. The sample was digested with Lys-C followed by trypsin after diluting the sample to 1 M urea. Cross-linked peptides were enriched by size exclusion chromatography and analyzed by MS as described previously [88]. Fragment ion spectra were assigned to cross-linked peptides using xQuest [214].

4.2.5 Nuclear Magnetic Resonance

NMR Spectroscopy

Prior to nuclear magnetic resonance (NMR) measurements, 0.02 % NaN3 was added to the sample containing 545 µM TNRC6B 599-683 (20 mM NaP (pH 6.5), 250 mM NaCl, 10% D2O). Measurements for backbone assignments were conducted at 278 K on a Bruker Avance III spectrometer with a magnetic field strength of 800 MHz, equipped with a TCI cryogenic probe head. All data sets were processed using NMRPipe [39]. Sequential resonance assignment was obtained from three-dimensional HNCA, CBCA-

CONH, and HNCACB experiments, employing constant time during ^{13}C evolution [187]. Assignments have been found for 86 % of all residues (excluding prolines, 73 of 85). Missing assignments for residues other than prolines were Q605, L607, W623, G624, W666, G667, N674, K677, W680, and G681. The three GW pairs could not be assigned unambiguously resonances present, due to the high flexibility and the resulting chemical shift degeneracy. These ambiguously assigned Trp resonances do not exhibit intensity changes upon Ago titration. Secondary structure analysis of the free protein was based on the difference of measured $^{13}C_\alpha$ and $^{13}C_\beta$ chemical shifts to random coil chemical shifts of the same nuclei [221]. Resonance assignments of TNRC6 peptides used in saturation transfer difference NMR experiments, were obtained using two dimensional homonuclear TOCSY, NOESY, and ROESY experiments [16][19][222]. Measurements for peptide resonance assignments were conducted at 298 K on Bruker Avance III spectrometers with magnetic field strengths of 500 and 800 MHz, equipped with a TXI cryogenic probe head. All assignments were done using CARA (http://cara.nmr.ch).

Saturation Transfer Difference NMR of TNRC6B Peptides and Argonaute 2

Saturation transfer difference (STD) NMR experiments [143] were performed on TNRC6B peptides and Ago2, ranging in concentrations between 160-625 µM (peptides) and 2-3.5 µM (Ago2) (20 mM NaP (pH 6.5), 250 mM NaCl, 10% D2O) on a Bruker Avance III 500 MHz spectrometer equipped with a TXI cryogenic probe head at 298 K. Protein was saturated by applying a series of 49 ms Gaussian pulses on the resonance frequency of upfield shifted Ago2 methyl resonances (-1 ppm) with a total saturation time between 0.25 s and 15 s. An STD amplification factor, which resembles the relative binding affinity of protons within a peptide, peptides of similar lengths, and different ligand:protein ratios, is calculated according to Mayer et al. [144]. In short, intensities of the STD NMR spectrum are divided by intensities of a reference 1D spectrum (with Gaussian pulses being off-resonance) and multiplied by the ligand excess.

^{15}N Relaxation Measurements of TNRC6 599-683

^{15}N relaxation measurements of free TNRC6B 599-681 were conducted on a Bruker Avance III 800 MHz NMR spectrometer equipped with a TXI cryogenic probe head at 298 K. R_1, R_2, and heteronuclear $^{15}N^1H$ NOEs were measured with gradient-enhanced, sensitivity-enhanced pulse sequences described by Farrow et al. [61] . The ^{15}N longitudinal relaxation rates (R_1) were measured with delays of 22, 43, 86, 173, 260, 346, 518, 691, 994, 1382, 1728, 1944, and 2160 ms, where delays of 22, 173, 346, 518, and 691 ms were measured in duplicates. The ^{15}N transverse relaxation rates (R_s) were measured

with delays of 5, 10, 20, 40, 80, 100, 140, 150, 200, 300, 400, and 500 ms, where delays of 5, 80, 100, and 200 ms were measured in duplicates. Peak volumes were calculated by using the software PINT (in manuscript).

NMR Binding Studies of TNRC6B 599-683 and Argonaute 2

TNRC6B 599-683 and Ago2 binding was monitored by measuring chemical shift perturbations and line width broadening. ^{1}H ^{15}N HSQC spectra were acquired of ^{15}N-labeled TNRC6B 599-683 with different protein ratios (1:0, 1:0.1, 1:1, TNRC6B599-681:Ago2). Measurements were performed on a Bruker Avance III 800 MHz spectrometer equipped with TXI cryogenic probe head at 298 K. Chemical shift perturbations, and peak volumes as a measure of line width were analyzed using SPARKY [75], and atom-specific chemical shift weighting was done according to Mulder et al. [151].

5 Appendix

Sequences TNRC6B and Ago2

>sp|Q9UPQ9|TNRC6B
MREKEQEREEQLMEDKKRKKEDKKKEATQKVTEQKTKVPEVTKPSLSQPTAASPIGSSP
SPPVNGGNNAKRVAVPNGQPPSAARYMPREVPPRFRCQQDHKVLLKRGQPPPPSCMLLGG
GAGPPPCTAPGANPNNAQVTGALLQSESGTAPDSTLGGAAASNYANSTWGSGASSNNGTS
PNPIHIWDKVIVDGSDMEEWPCIASKDTESSSENTTDNNSASNPGSEKSTLPGSTTSNKG
KGSQCQSASSGNECNLGVWKSDPKAKSVQSSNSTTENNNGLGNWRNVSGQDRIGPGSGFS
NFNPNSNPSAWPALVQEGTSRKGALETDNSNSSAQVSTVGQTSREQQSKMENAGVNFVVS
GREQAQIHNTDGPKNGNTNSLNLSSPNPMENKGMPFGMGLGNTSRSTDAPSQSTGDRKTG
SVGSWGAARGPSGTDTVSGQSNSGNNGNNGKEREDSWKGASVQKSTGSKNDSWDNNNRST
GGSWNFGPQDSNDNKWGEGNKMTSGVSQGEWKQPTGSDELKIGEWSGPNQPNSSTGAWDN
QKGHPLPENQGNAQAPCWGRSSSSTGSEVGGQSTGSNHKAGSSDSHNSGRRSYRPTHPDC
QAVLQTLLSRTDLDPRVLSNTGWGQTQIKQDTVWDIEEVPRPEGKSDKGTEGWESAATQT
KNSGGWGDAPSQSNQMKSGWGELSASTEWKDPKNTGGWNDYKNNNSSNWGGGRPDEKTPS
SWNENPSKDQGWGGGRQPNQGWSSGKNGWGEEVDQTKNSNWESSASKPVSGWGEGGQNEI
GTWGNGGNASLASKGGWEDCKRSPAWNETGRQPNSWNKQHQQQQPPQQPPPPQPEASGSW
GGPPPPPPGNVRPSNSSWSSGPQPATPKDEEPSGWEEPSPQSISRKMDIDDGTSAWGDPN
SYNYKNVNLWDKNSQGGPAPREPNLPTPMTSKSASVWSKSTPPAPDNGTSAWGEPNESSP
GWGEMDDTGASTTGWGNTPANAPNAMKPNSKSMQDGWGESDGPVTGARHPSWEEEEDGGV
WNTTGSQGSASSHNSASWGQGGKKQMKCSLKGGNNDSWMNPLAKQFSNMGLLSQTEDNPS
SKMDLSVGSLSDKKFDVDKRAMNLGDFNDIMRKDRSGFRPPNSKDMGTTDSGPYFEKLTL
PFSNQDGCLGDEAPCSPFSPSPSYKLSPSGSTLPNVSLGAIGTGLNPQNFAARQGGSHGL
FGNSTAQSRGLHTPVQPLNSSPSLRAQVPPQFISPQVSASMLKQFPNSGLSPGLFNVGPQ
LSPQQIAMLSQLPQIPQFQLACQLLLQQQQQQQLLQNQRKISQAVRQQQEQQLARMVSAL
QQQQQQQQRQPGMKHSPSHPVGPKPHLDNMVPNALNVGLPDLQTKGPIPGYGSGFSSGGM
DYGMVGGKEAGTESRFKQWTSMMEGLPSVATQEANMHKNGAIVAPGKTRGGSPYNQFDII
PGDTLGGHTGPAGDSWLPAKSPPTNKIGSKSSNASWPPEFQPGVPWKGIQNIDPESDPYV
TPGSVLGGTATSPIVDTDHQLLRDNTTGSNSSLNTSLPSPGAWPYSASDNSFTNVHSTSA
KFPDYKSTWSPDPIGHNPTHLSNKMWKNHISSRNTTPLPRPPPPGLTNPKPSSPWSSTAPR
SVRGWGTQDSRLASASTWSDGGSVRPSYWLVLHNLTPQIDGSTLRTICMQHGPLLTFHLN
LTQGTALIRYSTKQEAAKAQTALHMCVLGNTTILAEFATDDEVSRFLAQAQPPTPAATPS
APAAGWQSLETGQNQSDPVGPALNLFGGSTGLGQWSSSAGGSSGADLAGASLWGPPNYSS
SLWGVPTVEDPHRMGSPAPLLPGDLLGGGSDSI

>sp|Q9UKV8|AGO2
MYSGAGPALAPPAPPPPIQGYAFKPPPRPDFGTSGRTIKLQANFFEMDIPKIDIYHYELD
IKPEKCPRRVNREIVEHMVQHFKTQIFGDRKPVFDGRKNLYTAMPLPIGRDKVELEVTLP
GEGKDRIFKVSIKWVSCVSLQALHDALSGRLPSVPFETIQALDVVMRHLPSMRYTPVGRS
FFTASEGCSNPLGGGREVWFGFHQSVRPSLWKMMLNIDVSATAFYKAQPVIEFVCEVLDF
KSIEEQQKPLTDSQRVKFTKEIKGLKVEITHCGQMKRKYRVCNVTRRPASHQTFPLQQES
GQTVECTVAQYFKDRHKLVLRYPHLPCLQVGQEQKHTYLPLEVCNIVAGQRCIKKLTDNQ
TSTMIRATARSAPDRQEEISKLMRSASFNTDPYVREFGIMVKDEMTDVTGRVLQPPSILY
GGRNKAIATPVQGVWDMRNKQFHTGIEIKVWAIACFAPQRQCTEVHLKSFTEQLRKISRD
AGMPIQGQPCFCKYAQGADSVEPMFRHLKNTYAGLQLVVVILPGKTPVYAEVKRVGDTVL
GMATQCVQMKNVQRTTPQTLSNLCLKINVKLGGVNNILLPQGRPPVFQQPVIFLGADVTH
PPAGDGKKPSIAAVVGSMDAHPNRYCATVRVQQHRQEIIQDLAAMVRELLIQFYKSTRFK
PTRIIFYRDGVSEGQFQQVLHHELLAIREACIKLEKDYQPGITFIVVQKRHHTRLFCTDK
NERVGKSGNIPAGTTVDTKITHPTEFDFYLCSHAGIQGTSRPSHYHVLWDDNRFSSDELQ
ILTYQLCHTYVRCTRSVSIPAPAYYAHLVAFRARYHLVDKEHDSAEGSHTSGQSNGRDHQ
ALAKAVQVHQDTLRTMYFA

Secondary structure prediction TNRC6B

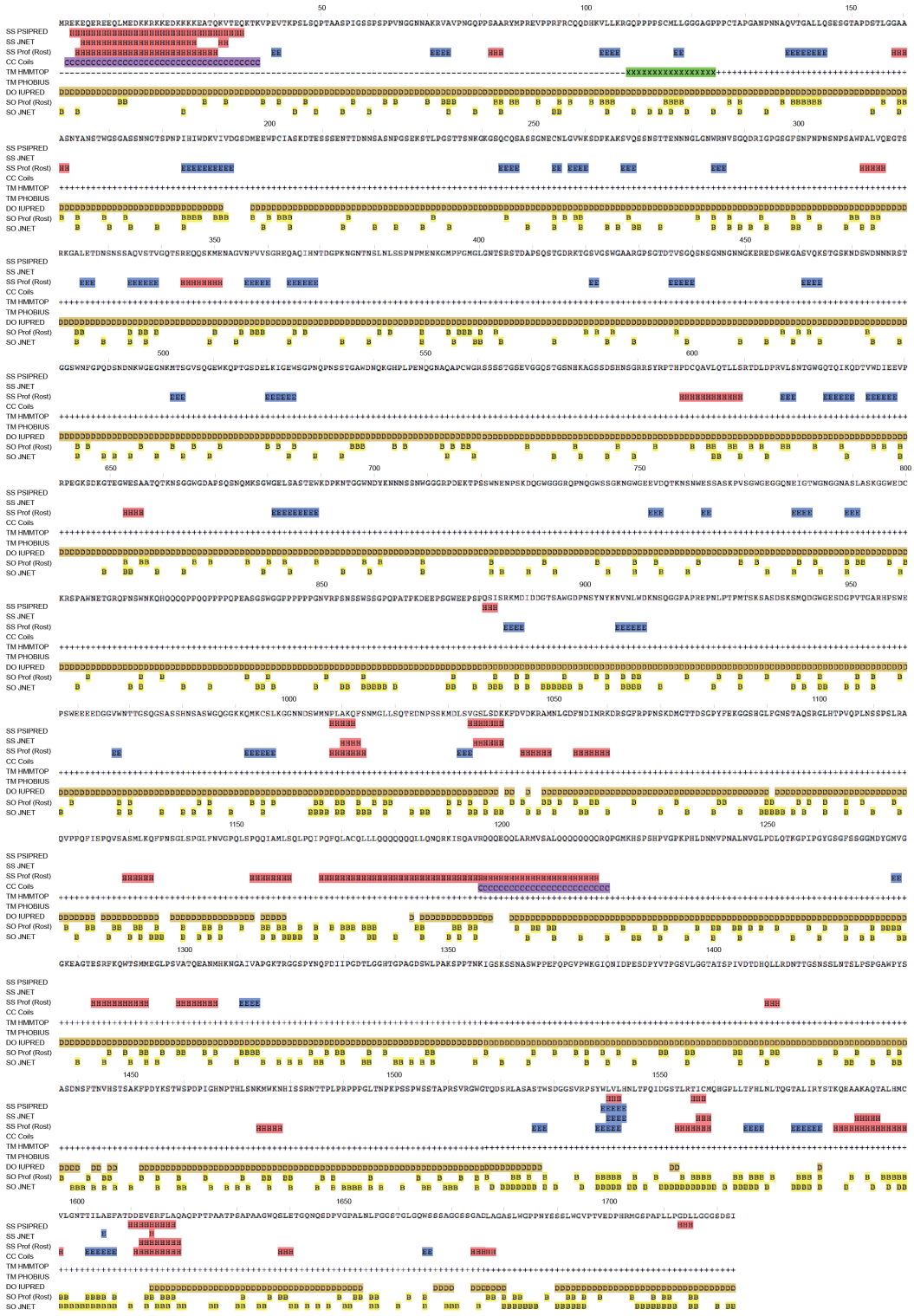

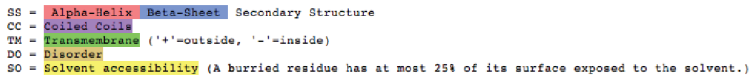

Figure 5.0.1: Secondary structure prediction of TNRC6B. Secondary structure prediction was performed with the program Quick2D [10] using different prediction algorithms for secondary structure (SS), coiled-coils (CC), and disordered (DO) regions. Structural features are color coded.

Secondary structure prediction Ago2

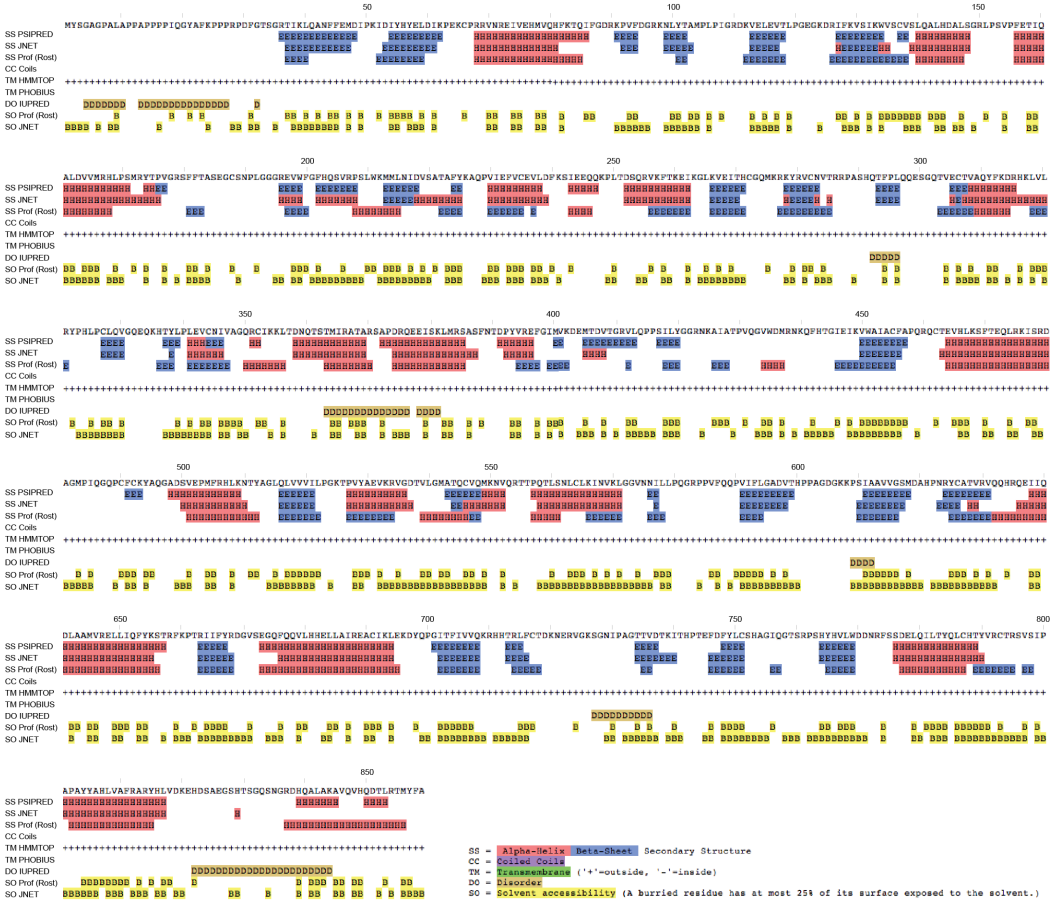

Figure 5.0.2: Secondary structure prediction of Ago2. Secondary structure prediction was performed with the program Quick2D 2006 using different prediction algorithms for secondary structure (SS), coiled-coils (CC), and disordered (DO) regions. Structural features are color coded.

Multiple sequence alignment TNRC6B

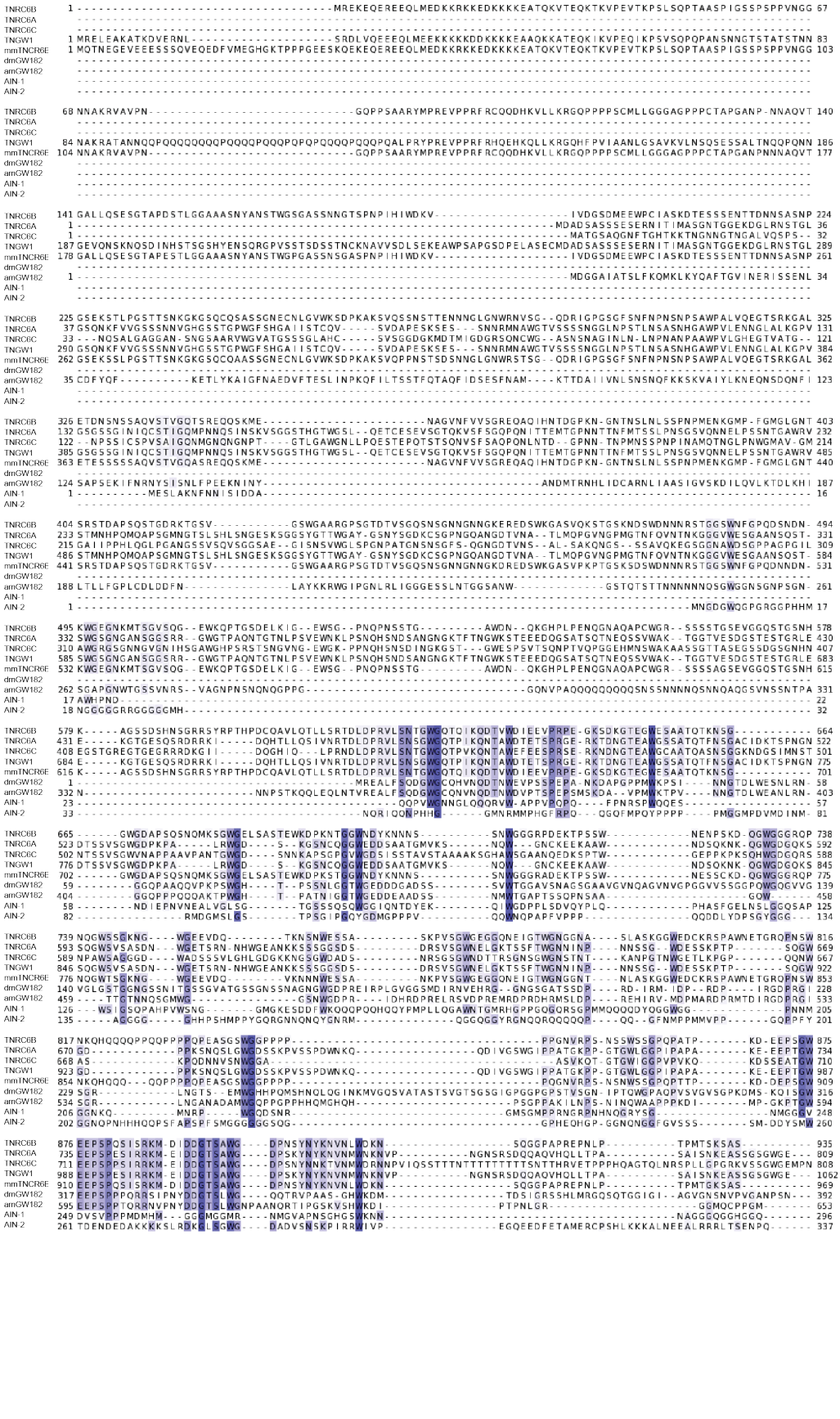

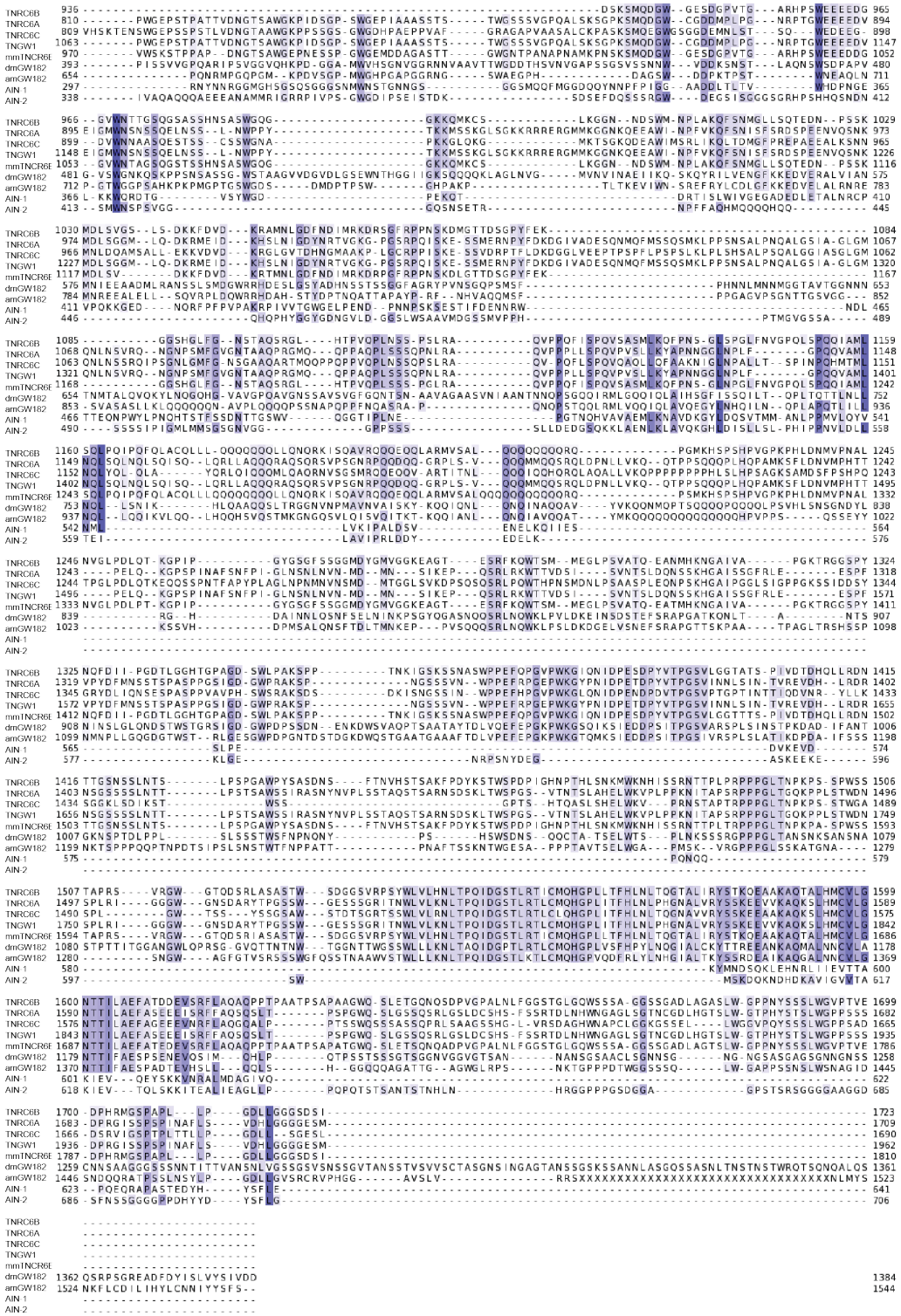

Figure 5.0.3: Multiple sequence alignment of TNRC6B homologues. TNRC6B homologues from selected organisms were aligned with MAFFT [105] using the Jalview software [216]. Conserved sequence motifs are shaded in blue.

Multiple sequence alignment Ago2

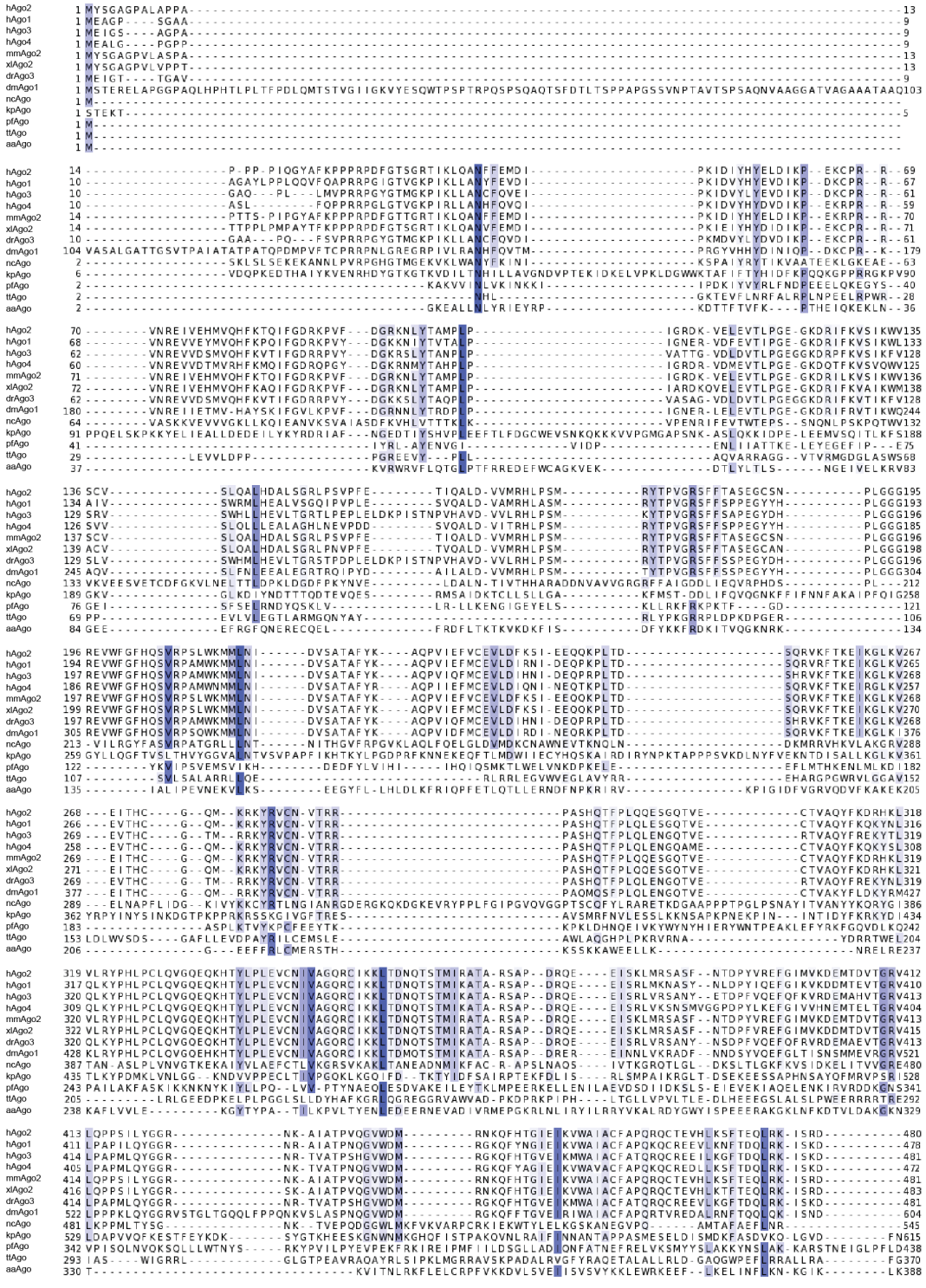

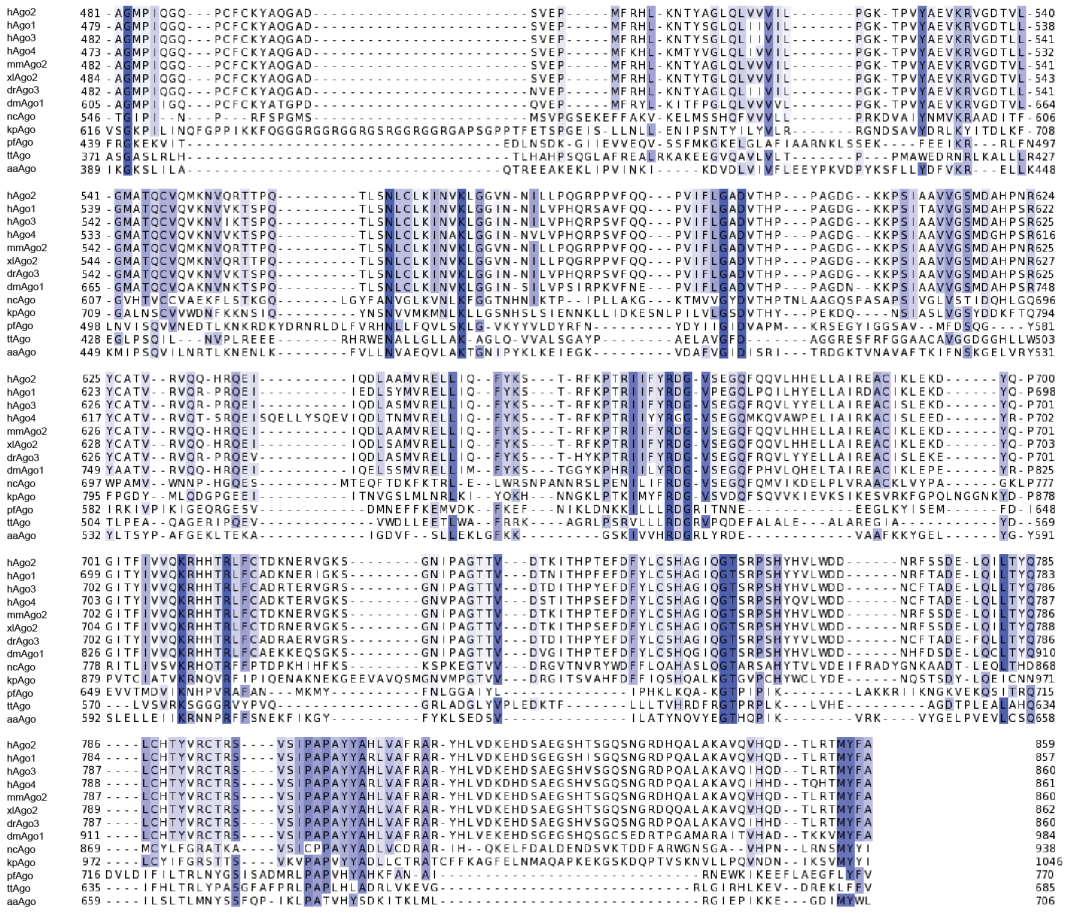

Figure 5.0.4: Multiple sequence alignment of Ago2 homologues. Ago2 homologues from selected organisms were aligned with MAFFT [105] using the Jalview software [216]. Conserved sequence motifs are shaded in blue.

Abbreviations

aa	amino acid
Ago	Argonaute
CD	circular dichroism
CRISPR	clustered regulatory interspaced short palindromic repeats
CSP	chemical shift perturbation
cv	column volume
C. elegans	*Caenorhabditis elegans*
DLS	dynamic light scattering
ds	double stranded
DUF	domain of unknown function
D. melanogaster	*Drosophila melanogaster*
ELM	european linear motif data bank
E. coli	*Escherichia coli*
e.g.	for example (exempli gratia)
GW-repeat	glycine-tryptophan or tryptophan-glycine repeat
GST	glutathione S-transferase
HCV	hepatitis C virus
HSQC	heteronuclear single quantum coherence
IPTG	isopropyl-?-D-thiogalactopyranosid
LC	low complexity
kDa	kilo dalton
K_D	dissociation constant
MID	middle
MS	mass spectrometry
min	minutes
miRNA	microRNA
miRNP	micro-ribonuleoprotein particle
mRNA	messenger RNA
MVBs	multivesicular bodies
NMR	nuclear magnetic resonance
nt	nucleotide
NOE	nuclear overhauser effect
PABP	poly(A)-binding protein protein
PAM2	poly(A)-binding protein-interacting motif 2
PAZ	PIWI-Argonaute-Zwille
P/GW-bodies	processing bodies
PBS	phosphate buffered saline
PDB	protein data bank

pf	*pyrococcus furiosus*
pH	potentia hydrogenii
piRNA	PIWI-interacting RNA
PTM	post translational modifications
pre-miRNA	precursor miRNA
pri-miRNA	primary miRNA
RISC	RNA-induced silencing complex
RITS	RNA-induced transcriptional silencing
RLC	RISC loading complex
RNAi	RNA interference
RNase	ribonuclease
rpm	revolutions per minute
RRM	RNA recognition motif
RT	room temperature
R_H	hydrodynamic radius
SDS-PAGE	sodium dodecyl sulfate polyacrylamide gel electrophoresis
SEC	size exclusion chromatography
siRNA	small interfering RNA
SLiM	short linear interaction motif
snoRNA	small nucleolar RNA
ss	single stranded
STD	saturation transfer difference
TGS	transcriptional gene silencing
TNRC6	trinucleotide repeat containing 6
TOCSY	total correlation spectroscopy
UBA	ubiquitin associated
UTR	untranslated region
v/v	volume per volume
wt	wild typ
w/v	weight per volume

Ala	alanine
Arg	arginine
Cys	cystein
Gln	glutamine
Gly	glycine
His	histidine
Ile	isoleucine
Leu	leucine
Lys	lysine
Met	methionine
Phe	phenylalanine
Ser	serine
Thr	threonine
Trp	tryptophan
Tyr	tyrosin
Val	valine

List of Figures

1.1.1 MiRNA biogenesis pathway. 3
1.2.1 Crystal structure of Ago2. 6
1.3.1 Schematic of TNRC6B domain organization. 9
1.7.1 MiRNA-mediated translational repression and decay. 15

2.1.1 Purification of TNRC6 constructs. 20
2.1.2 Schematic of TNRC6 constructs. 20
2.1.3 Schematic of Ago2 constructs. 21
2.1.4 The Ago2 MID domain and pfAgo full length protein are not sufficient to bind TNRC6B 599-683. 21
2.1.5 Purification and limited proteolysis of Ago. 22
2.2.1 Experimental setup of peptide array. 23
2.2.2 Peptide array identifies distinct Ago2 binding sites on TNRC6B. . . . 24
2.2.3 List of TNRC6B peptides spotted on the membrane with their Ago2 affinity indicated. 25
2.3.1 Peptide array for mutational analysis of peptide E11. 27
2.4.1 Schematic illustration of STD-NMR experiment applied to the protein receptor (Ago2) and ligand (peptide) complex. 30
2.4.2 STD amplification factors of measured peptides 33
2.5.1 Multiple sequence alignment of TNRC6B 599-683 orthologs. 34
2.5.2 CD spectrum, ^{15}N NMR relaxation data and heteronuclear NOE of TNRC6B 599-683. 35
2.5.3 Secondary chemical shifts calculated for TNRC6B 599-683. 36
2.6.1 Pulldown of proteins from HeLa lysate by TNRC6B 599-683. 37
2.6.2 TNRC6B 599-683 directly interacts with Ago2 and the complex does not aggregate upon binding. 39
2.6.3 FP measurement of TNRC6B 599-683:Ago2 interaction. 40
2.7.1 NMR titration experiments of TNRC6B 599-683 and Ago2. 41
2.8.1 The TNRC6B599-683:Ago2 interaction is mediated by Trps. 43

2.9.1 Crosslinking of TNRC6B 599-683:Ago2. 44
2.9.2 Crosslink map of TNRC6B 599-683:Ago2 analysis. 45
2.10.1 Schematic model of Ago2:TNRC6B 599-683 binding mode. 46
2.10.2 Model of Ago2:TNRC6B 599-683 interaction. 47

3.3.1 Surface properties of Ago2. 53
3.3.2 Ago mutations impairing GW182 binding. 54
3.3.3 Surface characteristics of Ago structures from different species. 55
3.4.1 Trp coordination in Ago2 binding pockets. 56
3.4.2 Spacing between TNRC6B Trps. 58
3.4.3 Exemplary crystal structure for LXXLL motif binding. 60

5.0.1 Secondary structure prediction of TNRC6B. 79
5.0.2 Secondary structure prediction of Ago2. 79
5.0.3 Multiple sequence alignment of TNRC6B homologues. 81
5.0.4 Multiple sequence alignment of Ago2 homologues. 83

List of Tables

2.6.1 Table of proteins pulled down together with TNRC6B 599-683 from HeLa lysate 38
2.9.1 Table of crosslinks identified by MS. 45

Bibliography

[1] A. A. Aravin, N. M. Naumova, A. V. Tulin, V. V. Vagin, Y. M. Rozovsky, and V. A. Gvozdev. Double-stranded RNA-mediated silencing of genomic tandem repeats and transposable elements in the D. melanogaster germline. *Curr. Biol.*, 11(13):1017–1027, Jul 2001.

[2] J. Azevedo, D. Garcia, D. Pontier, S. Ohnesorge, A. Yu, S. Garcia, L. Braun, M. Bergdoll, M. A. Hakimi, T. Lagrange, and O. Voinnet. Argonaute quenching and global changes in Dicer homeostasis caused by a pathogen-encoded GW repeat protein. *Genes Dev.*, 24(9):904–915, May 2010.

[3] J. E. Babiarz, J. G. Ruby, Y. Wang, D. P. Bartel, and R. Blelloch. Mouse ES cells express endogenous shRNAs, siRNAs, and other Microprocessor-independent, Dicer-dependent small RNAs. *Genes Dev.*, 22(20):2773–2785, Oct 2008.

[4] D. Baillat and R. Shiekhattar. Functional dissection of the human TNRC6 (GW182-related) family of proteins. *Mol. Cell. Biol.*, 29(15):4144–4155, Aug 2009.

[5] D. P. Bartel. MicroRNAs: genomics, biogenesis, mechanism, and function. *Cell*, 116(2):281–297, Jan 2004.

[6] D. P. Bartel. MicroRNAs: target recognition and regulatory functions. *Cell*, 136(2):215–233, Jan 2009.

[7] J. Bednenko, T. Noto, L. V. DeSouza, K. W. Siu, R. E. Pearlman, K. Mochizuki, and M. A. Gorovsky. Two GW repeat proteins interact with Tetrahymena thermophila argonaute and promote genome rearrangement. *Mol. Cell. Biol.*, 29(18):5020–5030, Sep 2009.

[8] I. Behm-Ansmant, J. Rehwinkel, T. Doerks, A. Stark, P. Bork, and E. Izaurralde. mRNA degradation by miRNAs and GW182 requires both CCR4:NOT deadenylase and DCP1:DCP2 decapping complexes. *Genes Dev.*, 20(14):1885–1898, Jul 2006.

[9] S. N. Bhattacharyya, R. Habermacher, U. Martine, E. I. Closs, and W. Filipowicz. Relief of microRNA-mediated translational repression in human cells subjected to stress. *Cell*, 125(6):1111–1124, Jun 2006.

[10] A. Biegert, C. Mayer, M. Remmert, J. Soding, and A. N. Lupas. The MPI Bioinformatics Toolkit for protein sequence analysis. *Nucleic Acids Res.*, 34(Web Server issue):W335–339, Jul 2006.

[11] K. Bohmert, I. Camus, C. Bellini, D. Bouchez, M. Caboche, and C. Benning. AGO1 defines a novel locus of Arabidopsis controlling leaf development. *EMBO J.*, 17(1):170–180, Jan 1998.

[12] M. T. Bohnsack, K. Czaplinski, and D. Gorlich. Exportin 5 is a RanGTP-dependent dsRNA-binding protein that mediates nuclear export of pre-miRNAs. *RNA*, 10(2):185–191, Feb 2004.

[13] A. Boland, E. Huntzinger, S. Schmidt, E. Izaurralde, and O. Weichenrieder. Crystal structure of the MID-PIWI lobe of a eukaryotic Argonaute protein. *Proc. Natl. Acad. Sci. U.S.A.*, 108(26):10466–10471, Jun 2011.

[14] A. Boland, F. Tritschler, S. Heimstadt, E. Izaurralde, and O. Weichenrieder. Crystal structure and ligand binding of the MID domain of a eukaryotic Argonaute protein. *EMBO Rep.*, 11(7):522–527, Jul 2010.

[15] G. M. Borchert, W. Lanier, and B. L. Davidson. RNA polymerase III transcribes human microRNAs. *Nat. Struct. Mol. Biol.*, 13(12):1097–1101, Dec 2006.

[16] A. A. Bothner-By, R. Stephens, L. Jumee, C. D. Warren, and R. W. Jeanloz. Structure determination of a tetrasaccharide: transient nuclear Overhauser effects in the rotating frame. *J Am Chem Soc*, 106(3):811–813, Feb 1984.

[17] J. E. Braun, E. Huntzinger, M. Fauser, and E. Izaurralde. GW182 proteins directly recruit cytoplasmic deadenylase complexes to miRNA targets. *Mol. Cell*, 44(1):120–133, Oct 2011.

[18] J. E. Braun, V. Truffault, A. Boland, E. Huntzinger, C. T. Chang, G. Haas, O. Weichenrieder, M. Coles, and E. Izaurralde. A direct interaction between DCP1 and XRN1 couples mRNA decapping to 5' exonucleolytic degradation. *Nat. Struct. Mol. Biol.*, 19(12):1324–1331, Dec 2012.

[19] L. Braunschweiler and R. Ernst. Coherence transfer by isotropic mixing: Application to proton correlation spectroscopy. *J Magn Reson*, 53:521–528, 1983.

[20] P. Brodersen and O. Voinnet. The diversity of RNA silencing pathways in plants. *Trends Genet.*, 22(5):268–280, May 2006.

[21] A. Buchberger. From UBA to UBX: new words in the ubiquitin vocabulary. *Trends Cell Biol.*, 12(5):216–221, May 2002.

[22] M. Buhler, A. Verdel, and D. Moazed. Tethering RITS to a nascent transcript initiates RNAi- and heterochromatin-dependent gene silencing. *Cell*, 125(5):873–886, Jun 2006.

[23] M. A. Carmell, A. Girard, H. J. van de Kant, D. Bourc'his, T. H. Bestor, D. G. de Rooij, and G. J. Hannon. MIWI2 is essential for spermatogenesis and repression of transposons in the mouse male germline. *Dev. Cell*, 12(4):503–514, Apr 2007.

[24] M. A. Carmell, Z. Xuan, M. Q. Zhang, and G. J. Hannon. The Argonaute family: tentacles that reach into RNAi, developmental control, stem cell maintenance, and tumorigenesis. *Genes Dev.*, 16(21):2733–2742, Nov 2002.

[25] R. W. Carthew and E. J. Sontheimer. Origins and Mechanisms of miRNAs and siRNAs. *Cell*, 136(4):642–655, Feb 2009.

[26] N. Chang, J. Yi, G. Guo, X. Liu, Y. Shang, T. Tong, Q. Cui, M. Zhan, M. Gorospe, and W. Wang. HuR uses AUF1 as a cofactor to promote p16INK4 mRNA decay. *Mol. Cell. Biol.*, 30(15):3875–3886, Aug 2010.

[27] M. Chekulaeva, W. Filipowicz, and R. Parker. Multiple independent domains of dGW182 function in miRNA-mediated repression in Drosophila. *RNA*, 15(5):794–803, May 2009.

[28] M. Chekulaeva, H. Mathys, J. T. Zipprich, J. Attig, M. Colic, R. Parker, and W. Filipowicz. miRNA repression involves GW182-mediated recruitment of CCR4-NOT through conserved W-containing motifs. *Nat. Struct. Mol. Biol.*, 18(11), 2011.

[29] M. Chekulaeva, R. Parker, and W. Filipowicz. The GW/WG repeats of Drosophila GW182 function as effector motifs for miRNA-mediated repression. *Nucleic Acids Res.*, 38(19):6673–6683, Oct 2010.

[30] S. Cheloufi, C. O. Dos Santos, M. M. Chong, and G. J. Hannon. A dicer-independent miRNA biogenesis pathway that requires Ago catalysis. *Nature*, 465(7298):584–589, Jun 2010.

[31] C. Y. Chen, D. Zheng, Z. Xia, and A. B. Shyu. Ago-TNRC6 triggers microRNA-mediated decay by promoting two deadenylation steps. *Nat. Struct. Mol. Biol.*, 16(11):1160–1166, Nov 2009.

[32] T. P. Chendrimada, R. I. Gregory, E. Kumaraswamy, J. Norman, N. Cooch, K. Nishikura, and R. Shiekhattar. TRBP recruits the Dicer complex to Ago2 for microRNA processing and gene silencing. *Nature*, 436(7051):740–744, Aug 2005.

[33] C. Y. Chu and T. M. Rana. Translation repression in human cells by microRNA-induced gene silencing requires RCK/p54. *PLoS Biol.*, 4(7):e210, Jul 2006.

[34] D. Cifuentes, H. Xue, D. W. Taylor, H. Patnode, Y. Mishima, S. Cheloufi, E. Ma, S. Mane, G. J. Hannon, N. D. Lawson, S. A. Wolfe, and A. J. Giraldez. A novel miRNA processing pathway independent of Dicer requires Argonaute2 catalytic activity. *Science*, 328(5986):1694–1698, Jun 2010.

[35] A. Clery, M. Blatter, and F. H. Allain. RNA recognition motifs: boring? Not quite. *Curr. Opin. Struct. Biol.*, 18(3):290–298, Jun 2008.

[36] J. Coller and R. Parker. General translational repression by activators of mRNA decapping. *Cell*, 122(6):875–886, Sep 2005.

[37] A. Cooke, A. Prigge, and M. Wickens. Translational repression by deadenylases. *J. Biol. Chem.*, 285(37):28506–28513, Sep 2010.

[38] B. Czech, C. D. Malone, R. Zhou, A. Stark, C. Schlingeheyde, M. Dus, N. Perrimon, M. Kellis, J. A. Wohlschlegel, R. Sachidanandam, G. J. Hannon, and J. Brennecke. An endogenous small interfering RNA pathway in Drosophila. *Nature*, 453(7196):798–802, Jun 2008.

[39] F. Delaglio, S. Grzesiek, G. W. Vuister, G. Zhu, J. Pfeifer, and A. Bax. NMRPipe: a multidimensional spectral processing system based on UNIX pipes. *J. Biomol. NMR*, 6(3):277–293, Nov 1995.

[40] A. M. Denli, B. B. Tops, R. H. Plasterk, R. F. Ketting, and G. J. Hannon. Processing of primary microRNAs by the Microprocessor complex. *Nature*, 432(7014):231–235, Nov 2004.

[41] S. Diederichs and D. A. Haber. Dual role for argonautes in microRNA processing and posttranscriptional regulation of microRNA expression. *Cell*, 131(6):1097–1108, Dec 2007.

[42] F. Diella, N. Haslam, C. Chica, A. Budd, S. Michael, N. P. Brown, G. Trave, and T. J. Gibson. Understanding eukaryotic linear motifs and their role in cell signaling and regulation. *Front. Biosci.*, 13:6580–6603, 2008.

[43] L. Ding and M. Han. GW182 family proteins are crucial for microRNA-mediated gene silencing. *Trends Cell Biol.*, 17(8):411–416, Aug 2007.

[44] L. Ding, A. Spencer, K. Morita, and M. Han. The developmental timing regulator AIN-1 interacts with miRISCs and may target the argonaute protein ALG-1 to cytoplasmic P bodies in C. elegans. *Mol. Cell*, 19(4):437–447, Aug 2005.

[45] M. El-Shami, D. Pontier, S. Lahmy, L. Braun, C. Picart, D. Vega, M. A. Hakimi, S. E. Jacobsen, R. Cooke, and T. Lagrange. Reiterated WG/GW motifs form functionally and evolutionarily conserved ARGONAUTE-binding platforms in RNAi-related components. *Genes Dev.*, 21(20):2539–2544, Oct 2007.

[46] S. M. Elbashir, W. Lendeckel, and T. Tuschl. RNA interference is mediated by 21- and 22-nucleotide RNAs. *Genes Dev.*, 15(2):188–200, Jan 2001.

[47] E. Elkayam, C. D. Kuhn, A. Tocilj, A. D. Haase, E. M. Greene, G. J. Hannon, and L. Joshua-Tor. The structure of human argonaute-2 in complex with miR-20a. *Cell*, 150(1):100–110, Jul 2012.

[48] P. Emsley, B. Lohkamp, W. G. Scott, and K. Cowtan. Features and development of Coot. *Acta Crystallogr. D Biol. Crystallogr.*, 66(Pt 4):486–501, Apr 2010.

[49] C. Ender, A. Krek, M. R. Friedlander, M. Beitzinger, L. Weinmann, W. Chen, S. Pfeffer, N. Rajewsky, and G. Meister. A human snoRNA with microRNA-like functions. *Mol. Cell*, 32(4):519–528, Nov 2008.

[50] A. Eulalio, I. Behm-Ansmant, D. Schweizer, and E. Izaurralde. P-body formation is a consequence, not the cause, of RNA-mediated gene silencing. *Mol. Cell. Biol.*, 27(11):3970–3981, Jun 2007.

[51] A. Eulalio, S. Helms, C. Fritzsch, M. Fauser, and E. Izaurralde. A C-terminal silencing domain in GW182 is essential for miRNA function. *RNA*, 15(6):1067–1077, Jun 2009.

[52] A. Eulalio, E. Huntzinger, and E. Izaurralde. GW182 interaction with Argonaute is essential for miRNA-mediated translational repression and mRNA decay. *Nat. Struct. Mol. Biol.*, 15(4):346–353, Apr 2008.

[53] A. Eulalio, F. Tritschler, R. Buttner, O. Weichenrieder, E. Izaurralde, and V. Truffault. The RRM domain in GW182 proteins contributes to miRNA-mediated gene silencing. *Nucleic Acids Res.*, 37(9):2974–2983, 2009.

[54] A. Eulalio, F. Tritschler, and E. Izaurralde. The GW182 protein family in animal cells: new insights into domains required for miRNA-mediated gene silencing. *RNA*, 15(8):1433–1442, Aug 2009.

[55] T. Eystathioy, E. K. Chan, S. A. Tenenbaum, J. D. Keene, K. Griffith, and M. J. Fritzler. A phosphorylated cytoplasmic autoantigen, GW182, associates with a unique population of human mRNAs within novel cytoplasmic speckles. *Mol. Biol. Cell*, 13(4):1338–1351, Apr 2002.

[56] T. Eystathioy, A. Jakymiw, E. K. Chan, B. Seraphin, N. Cougot, and M. J. Fritzler. The GW182 protein colocalizes with mRNA degradation associated proteins hDcp1 and hLSm4 in cytoplasmic GW bodies. *RNA*, 9(10):1171–1173, Oct 2003.

[57] M. R. Fabian, M. K. Cieplak, F. Frank, M. Morita, J. Green, T. Srikumar, B. Nagar, T. Yamamoto, B. Raught, T. F. Duchaine, and N. Sonenberg. miRNA-mediated deadenylation is orchestrated by GW182 through two conserved motifs that interact with CCR4-NOT. *Nat. Struct. Mol. Biol.*, 18(11):1211–1217, Nov 2011.

[58] M. R. Fabian, G. Mathonnet, T. Sundermeier, H. Mathys, J. T. Zipprich, Y. V. Svitkin, F. Rivas, M. Jinek, J. Wohlschlegel, J. A. Doudna, C. Y. Chen, A. B. Shyu, J. R. Yates, G. J. Hannon, W. Filipowicz, T. F. Duchaine, and N. Sonenberg. Mammalian miRNA RISC recruits CAF1 and PABP to affect PABP-dependent deadenylation. *Mol. Cell*, 35(6):868–880, Sep 2009.

[59] M. R. Fabian and N. Sonenberg. The mechanics of miRNA-mediated gene silencing: a look under the hood of miRISC. *Nat. Struct. Mol. Biol.*, 19(6):586–593, Jun 2012.

[60] C. R. Faehnle and L. Joshua-Tor. Argonautes confront new small RNAs. *Curr Opin Chem Biol*, 11(5):569–577, Oct 2007.

[61] N. A. Farrow, R. Muhandiram, A. U. Singer, S. M. Pascal, C. M. Kay, G. Gish, S. E. Shoelson, T. Pawson, J. D. Forman-Kay, and L. E. Kay. Backbone dynamics of a free and phosphopeptide-complexed Src homology 2 domain studied by 15N NMR relaxation. *Biochemistry*, 33(19):5984–6003, May 1994.

[62] A. Fire, S. Xu, M. K. Montgomery, S. A. Kostas, S. E. Driver, and C. C. Mello. Potent and specific genetic interference by double-stranded RNA in Caenorhabditis elegans. *Nature*, 391(6669):806–811, Feb 1998.

[63] K. Forstemann, Y. Tomari, T. Du, V. V. Vagin, A. M. Denli, D. P. Bratu, C. Klattenhoff, W. E. Theurkauf, and P. D. Zamore. Normal microRNA maturation and germ-line stem cell maintenance requires Loquacious, a double-stranded RNA-binding domain protein. *PLoS Biol.*, 3(7):e236, Jul 2005.

[64] F. Frank, N. Sonenberg, and B. Nagar. Structural basis for 5'-nucleotide base-specific recognition of guide RNA by human AGO2. *Nature*, 465(7299):818–822, Jun 2010.

[65] S. Frey and D. Gorlich. A saturated FG-repeat hydrogel can reproduce the permeability properties of nuclear pore complexes. *Cell*, 130(3):512–523, Aug 2007.

[66] R. C. Friedman, K. K. Farh, C. B. Burge, and D. P. Bartel. Most mammalian mRNAs are conserved targets of microRNAs. *Genome Res.*, 19(1):92–105, Jan 2009.

[67] S. A. Fromm, V. Truffault, J. Kamenz, J. E. Braun, N. A. Hoffmann, E. Izaurralde, and R. Sprangers. The structural basis of Edc3- and Scd6-mediated activation of the Dcp1:Dcp2 mRNA decapping complex. *EMBO J.*, 31(2):279–290, Jan 2012.

[68] T. Fukaya and Y. Tomari. MicroRNAs mediate gene silencing via multiple different pathways in drosophila. *Mol. Cell*, 48(6):825–836, Dec 2012.

[69] K. Gavrilov and W. M. Saltzman. Therapeutic siRNA: principles, challenges, and strategies. *Yale J Biol Med*, 85(2):187–200, Jun 2012.

[70] M. Ghildiyal, H. Seitz, M. D. Horwich, C. Li, T. Du, S. Lee, J. Xu, E. L. Kittler, M. L. Zapp, Z. Weng, and P. D. Zamore. Endogenous siRNAs derived from transposons and mRNAs in Drosophila somatic cells. *Science*, 320(5879):1077–1081, May 2008.

[71] M. Ghildiyal and P. D. Zamore. Small silencing RNAs: an expanding universe. *Nat. Rev. Genet.*, 10(2):94–108, Feb 2009.

[72] D. Gibbings, P. Leblanc, F. Jay, D. Pontier, F. Michel, Y. Schwab, S. Alais, T. Lagrange, and O. Voinnet. Human prion protein binds Argonaute and promotes accumulation of microRNA effector complexes. *Nat. Struct. Mol. Biol.*, 19(5):517–524, May 2012.

[73] D. J. Gibbings, C. Ciaudo, M. Erhardt, and O. Voinnet. Multivesicular bodies associate with components of miRNA effector complexes and modulate miRNA activity. *Nat. Cell Biol.*, 11(9):1143–1149, Sep 2009.

[74] A. Giner, L. Lakatos, M. Garcia-Chapa, J. J. Lopez-Moya, and J. Burgyan. Viral protein inhibits RISC activity by argonaute binding through conserved WG/GW motifs. *PLoS Pathog.*, 6(7):e1000996, 2010.

[75] T. Goddard and D. Kneller. Sarky 3. *University of Calofornia*, 1994.

[76] R. I. Gregory, T. P. Chendrimada, N. Cooch, and R. Shiekhattar. Human RISC couples microRNA biogenesis and posttranscriptional gene silencing. *Cell*, 123(4):631–640, Nov 2005.

[77] R. I. Gregory, K. P. Yan, G. Amuthan, T. Chendrimada, B. Doratotaj, N. Cooch, and R. Shiekhattar. The Microprocessor complex mediates the genesis of microRNAs. *Nature*, 432(7014):235–240, Nov 2004.

[78] S. Griffiths-Jones, H. K. Saini, S. van Dongen, and A. J. Enright. miRBase: tools for microRNA genomics. *Nucleic Acids Res.*, 36(Database issue):D154–158, Jan 2008.

[79] H. Guo, N. T. Ingolia, J. S. Weissman, and D. P. Bartel. Mammalian microRNAs predominantly act to decrease target mRNA levels. *Nature*, 466(7308):835–840, Aug 2010.

[80] A. D. Haase, L. Jaskiewicz, H. Zhang, S. Laine, R. Sack, A. Gatignol, and W. Filipowicz. TRBP, a regulator of cellular PKR and HIV-1 virus expression, interacts with Dicer and functions in RNA silencing. *EMBO Rep.*, 6(10):961–967, Oct 2005.

[81] A. J. Hamilton and D. C. Baulcombe. A species of small antisense RNA in posttranscriptional gene silencing in plants. *Science*, 286(5441):950–952, Oct 1999.

[82] C. M. Hammell, I. Lubin, P. R. Boag, T. K. Blackwell, and V. Ambros. nhl-2 Modulates microRNA activity in Caenorhabditis elegans. *Cell*, 136(5):926–938, Mar 2009.

[83] J. Han, Y. Lee, K. H. Yeom, Y. K. Kim, H. Jin, and V. N. Kim. The Drosha-DGCR8 complex in primary microRNA processing. *Genes Dev.*, 18(24):3016–3027, Dec 2004.

[84] T. W. Han, M. Kato, S. Xie, L. C. Wu, H. Mirzaei, J. Pei, M. Chen, Y. Xie, J. Allen, G. Xiao, and S. L. McKnight. Cell-free formation of RNA granules: bound RNAs identify features and components of cellular assemblies. *Cell*, 149(4):768–779, May 2012.

[85] D. Hanahan. Studies on transformation of Escherichia coli with plasmids. *J. Mol. Biol.*, 166(4):557–580, Jun 1983.

[86] X. J. He, Y. F. Hsu, S. Zhu, A. T. Wierzbicki, O. Pontes, C. S. Pikaard, H. L. Liu, C. S. Wang, H. Jin, and J. K. Zhu. An effector of RNA-directed DNA methylation in arabidopsis is an ARGONAUTE 4- and RNA-binding protein. *Cell*, 137(3):498–508, May 2009.

[87] J. I. Henke, D. Goergen, J. Zheng, Y. Song, C. G. Schuttler, C. Fehr, C. Junemann, and M. Niepmann. microRNA-122 stimulates translation of hepatitis C virus RNA. *EMBO J.*, 27(24):3300–3310, Dec 2008.

[88] F. Herzog, A. Kahraman, D. Boehringer, R. Mak, A. Bracher, T. Walzthoeni, A. Leitner, M. Beck, F. U. Hartl, N. Ban, L. Malmstrom, and R. Aebersold. Structural probing of a protein phosphatase 2A network by chemical cross-linking and mass spectrometry. *Science*, 337(6100):1348–1352, Sep 2012.

[89] J. Hock and G. Meister. The Argonaute protein family. *Genome Biol.*, 9(2):210, 2008.

[90] H. Y. Hu, Z. Yan, Y. Xu, H. Hu, C. Menzel, Y. H. Zhou, W. Chen, and P. Khaitovich. Sequence features associated with microRNA strand selection in humans and flies. *BMC Genomics*, 10:413, 2009.

[91] D. T. Humphreys, B. J. Westman, D. I. Martin, and T. Preiss. MicroRNAs control translation initiation by inhibiting eukaryotic initiation factor 4E/cap and poly(A) tail function. *Proc. Natl. Acad. Sci. U.S.A.*, 102(47):16961–16966, Nov 2005.

[92] E. Huntzinger, J. E. Braun, S. Heimstadt, L. Zekri, and E. Izaurralde. Two PABPC1-binding sites in GW182 proteins promote miRNA-mediated gene silencing. *EMBO J.*, 29(24):4146–4160, Dec 2010.

[93] E. Huntzinger and E. Izaurralde. Gene silencing by microRNAs: contributions of translational repression and mRNA decay. *Nat. Rev. Genet.*, 12(2):99–110, Feb 2011.

[94] E. Huntzinger, D. Kuzuoglu-Ozturk, J. E. Braun, A. Eulalio, L. Wohlbold, and E. Izaurralde. The interactions of GW182 proteins with PABP and deadenylases are required for both translational repression and degradation of miRNA targets. *Nucleic Acids Res.*, 41(2):978–994, Jan 2013.

[95] G. Hutvagner, J. McLachlan, A. E. Pasquinelli, E. Balint, T. Tuschl, and P. D. Zamore. A cellular function for the RNA-interference enzyme Dicer in the maturation of the let-7 small temporal RNA. *Science*, 293(5531):834–838, Aug 2001.

[96] G. Hutvagner and M. J. Simard. Argonaute proteins: key players in RNA silencing. *Nat. Rev. Mol. Cell Biol.*, 9(1):22–32, Jan 2008.

[97] S. Iwasaki, M. Kobayashi, M. Yoda, Y. Sakaguchi, S. Katsuma, T. Suzuki, and Y. Tomari. Hsc70/Hsp90 chaperone machinery mediates ATP-dependent RISC loading of small RNA duplexes. *Mol. Cell*, 39(2):292–299, Jul 2010.

[98] S. Iwasaki and Y. Tomari. Argonaute-mediated translational repression (and activation). *Fly (Austin)*, 3(3):204–206, 2009.

[99] B. A. Janowski, J. Hu, and D. R. Corey. Silencing gene expression by targeting chromosomal DNA with antigene peptide nucleic acids and duplex RNAs. *Nat Protoc*, 1(1):436–443, 2006.

[100] B. A. Janowski, K. E. Huffman, J. C. Schwartz, R. Ram, R. Nordsell, D. S. Shames, J. D. Minna, and D. R. Corey. Involvement of AGO1 and AGO2 in mammalian transcriptional silencing. *Nat. Struct. Mol. Biol.*, 13(9):787–792, Sep 2006.

[101] M. Jinek, M. R. Fabian, S. M. Coyle, N. Sonenberg, and J. A. Doudna. Structural insights into the human GW182-PABC interaction in microRNA-mediated deadenylation. *Nat. Struct. Mol. Biol.*, 17(2):238–240, Feb 2010.

[102] M. Johnston, M. C. Geoffroy, A. Sobala, R. Hay, and G. Hutvagner. HSP90 protein stabilizes unloaded argonaute complexes and microscopic P-bodies in human cells. *Mol. Biol. Cell*, 21(9):1462–1469, May 2010.

[103] W. M. Karlowski, A. Zielezinski, J. Carrere, D. Pontier, T. Lagrange, and R. Cooke. Genome-wide computational identification of WG/GW Argonaute-binding proteins in Arabidopsis. *Nucleic Acids Res.*, 38(13):4231–4245, Jul 2010.

[104] M. Kato, T. W. Han, S. Xie, K. Shi, X. Du, L. C. Wu, H. Mirzaei, E. J. Goldsmith, J. Longgood, J. Pei, N. V. Grishin, D. E. Frantz, J. W. Schneider, S. Chen, L. Li, M. R. Sawaya, D. Eisenberg, R. Tycko, and S. L. McKnight. Cell-free formation of RNA granules: low complexity sequence domains form dynamic fibers within hydrogels. *Cell*, 149(4):753–767, May 2012.

[105] K. Katoh, K. Kuma, H. Toh, and T. Miyata. MAFFT version 5: improvement in accuracy of multiple sequence alignment. *Nucleic Acids Res.*, 33(2):511–518, 2005.

[106] Y. Kawamura, K. Saito, T. Kin, Y. Ono, K. Asai, T. Sunohara, T. N. Okada, M. C. Siomi, and H. Siomi. Drosophila endogenous small RNAs bind to Argonaute 2 in somatic cells. *Nature*, 453(7196):793–797, Jun 2008.

[107] M. Kedde, M. J. Strasser, B. Boldajipour, J. A. Oude Vrielink, K. Slanchev, C. le Sage, R. Nagel, P. M. Voorhoeve, J. van Duijse, U. A. Orom, A. H. Lund, A. Perrakis, E. Raz, and R. Agami. RNA-binding protein Dnd1 inhibits microRNA access to target mRNA. *Cell*, 131(7):1273–1286, Dec 2007.

[108] M. Kedde, M. van Kouwenhove, W. Zwart, J. A. Oude Vrielink, R. Elkon, and R. Agami. A Pumilio-induced RNA structure switch in p27-3' UTR controls miR-221 and miR-222 accessibility. *Nat. Cell Biol.*, 12(10):1014–1020, Oct 2010.

[109] A. Khvorova, A. Reynolds, and S. D. Jayasena. Functional siRNAs and miRNAs exhibit strand bias. *Cell*, 115(2):209–216, Oct 2003.

[110] D. H. Kim, L. M. Villeneuve, K. V. Morris, and J. J. Rossi. Argonaute-1 directs siRNA-mediated transcriptional gene silencing in human cells. *Nat. Struct. Mol. Biol.*, 13(9):793–797, Sep 2006.

[111] H. H. Kim, Y. Kuwano, S. Srikantan, E. K. Lee, J. L. Martindale, and M. Gorospe. HuR recruits let-7/RISC to repress c-Myc expression. *Genes Dev.*, 23(15):1743–1748, Aug 2009.

[112] V. N. Kim, J. Han, and M. C. Siomi. Biogenesis of small RNAs in animals. *Nat. Rev. Mol. Cell Biol.*, 10(2):126–139, Feb 2009.

[113] Y. Kirino and Z. Mourelatos. Mouse Piwi-interacting RNAs are 2'-O-methylated at their 3' termini. *Nat. Struct. Mol. Biol.*, 14(4):347–348, Apr 2007.

[114] A. Kozomara and S. Griffiths-Jones. miRBase: integrating microRNA annotation and deep-sequencing data. *Nucleic Acids Res.*, 39(Database issue):D152–157, Jan 2011.

[115] J. Krol, I. Loedige, and W. Filipowicz. The widespread regulation of microRNA biogenesis, function and decay. *Nat. Rev. Genet.*, 11(9):597–610, Sep 2010.

[116] U. K. Laemmli. Cleavage of structural proteins during the assembly of the head of bacteriophage T4. *Nature*, 227(5259):680–685, Aug 1970.

[117] D. Lazzaretti, I. Tournier, and E. Izaurralde. The C-terminal domains of human TNRC6A, TNRC6B, and TNRC6C silence bound transcripts independently of Argonaute proteins. *RNA*, 15(6):1059–1066, Jun 2009.

[118] R. C. Lee, R. L. Feinbaum, and V. Ambros. The C. elegans heterochronic gene lin-4 encodes small RNAs with antisense complementarity to lin-14. *Cell*, 75(5):843–854, Dec 1993.

[119] Y. Lee, C. Ahn, J. Han, H. Choi, J. Kim, J. Yim, J. Lee, P. Provost, O. Radmark, S. Kim, and V. N. Kim. The nuclear RNase III Drosha initiates microRNA processing. *Nature*, 425(6956):415–419, Sep 2003.

[120] Y. Lee, I. Hur, S. Y. Park, Y. K. Kim, M. R. Suh, and V. N. Kim. The role of PACT in the RNA silencing pathway. *EMBO J.*, 25(3):522–532, Feb 2006.

[121] Y. Lee, K. Jeon, J. T. Lee, S. Kim, and V. N. Kim. MicroRNA maturation: stepwise processing and subcellular localization. *EMBO J.*, 21(17):4663–4670, Sep 2002.

[122] Y. Lee, M. Kim, J. Han, K. H. Yeom, S. Lee, S. H. Baek, and V. N. Kim. MicroRNA genes are transcribed by RNA polymerase II. *EMBO J.*, 23(20):4051–4060, Oct 2004.

[123] Y. S. Lee, S. Pressman, A. P. Andress, K. Kim, J. L. White, J. J. Cassidy, X. Li, K. Lubell, d. o. H. Lim, I. S. Cho, K. Nakahara, J. B. Preall, P. Bellare, E. J. Sontheimer, and R. W. Carthew. Silencing by small RNAs is linked to endosomal trafficking. *Nat. Cell Biol.*, 11(9):1150–1156, Sep 2009.

[124] A. K. Leung, J. M. Calabrese, and P. A. Sharp. Quantitative analysis of Argonaute protein reveals microRNA-dependent localization to stress granules. *Proc. Natl. Acad. Sci. U.S.A.*, 103(48):18125–18130, Nov 2006.

[125] C. F. Li, O. Pontes, M. El-Shami, I. R. Henderson, Y. V. Bernatavichute, S. W. Chan, T. Lagrange, C. S. Pikaard, and S. E. Jacobsen. An ARGONAUTE4-containing nuclear processing center colocalized with Cajal bodies in Arabidopsis thaliana. *Cell*, 126(1):93–106, Jul 2006.

[126] S. L. Lian, S. Li, G. X. Abadal, B. A. Pauley, M. J. Fritzler, and E. K. Chan. The C-terminal half of human Ago2 binds to multiple GW-rich regions of GW182 and requires GW182 to mediate silencing. *RNA*, 15(5):804–813, May 2009.

[127] H. Lin and A. C. Spradling. A novel group of pumilio mutations affects the asymmetric division of germline stem cells in the Drosophila ovary. *Development*, 124(12):2463–2476, Jun 1997.

[128] A. Lingel and M. Sattler. Novel modes of protein-RNA recognition in the RNAi pathway. *Curr. Opin. Struct. Biol.*, 15(1):107–115, Feb 2005.

[129] A. Lingel, B. Simon, E. Izaurralde, and M. Sattler. Structure and nucleic-acid binding of the Drosophila Argonaute 2 PAZ domain. *Nature*, 426(6965):465–469, Nov 2003.

[130] J. Liu, M. A. Carmell, F. V. Rivas, C. G. Marsden, J. M. Thomson, J. J. Song, S. M. Hammond, L. Joshua-Tor, and G. J. Hannon. Argonaute2 is the catalytic engine of mammalian RNAi. *Science*, 305(5689):1437–1441, Sep 2004.

[131] J. Liu, F. V. Rivas, J. Wohlschlegel, J. R. Yates, R. Parker, and G. J. Hannon. A role for the P-body component GW182 in microRNA function. *Nat. Cell Biol.*, 7(12):1261–1266, Dec 2005.

[132] Q. Liu, T. A. Rand, S. Kalidas, F. Du, H. E. Kim, D. P. Smith, and X. Wang. R2D2, a bridge between the initiation and effector steps of the Drosophila RNAi pathway. *Science*, 301(5641):1921–1925, Sep 2003.

[133] X. Liu, F. Jiang, S. Kalidas, D. Smith, and Q. Liu. Dicer-2 and R2D2 coordinately bind siRNA to promote assembly of the siRISC complexes. *RNA*, 12(8):1514–1520, Aug 2006.

[134] Y. Liu, X. Ye, F. Jiang, C. Liang, D. Chen, J. Peng, L. N. Kinch, N. V. Grishin, and Q. Liu. C3PO, an endoribonuclease that promotes RNAi by facilitating RISC activation. *Science*, 325(5941):750–753, Aug 2009.

[135] I. Loedige, D. Gaidatzis, R. Sack, G. Meister, and W. Filipowicz. The mammalian TRIM-NHL protein TRIM71/LIN-41 is a repressor of mRNA function. *Nucleic Acids Res.*, 41(1):518–532, Jan 2013.

[136] E. Lund, S. Guttinger, A. Calado, J. E. Dahlberg, and U. Kutay. Nuclear export of microRNA precursors. *Science*, 303(5654):95–98, Jan 2004.

[137] J. B. Ma, K. Ye, and D. J. Patel. Structural basis for overhang-specific small interfering RNA recognition by the PAZ domain. *Nature*, 429(6989):318–322, May 2004.

[138] J. B. Ma, Y. R. Yuan, G. Meister, Y. Pei, T. Tuschl, and D. J. Patel. Structural basis for 5'-end-specific recognition of guide RNA by the A. fulgidus Piwi protein. *Nature*, 434(7033):666–670, Mar 2005.

[139] I. J. MacRae, E. Ma, M. Zhou, C. V. Robinson, and J. A. Doudna. In vitro reconstitution of the human RISC-loading complex. *Proc. Natl. Acad. Sci. U.S.A.*, 105(2):512–517, Jan 2008.

[140] E. Maniataki and Z. Mourelatos. A human, ATP-independent, RISC assembly machine fueled by pre-miRNA. *Genes Dev.*, 19(24):2979–2990, Dec 2005.

[141] P. A. Maroney, Y. Yu, J. Fisher, and T. W. Nilsen. Evidence that microRNAs are associated with translating messenger RNAs in human cells. *Nat. Struct. Mol. Biol.*, 13(12):1102–1107, Dec 2006.

[142] J. Martinez and T. Tuschl. RISC is a 5' phosphomonoester-producing RNA endonuclease. *Genes Dev.*, 18(9):975–980, May 2004.

[143] M. Mayer and B. Meyer. Characterization of ligand binding by saturation transfer difference NMR spectroscopy. *Angew Chem Int Ed Engl*, 38:1784–1788, 1999.

[144] M. Mayer and B. Meyer. *J Am Chem Soc*, 123(25):6108–17, 2001.

[145] G. Meister, M. Landthaler, A. Patkaniowska, Y. Dorsett, G. Teng, and T. Tuschl. Human Argonaute2 mediates RNA cleavage targeted by miRNAs and siRNAs. *Mol. Cell*, 15(2):185–197, Jul 2004.

[146] G. Meister, M. Landthaler, L. Peters, P. Y. Chen, H. Urlaub, R. Luhrmann, and T. Tuschl. Identification of novel argonaute-associated proteins. *Curr. Biol.*, 15(23):2149–2155, Dec 2005.

[147] S. Mi, T. Cai, Y. Hu, Y. Chen, E. Hodges, F. Ni, L. Wu, S. Li, H. Zhou, C. Long, S. Chen, G. J. Hannon, and Y. Qi. Sorting of small RNAs into Arabidopsis argonaute complexes is directed by the 5' terminal nucleotide. *Cell*, 133(1):116–127, Apr 2008.

[148] K. Miyoshi, T. N. Okada, H. Siomi, and M. C. Siomi. Characterization of the miRNA-RISC loading complex and miRNA-RISC formed in the Drosophila miRNA pathway. *RNA*, 15(7):1282–1291, Jul 2009.

[149] T. Miyoshi, A. Takeuchi, H. Siomi, and M. C. Siomi. A direct role for Hsp90 in pre-RISC formation in Drosophila. *Nat. Struct. Mol. Biol.*, 17(8):1024–1026, Aug 2010.

[150] B. Moussian, H. Schoof, A. Haecker, G. Jurgens, and T. Laux. Role of the ZWILLE gene in the regulation of central shoot meristem cell fate during Arabidopsis embryogenesis. *EMBO J.*, 17(6):1799–1809, Mar 1998.

[151] F. A. Mulder, D. Schipper, R. Bott, and R. Boelens. Altered flexibility in the substrate-binding site of related native and engineered high-alkaline Bacillus subtilisins. *J. Mol. Biol.*, 292(1):111–123, Sep 1999.

[152] K. Nakanishi, D. E. Weinberg, D. P. Bartel, and D. J. Patel. Structure of yeast Argonaute with guide RNA. *Nature*, 486(7403):368–374, Jun 2012.

[153] C. Napoli, C. Lemieux, and R. Jorgensen. Introduction of a Chimeric Chalcone Synthase Gene into Petunia Results in Reversible Co-Suppression of Homologous Genes in trans. *Plant Cell*, 2(4):279–289, Apr 1990.

[154] R. A. Neumuller, J. Betschinger, A. Fischer, N. Bushati, I. Poernbacher, K. Mechtler, S. M. Cohen, and J. A. Knoblich. Mei-P26 regulates microRNAs and cell growth in the Drosophila ovarian stem cell lineage. *Nature*, 454(7201):241–245, Jul 2008.

[155] K. Nishi, A. Nishi, T. Nagasawa, and K. Ui-Tei. Human TNRC6A is an Argonaute-navigator protein for microRNA-mediated gene silencing in the nucleus. *RNA*, 19(1):17–35, Jan 2013.

[156] C. L. Noland, E. Ma, and J. A. Doudna. siRNA repositioning for guide strand selection by human Dicer complexes. *Mol. Cell*, 43(1):110–121, Jul 2011.

[157] M. J. Nolde, N. Saka, K. L. Reinert, and F. J. Slack. The Caenorhabditis elegans pumilio homolog, puf-9, is required for the 3'UTR-mediated repression of the let-7 microRNA target gene, hbl-1. *Dev. Biol.*, 305(2):551–563, May 2007.

[158] M. Nowotny, S. A. Gaidamakov, R. J. Crouch, and W. Yang. Crystal structures of RNase H bound to an RNA/DNA hybrid: substrate specificity and metal-dependent catalysis. *Cell*, 121(7):1005–1016, Jul 2005.

[159] A. Nykanen, B. Haley, and P. D. Zamore. ATP requirements and small interfering RNA structure in the RNA interference pathway. *Cell*, 107(3):309–321, Nov 2001.

[160] T. Ohrt, J. Mutze, W. Staroske, L. Weinmann, J. Hock, K. Crell, G. Meister, and P. Schwille. Fluorescence correlation spectroscopy and fluorescence cross-correlation spectroscopy reveal the cytoplasmic origination of loaded nuclear RISC in vivo in human cells. *Nucleic Acids Res.*, 36(20):6439–6449, Nov 2008.

[161] K. Okamura, W. J. Chung, J. G. Ruby, H. Guo, D. P. Bartel, and E. C. Lai. The Drosophila hairpin RNA pathway generates endogenous short interfering RNAs. *Nature*, 453(7196):803–806, Jun 2008.

[162] K. Okamura, J. W. Hagen, H. Duan, D. M. Tyler, and E. C. Lai. The mirtron pathway generates microRNA-class regulatory RNAs in Drosophila. *Cell*, 130(1):89–100, Jul 2007.

[163] P. H. Olsen and V. Ambros. The lin-4 regulatory RNA controls developmental timing in Caenorhabditis elegans by blocking LIN-14 protein synthesis after the initiation of translation. *Dev. Biol.*, 216(2):671–680, Dec 1999.

[164] T. I. Orban and E. Izaurralde. Decay of mRNAs targeted by RISC requires XRN1, the Ski complex, and the exosome. *RNA*, 11(4):459–469, Apr 2005.

[165] U. A. Orom, F. C. Nielsen, and A. H. Lund. MicroRNA-10a binds the 5'UTR of ribosomal protein mRNAs and enhances their translation. *Mol. Cell*, 30(4):460–471, May 2008.

[166] R. Parker and U. Sheth. P bodies and the control of mRNA translation and degradation. *Mol. Cell*, 25(5):635–646, Mar 2007.

[167] J. F. Partridge, J. L. DeBeauchamp, A. M. Kosinski, D. L. Ulrich, M. J. Hadler, and V. J. Noffsinger. Functional separation of the requirements for establishment and maintenance of centromeric heterochromatin. *Mol. Cell*, 26(4):593–602, May 2007.

[168] K. M. Pauley, T. Eystathioy, A. Jakymiw, J. C. Hamel, M. J. Fritzler, and E. K. Chan. Formation of GW bodies is a consequence of microRNA genesis. *EMBO Rep.*, 7(9):904–910, Sep 2006.

[169] C. P. Petersen, M. E. Bordeleau, J. Pelletier, and P. A. Sharp. Short RNAs repress translation after initiation in mammalian cells. *Mol. Cell*, 21(4):533–542, Feb 2006.

[170] S. Petri, A. Dueck, G. Lehmann, N. Putz, S. Rudel, E. Kremmer, and G. Meister. Increased siRNA duplex stability correlates with reduced off-target and elevated on-target effects. *RNA*, 17(4):737–749, Apr 2011.

[171] R. S. Pillai, S. N. Bhattacharyya, C. G. Artus, T. Zoller, N. Cougot, E. Basyuk, E. Bertrand, and W. Filipowicz. Inhibition of translational initiation by Let-7 MicroRNA in human cells. *Science*, 309(5740):1573–1576, Sep 2005.

[172] D. Pontier, G. Yahubyan, D. Vega, A. Bulski, J. Saez-Vasquez, M. A. Hakimi, S. Lerbs-Mache, V. Colot, and T. Lagrange. Reinforcement of silencing at transposons and highly repeated sequences requires the concerted action of two distinct RNA polymerases IV in Arabidopsis. *Genes Dev.*, 19(17):2030–2040, Sep 2005.

[173] H. H. Qi, P. P. Ongusaha, J. Myllyharju, D. Cheng, O. Pakkanen, Y. Shi, S. W. Lee, J. Peng, and Y. Shi. Prolyl 4-hydroxylation regulates Argonaute 2 stability. *Nature*, 455(7211):421–424, Sep 2008.

[174] T. M. Rana. Illuminating the silence: understanding the structure and function of small RNAs. *Nat. Rev. Mol. Cell Biol.*, 8(1):23–36, Jan 2007.

[175] J. Rehwinkel, I. Behm-Ansmant, D. Gatfield, and E. Izaurralde. A crucial role for GW182 and the DCP1:DCP2 decapping complex in miRNA-mediated gene silencing. *RNA*, 11(11):1640–1647, Nov 2005.

[176] F. V. Rivas, N. H. Tolia, J. J. Song, J. P. Aragon, J. Liu, G. J. Hannon, and L. Joshua-Tor. Purified Argonaute2 and an siRNA form recombinant human RISC. *Nat. Struct. Mol. Biol.*, 12(4):340–349, Apr 2005.

[177] G. B. Robb, K. M. Brown, J. Khurana, and T. M. Rana. Specific and potent RNAi in the nucleus of human cells. *Nat. Struct. Mol. Biol.*, 12(2):133–137, Feb 2005.

[178] G. B. Robb and T. M. Rana. RNA helicase A interacts with RISC in human cells and functions in RISC loading. *Mol. Cell*, 26(4):523–537, May 2007.

[179] J. G. Ruby, C. Jan, C. Player, M. J. Axtell, W. Lee, C. Nusbaum, H. Ge, and D. P. Bartel. Large-scale sequencing reveals 21U-RNAs and additional microRNAs and endogenous siRNAs in C. elegans. *Cell*, 127(6):1193–1207, Dec 2006.

[180] J. G. Ruby, C. H. Jan, and D. P. Bartel. Intronic microRNA precursors that bypass Drosha processing. *Nature*, 448(7149):83–86, Jul 2007.

[181] S. Rudel, A. Flatley, L. Weinmann, E. Kremmer, and G. Meister. A multifunctional human Argonaute2-specific monoclonal antibody. *RNA*, 14(6):1244–1253, Jun 2008.

[182] S. Rudel, Y. Wang, R. Lenobel, R. Korner, H. H. Hsiao, H. Urlaub, D. Patel, and G. Meister. Phosphorylation of human Argonaute proteins affects small RNA binding. *Nucleic Acids Res.*, 39(6):2330–2343, Mar 2011.

[183] A. Rybak, H. Fuchs, K. Hadian, L. Smirnova, E. A. Wulczyn, G. Michel, R. Nitsch, D. Krappmann, and F. G. Wulczyn. The let-7 target gene mouse lin-41 is a stem cell specific E3 ubiquitin ligase for the miRNA pathway protein Ago2. *Nat. Cell Biol.*, 11(12):1411–1420, Dec 2009.

[184] K. Saito, A. Ishizuka, H. Siomi, and M. C. Siomi. Processing of pre-microRNAs by the Dicer-1-Loquacious complex in Drosophila cells. *PLoS Biol.*, 3(7):e235, Jul 2005.

[185] K. Saito, Y. Sakaguchi, T. Suzuki, T. Suzuki, H. Siomi, and M. C. Siomi. Pimet, the Drosophila homolog of HEN1, mediates 2'-O-methylation of Piwi- interacting RNAs at their 3' ends. *Genes Dev.*, 21(13):1603–1608, Jul 2007.

[186] J. Sambrook, E. Fritsch, and F. Maniatis. Molecular cloning: A Laboratory Manual. *Cold Spring Harbour Laboratory Press*, Cold Spring Harbour , N.Y. 1989.

[187] M. Sattler, J. Schleucher, and C. Griesinger. Heteronuclear multidimensional NMR experiments for the structure determination of proteins in solution employing pulsed field gradients. *Prog Nucl Magn Reson Spectrosc*, 34:93–158, 1999.

[188] N. T. Schirle and I. J. MacRae. The crystal structure of human Argonaute2. *Science*, 336(6084):1037–1040, May 2012.

[189] J. C. Schwamborn, E. Berezikov, and J. A. Knoblich. The TRIM-NHL protein TRIM32 activates microRNAs and prevents self-renewal in mouse neural progenitors. *Cell*, 136(5):913–925, Mar 2009.

[190] D. S. Schwarz, G. Hutvagner, T. Du, Z. Xu, N. Aronin, and P. D. Zamore. Asymmetry in the assembly of the RNAi enzyme complex. *Cell*, 115(2):199–208, Oct 2003.

[191] D. S. Schwarz, Y. Tomari, and P. D. Zamore. The RNA-induced silencing complex is a Mg2+-dependent endonuclease. *Curr. Biol.*, 14(9):787–791, May 2004.

[192] S. Schwarzinger, G. J. Kroon, T. R. Foss, J. Chung, P. E. Wright, and H. J. Dyson. Sequence-dependent correction of random coil NMR chemical shifts. *J. Am. Chem. Soc.*, 123(13):2970–2978, Apr 2001.

[193] B. Shen and H. M. Goodman. Uridine addition after microRNA-directed cleavage. *Science*, 306(5698):997, Nov 2004.

[194] U. Sheth and R. Parker.

[195] T. F. Smith. Diversity of WD-repeat proteins. *Subcell. Biochem.*, 48:20–30, 2008.

[196] J. J. Song, S. K. Smith, G. J. Hannon, and L. Joshua-Tor. Crystal structure of Argonaute and its implications for RISC slicer activity. *Science*, 305(5689):1434–1437, Sep 2004.

[197] M. Stevenson. Therapeutic potential of RNA interference. *N. Engl. J. Med.*, 351(17):1772–1777, Oct 2004.

[198] H. Su, S. Meng, Y. Lu, M. I. Trombly, J. Chen, C. Lin, A. Turk, and X. Wang. Mammalian hyperplastic discs homolog EDD regulates miRNA-mediated gene silencing. *Mol. Cell*, 43(1):97–109, Jul 2011.

[199] H. Su, M. I. Trombly, J. Chen, and X. Wang. Essential and overlapping functions for mammalian Argonautes in microRNA silencing. *Genes Dev.*, 23(3):304–317, Feb 2009.

[200] V. Su and A. F. Lau. Ubiquitin-like and ubiquitin-associated domain proteins: significance in proteasomal degradation. *Cell. Mol. Life Sci.*, 66(17):2819–2833, Sep 2009.

[201] K. Takimoto, M. Wakiyama, and S. Yokoyama. Mammalian GW182 contains multiple Argonaute-binding sites and functions in microRNA-mediated translational repression. *RNA*, 15(6):1078–1089, Jun 2009.

[202] K. Tiemann and J. J. Rossi. RNAi-based therapeutics-current status, challenges and prospects. *EMBO Mol Med*, 1(3):142–151, Jun 2009.

[203] S. Till, E. Lejeune, R. Thermann, M. Bortfeld, M. Hothorn, D. Enderle, C. Heinrich, M. W. Hentze, and A. G. Ladurner. A conserved motif in Argonaute-interacting proteins mediates functional interactions through the Argonaute PIWI domain. *Nat. Struct. Mol. Biol.*, 14(10):897–903, Oct 2007.

[204] Y. Tomari, C. Matranga, B. Haley, N. Martinez, and P. D. Zamore. A protein sensor for siRNA asymmetry. *Science*, 306(5700):1377–1380, Nov 2004.

[205] P. Tompa. Intrinsically unstructured proteins. *Trends Biochem. Sci.*, 27(10):527–533, Oct 2002.

[206] P. Tompa, J. Prilusky, I. Silman, and J. L. Sussman. Structural disorder serves as a weak signal for intracellular protein degradation. *Proteins*, 71(2):903–909, May 2008.

[207] T. Treiber, N. Treiber, and G. Meister. Regulation of microRNA biogenesis and function. *Thromb. Haemost.*, 107(4):605–610, Apr 2012.

[208] F. Tritschler, J. E. Braun, A. Eulalio, V. Truffault, E. Izaurralde, and O. Weichenrieder. Structural basis for the mutually exclusive anchoring of P body components EDC3 and Tral to the DEAD box protein DDX6/Me31B. *Mol. Cell*, 33(5):661–668, Mar 2009.

[209] T. Tuschl. RNA interference and small interfering RNAs. *Chembiochem*, 2(4):239–245, Apr 2001.

[210] H. Valadi, K. Ekstrom, A. Bossios, M. Sjostrand, J. J. Lee, and J. O. Lotvall. Exosome-mediated transfer of mRNAs and microRNAs is a novel mechanism of genetic exchange between cells. *Nat. Cell Biol.*, 9(6):654–659, Jun 2007.

[211] A. R. van der Krol, L. A. Mur, P. de Lange, J. N. Mol, and A. R. Stuitje. Inhibition of flower pigmentation by antisense CHS genes: promoter and minimal sequence requirements for the antisense effect. *Plant Mol. Biol.*, 14(4):457–466, Apr 1990.

[212] S. Vasudevan, Y. Tong, and J. A. Steitz. Switching from repression to activation: microRNAs can up-regulate translation. *Science*, 318(5858):1931–1934, Dec 2007.

[213] A. Verdel, S. Jia, S. Gerber, T. Sugiyama, S. Gygi, S. I. Grewal, and D. Moazed. RNAi-mediated targeting of heterochromatin by the RITS complex. *Science*, 303(5658):672–676, Jan 2004.

[214] T. Walzthoeni, M. Claassen, A. Leitner, F. Herzog, S. Bohn, F. Forster, M. Beck, and R. Aebersold. False discovery rate estimation for cross-linked peptides identified by mass spectrometry. *Nat. Methods*, 9(9):901–903, Sep 2012.

[215] Y. Wang, G. Sheng, S. Juranek, T. Tuschl, and D. J. Patel. Structure of the guide-strand-containing argonaute silencing complex. *Nature*, 456(7219):209–213, Nov 2008.

[216] A. M. Waterhouse, J. B. Procter, D. M. Martin, M. Clamp, and G. J. Barton. Jalview Version 2–a multiple sequence alignment editor and analysis workbench. *Bioinformatics*, 25(9):1189–1191, May 2009.

[217] P. M. Waterhouse, M. B. Wang, and T. Lough. Gene silencing as an adaptive defence against viruses. *Nature*, 411(6839):834–842, Jun 2001.

[218] L. Weinmann, J. Hock, T. Ivacevic, T. Ohrt, J. Mutze, P. Schwille, E. Kremmer, V. Benes, H. Urlaub, and G. Meister. Importin 8 is a gene silencing factor that targets argonaute proteins to distinct mRNAs. *Cell*, 136(3):496–507, Feb 2009.

[219] B. Wightman, I. Ha, and G. Ruvkun. Posttranscriptional regulation of the heterochronic gene lin-14 by lin-4 mediates temporal pattern formation in C. elegans. *Cell*, 75(5):855–862, Dec 1993.

[220] J. Winter, S. Jung, S. Keller, R. I. Gregory, and S. Diederichs. Many roads to maturity: microRNA biogenesis pathways and their regulation. *Nat. Cell Biol.*, 11(3):228–234, Mar 2009.

[221] D. S. Wishart, C. G. Bigam, A. Holm, R. S. Hodges, and B. D. Sykes. 1H, 13C and 15N random coil NMR chemical shifts of the common amino acids. I. Investigations of nearest-neighbor effects. *J. Biomol. NMR*, 5(1):67–81, Jan 1995.

[222] K. Wuthrich. NMR of proteins and nucleic acid. *Wiley*, 1986.

[223] Z. Yang, A. Jakymiw, M. R. Wood, T. Eystathioy, R. L. Rubin, M. J. Fritzler, and E. K. Chan. GW182 is critical for the stability of GW bodies expressed during the cell cycle and cell proliferation. *J. Cell. Sci.*, 117(Pt 23):5567–5578, Nov 2004.

[224] B. Yao, S. Li, H. M. Jung, S. L. Lian, G. X. Abadal, F. Han, M. J. Fritzler, and E. K. Chan. Divergent GW182 functional domains in the regulation of translational silencing. *Nucleic Acids Res.*, 39(7):2534–2547, Apr 2011.

[225] X. Ye, N. Huang, Y. Liu, Z. Paroo, C. Huerta, P. Li, S. Chen, Q. Liu, and H. Zhang. Structure of C3PO and mechanism of human RISC activation. *Nat. Struct. Mol. Biol.*, 18(6):650–657, Jun 2011.

[226] R. Yi, Y. Qin, I. G. Macara, and B. R. Cullen. Exportin-5 mediates the nuclear export of pre-microRNAs and short hairpin RNAs. *Genes Dev.*, 17(24):3011–3016, Dec 2003.

[227] E. Yigit, P. J. Batista, Y. Bei, K. M. Pang, C. C. Chen, N. H. Tolia, L. Joshua-Tor, S. Mitani, M. J. Simard, and C. C. Mello. Analysis of the C. elegans Argonaute family reveals that distinct Argonautes act sequentially during RNAi. *Cell*, 127(4):747–757, Nov 2006.

[228] M. Yoda, T. Kawamata, Z. Paroo, X. Ye, S. Iwasaki, Q. Liu, and Y. Tomari. ATP-dependent human RISC assembly pathways. *Nat. Struct. Mol. Biol.*, 17(1):17–23, Jan 2010.

[229] N. J. Yoo, S. Y. Hur, M. S. Kim, J. Y. Lee, and S. H. Lee. Immunohistochemical analysis of RNA-induced silencing complex-related proteins AGO2 and TNRC6A in prostate and esophageal cancers. *APMIS*, 118(4):271–276, Apr 2010.

[230] Y. R. Yuan, Y. Pei, J. B. Ma, V. Kuryavyi, M. Zhadina, G. Meister, H. Y. Chen, Z. Dauter, T. Tuschl, and D. J. Patel. Crystal structure of A. aeolicus argonaute, a site-specific DNA-guided endoribonuclease, provides insights into RISC-mediated mRNA cleavage. *Mol. Cell*, 19(3):405–419, Aug 2005.

[231] L. Zekri, E. Huntzinger, S. Heimstadt, and E. Izaurralde. The silencing domain of GW182 interacts with PABPC1 to promote translational repression and degradation of microRNA targets and is required for target release. *Mol. Cell. Biol.*, 29(23):6220–6231, Dec 2009.

[232] Y. Zeng, H. Sankala, X. Zhang, and P. R. Graves. Phosphorylation of Argonaute 2 at serine-387 facilitates its localization to processing bodies. *Biochem. J.*, 413(3):429–436, Aug 2008.

[233] H. Zhang and J. K. Zhu. RNA-directed DNA methylation. *Curr. Opin. Plant Biol.*, 14(2):142–147, Apr 2011.

[234] A. Zielezinski and W. M. Karlowski. Agos–a universal web tool for GW Argonaute-binding domain prediction. *Bioinformatics*, 27(9):1318–1319, May 2011.

[235] J. T. Zipprich, S. Bhattacharyya, H. Mathys, and W. Filipowicz. Importance of the C-terminal domain of the human GW182 protein TNRC6C for translational repression. *RNA*, 15(5):781–793, May 2009.

Acknowledgements

I would like to thank all people who contributed to this work.

First and foremost, I thank Gunter Meister for giving me the great opportunity to realize my PhD in his group. Thanks for your support and the freedom to accomplish the project the way I did.

Big thanks to Dierk Niessing for accommodating me in Munich for more than two years and pushing forward my PhD. I'm grateful for your encouragement and guidance.

I would like to express my gratitude to Klaus Förstemann for officially supervising this thesis.

I thank the remaining members of my thesis committee Michael Sattler, Esben Lorentzen and Tobias Walther for your impulses.

My project could not have been successful without my collaboration partners Janosch Hennig and Franz Herzog. Many thanks for your excellent work and help.

There are many more people I would like to thank. My appreciation goes to all colleagues I have met in the Meister, Conti, Walther, Niessing and Sattler labs for making me quickly feel comfortable and teaching me the right skills to advance my project.

Extra thanks go to Alex, Anne, Anne, Danny, Justine, Ira, Tina, Lena, Doris, Roland, Lisa, Vroni, Steffi and Frauke.

Finally, I would like to thank my family and Thomas for their unconditional support.